ACTUATOR LOAD CALCULATION TOOL FOR A MULTIAXIAL TEST SYSTEM OF A ROTATING BEAM LIKE AEROSTRUCTURE

A THESIS SUBMITTED TO
THE GRADUATE SCHOOL OF NATURAL AND APPLIED SCIENCES
OF
MIDDLE EAST TECHNICAL UNIVERSITY

BY

AFİF UMUR LİMON

IN PARTIAL FULFILLMENT OF THE REQUIREMENTS
FOR
THE DEGREE OF MASTER OF SCIENCE
IN
AEROSPACE ENGINEERING

DECEMBER 2018

Approval of the thesis:

ACTUATOR LOAD CALCULATION TOOL FOR A MULTIAXIAL TEST SYSTEM OF A ROTATING BEAM LIKE AEROSTRUCTURE

submitted by **AFİF UMUR LİMON** in partial fulfillment of the requirements for the degree of **Master of Science in Aerospace Engineering Department, Middle East Technical University** by,

Prof. Dr. Halil Kalıpçılar
Director, Graduate School of **Natural and Applied Sciences** ________________

Prof. Dr. İsmail Hakkı Tuncer
Head of Department, **Aerospace Engineering** ________________

Assoc. Prof. Dr. Demirkan Çöker
Supervisor, **Aerospace Engineering Dept., METU** ________________

Examining Committee Members:

Prof. Dr. Ozan Tekinalp
Aerospace Engineering Dept., METU ________________

Assoc. Prof. Dr. Demirkan Çöker
Aerospace Engineering Dept., METU ________________

Prof. Dr. Altan Kayran
Aerospace Engineering Dept., METU ________________

Prof. Dr. Kemal Levend Parnas
Mechanical Engineering Dept., TED University ________________

Assoc. Prof. Dr. Ercan Gürses
Aerospace Engineering Dept., METU ________________

Date: 18.12.2018

I hereby declare that all the information in this document has been obtained and presented in accordance with academic rules and ethical conduct. I also declare that, as required by these rules and conduct, I have fully cited and referenced all material and results that are not original to this work.

Name, Last Name: Afif Umur Limon

Signature:

ABSTRACT

ACTUATOR LOAD CALCULATION TOOL FOR A MULTIAXIAL TEST SYSTEM OF A ROTATING BEAM LIKE AEROSTRUCTURE

Limon, Afif Umur

M.S., Department of Aerospace Engineering

Supervisor: Assoc. Prof. Dr. Demirkan Çöker

December 2018, 98 pages

Design and analysis of new helicopter blades need to be verified by testing under combined multiaxial loading including centrifugal force, chord bending, beam bending and torsion loadings. In this thesis, an actuator load calculation tool for a rotating beam like aerospace structure structural test system is developed and is verified by multiaxial testing of a dummy component.

The actuator load calculation tool development consists of an analysis and testing part. A dummy structural component is designed and analyzed with a commercial FEM software. A dynamic analysis model of the helicopter blade structural test system is conducted using a commercial multibody dynamic simulation software. The model is used to find the strain data on the dummy component using the modules of multibody dynamic simulation software. Calibration dynamic analysis model is created for the calculation of calibration coefficients for the dummy component. By using calibration coefficients and strain data found from dynamic analysis model of the test setup, section loads on the dummy component are calculated.

For the testing part, a dummy component is manufactured, and is wired with strain gages, after which calibration and crosstalk compensation operations are accomplished, and the section loads on the dummy component are measured from the multiaxial test. Using measurements of six strain bridges, chord bending, beam bending, torque, and centrifugal force, on two different sections are calculated. The developed methodology is validated by executing a multiaxial test on the dummy component with a combined loading of chord bending, beam bending, torsion, and centrifugal force loading, resulting in an average absolute percentage error rate of 4.92% between the testing and estimated section loads. The tool developed in this thesis can be used for the calculation of actuator loads in the multiaxial loading test of real helicopter blades by importing the finite element model and the composite material properties of the actual helicopter blade.

Keywords: Aerospace Structural Testing, Structural Design and Analysis, Finite Element Analysis, Dynamic Analysis of Mechanical Systems, Strain-based Sensor Calibration

ÖZ

DÖNER KİRİŞ BENZERİ HAVACILIK YAPILARININ ÇOK EKSENLİ YAPISAL TESTİ İÇİN EYLEYİCİ YÜKÜ HESAPLAMA ALGORİTMASI

Limon, Afif Umur
Yüksek Lisans, Havacılık ve Uzay Mühendisliği Bölümü
Tez Yöneticisi: Doç. Dr. Demirkan Çöker

Aralık 2018, 98 sayfa

Yeni helikopter pallerinin tasarım ve analizleri merkezcil kuvvet, veter bükülmesi, kiriş bükülmesi ve burulma yüklerinin uygulandığı çok eksenli testler ile doğrulanmalıdır. Bu çalışmada, döner kiriş benzeri havacılık yapılarının yapısal test sistemi eyleyici yükü hesaplama algoritması geliştirilmiştir ve bu algoritma taklit bir havacılık yapısı üzerinde uygulanan çok eksenli test ile doğrulanmıştır.

Hidrolik eyleyici yük hesaplama aracı geliştirilmesi süreci analiz ve test olarak iki aşamadan oluşmaktadır. Taklit bir parça bilgisayar ortamında tasarlanarak ticari bir sonlu elemanlar yazılımı kullanılarak analiz edilmiştir. Helikopter pali yapısal test sisteminin dinamik analiz modeli ticari amaçlı üretilmiş çok parçalı dinamik simülasyon yazılımı kullanılarak oluşturulmuştur. Bu model, bu yazılımın modülleri yardımıyla taklit parça üzerindeki gerinim değerlerinin hesaplanmasında kullanılmıştır. Kalibrasyon dinamik analiz modeli, taklit parçanın kalibrasyon katsayılarını bulmak için oluşturulmuştur. Bu kalibrasyon katsayıları ve dinamik analiz modelinden bulunan gerinim değerleri kullanılarak taklit parça üzerindeki kesit yükleri hesaplanmıştır.

Test bölümü için üretilen taklit parça üzerine kalibrasyon ve çapraz karışma giderim uygulamaları yapılacak olan gerinim pulları yapıştırılmıştır ve bu parça üzerinde çok eksenli bir test uygulanarak kesit yükleri ölçülmüştür. Veter bükülmesi, kiriş bükülmesi, burulma ve merkezcil kuvvetini ölçebilen altı adet gerinim köprüsünden elde edilen ölçümler kullanılarak iki kesitteki kesit yükleri bulunmuştur. Geliştirilen metot, taklit parça üzerinde veter bükülmesi, kiriş bükülmesi, burulma ve merkezcil kuvvet yüklerinden oluşan kombine bir yüklemenin uygulandığı çok eksenli bir test ile test ölçümleri ve hesaplanan kesit yükleri arasında ortalama %4.92 hata oranıyla doğrulanmıştır. Bu tezde geliştirilen araç gerçek helikopter pallerinin çok eksenli testlerindeki hidrolik eyleyici yüklerinin hesaplanmasında helikopter palinin sonlu elemanlar modeli ve malzeme özellikleri içine yüklenerek kullanılabilecektir.

Anahtar Kelimeler: Havacılık ve Uzay Yapısal Testleri, Yapısal Tasarım ve Analiz, Sonlu Elemanlar Analizi, Mekanik Sistemlerin Dinamik Analizi, Gerinim Tabanlı Sensor Kalibrasyonu

To my family, and my love

ACKNOWLEDGEMENTS

I would like to express my greatest gratitude to my supervisor Assoc. Prof. Dr. Demirkan Çöker, for giving me an opportunity to work with him, allowing me to benefit from his invaluable comments and experiences and his endless patience throughout my study.

I want to express my gratitude to thesis examining committee members Prof. Dr. Ozan Tekinalp, Prof. Dr. Altan Kayran, Prof. Dr. Kemal Levend Parnas, and Assoc. Prof. Dr. Ercan Gürses for their valuable feedbacks about my study.

I am also indebted to my colleague in TAI Structural Test, Yusuf Ulu for his support during the studies, his advice during the thesis subject determination and tutoring in MSC Adams software.

I must also express my gratitude to my colleagues Levent Ulu, Mustafa İçen, Fırat Temel, Berkay Önsü, Gülay Yılmaz Çimen and Sinan Dalkılıç. Without their help, this study would not have finished. Additionally, I must also thank to technicians in the laboratory Mehmet Aras, Oktay Sevil and Mesut Talha Güven for their passionate participation.

I would like to thank to my father Atila, my mother Güler and my sister Umay for their unfailing support and continuous encouragement throughout my years of study and through the process of researching and writing this thesis. This accomplishment would not have been possible without them.

I would like to express my deepest gratitude to İzel Gülcan, my love, for loving me and her endless patience throughout my study.

I also appreciate the support of my dearest friends Murat Şenipek, Metehan Yayla, Ramin Rouzbar, Yoseph Yang, Selahattin Burak Sarsılmaz, Harun Tıraş and Ezgi Orbay Akcengiz for always promoting me and believing in me.

I would like to thank to Aerospace Engineering Department Secretary for Student Affairs, Derya Kaya Topa for her help during registration and thesis submission progress, and relations with Graduate School of Natural and Applied Sciences and Registrar's Office.

I would like to express my thanks to Queen, ACDC Mor ve Ötesi and Athena for their motivating songs to give strength to me to continue in my darkest hours.

I also thank to TAI (Turkish Aerospace Industries) for continuous support during my thesis study.

TABLE OF CONTENTS

LIST OF TABLES

TABLES

LIST OF FIGURES

FIGURES

LIST OF SYMBOLS

ρ	Density
E	Young's Modulus
ν	Poisson's Ratio
G	Shear Modulus
ε	Strain
V	Voltage

LIST OF ABBREVIATIONS

BB	Beam Bending
BC	Boundary Conditions
CAD	Computer-aided Design
CB	Chord Bending
CF	Centrifugal Force
CG	Center of Gravity
DAQ	Data Acquisition System
EU	Engineering Unit
FEA	Finite Element Analysis
FEM	Finite Element Model
HPU	Hydraulic Power Unit
HSM	Hydraulic Service Manifold
MBD	Multibody Dynamics
METU	Middle East Technical University
MNF	Modal Neutral File
RF	Reserve Factor
TAI	Turkish Aerospace Industries
TQ	Torque

CHAPTER 1

INTRODUCTION

1.1 Definition of Helicopter Blade Structural Tests

In today’s world, all the design phases are generally completed in the computer environment. Structural design and analysis work done in the computer environment during the design phase of the helicopters must be tested by simulating the design conditions and loads before the first flight [1]. Certification authorities also demand to see that the designed structure can withstand ultimate loads for at least 3 seconds in static tests and imitative cycling loads under dynamic test conditions [2]. All the activities carried out to prove the helicopter blade theoretical strength in the real-world environment is the goal of helicopter blade structural tests. Considering the importance of the helicopter main rotor blades for helicopter flights, helicopter blade structural testing is a crucial part of helicopter design process.

1.2 Definition of Helicopter Blade Structural Test System

Helicopter blade structural test system at Turkish Aerospace Industries (TAI) is used during the thesis study, and it is explained briefly in this section.

At the TAI facilities, a test rig for helicopter blade structural tests was designed, manufactured, and assembled for design verification procedures of helicopter rotor blades. The test system has the capability of testing a wide range of helicopter blades by its modular design philosophy. The system can apply centrifugal force, beam bending, chord bending, and torsion loads on the test article. All applicable loads can be applied as oscillatory loads with constant or variable amplitudes with the help of hydraulic actuators and load introduction structures assembled on cars, which can move only linearly. The cars were also designed to minimize cross coupling of these loads with a specialized gimbal system. A system consisting of dead weights called counterbalance system is used to balance the weights of the actuators, fixed rods, and load application unit components. Moreover, it has a separate section for the calibration of test articles on the left-hand side of the test system. A general overview of the test system can be seen in Figure 1.

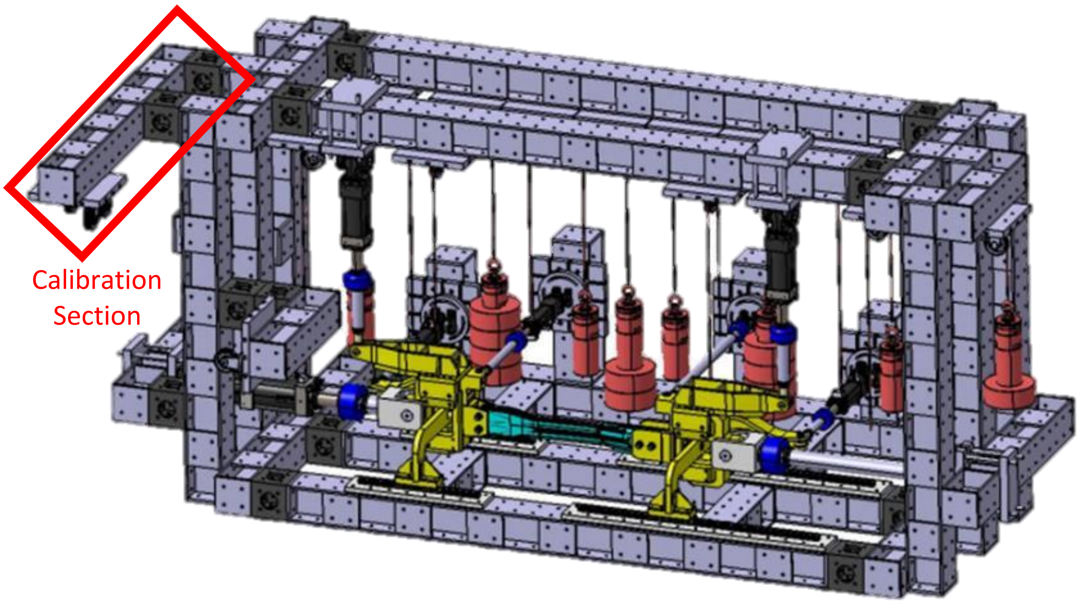

Figure 1: Helicopter Blade Structural Test System [3]

Helicopter blade structural test system is very complex and complicated to understand by just looking the Figure 1. All unnecessary parts like support structures, counterbalance system, and calibration section are made transparent in Figure 2 to make the system simpler. In this simplified figure, all the necessary and critical loading parts and the helicopter blade can be seen. This part creates the main focus area of this study. Even the simplified view of the test system is complicated.

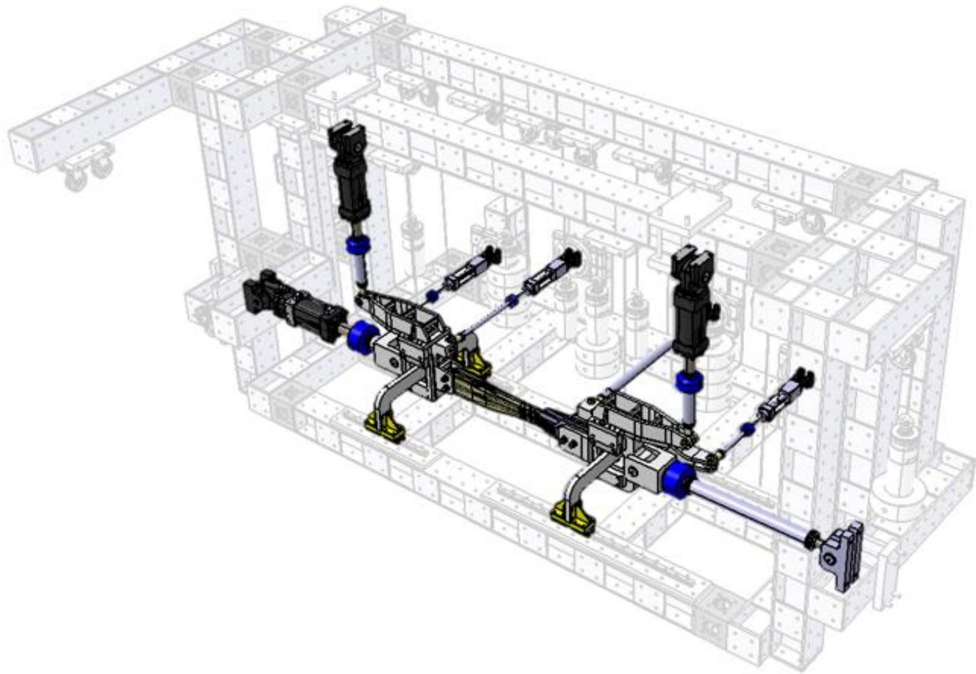

Figure 2: Helicopter Blade Structural Test System Simplified View [3]

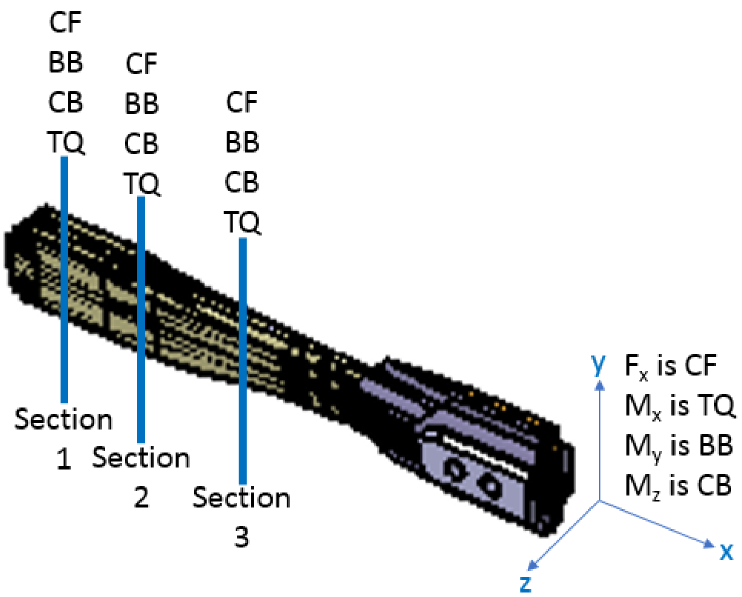

Figure 3: Demanded Loads and Sections on Helicopter Main Rotor Blade Spar Root Zone [3]

Even seeing the simplified view of the test system does not make the system comprehensible. The design process of the test system will be told to make it clear.

First, the helicopter blade main rotor blade spar root zone is sent to the helicopter structural test team with the demand of predetermined multiaxial loading on three sections. Test requesters demanded to see different centrifugal force loading (CF), beam bending loading (BB), chord bending loading (CB), and torsion (pitch moment) loading (TQ) on these three different sections. All the loading is cycling and represents the real-life loads on helicopter lifespan. Directional loading information and representative section locations can be seen in Figure 3.

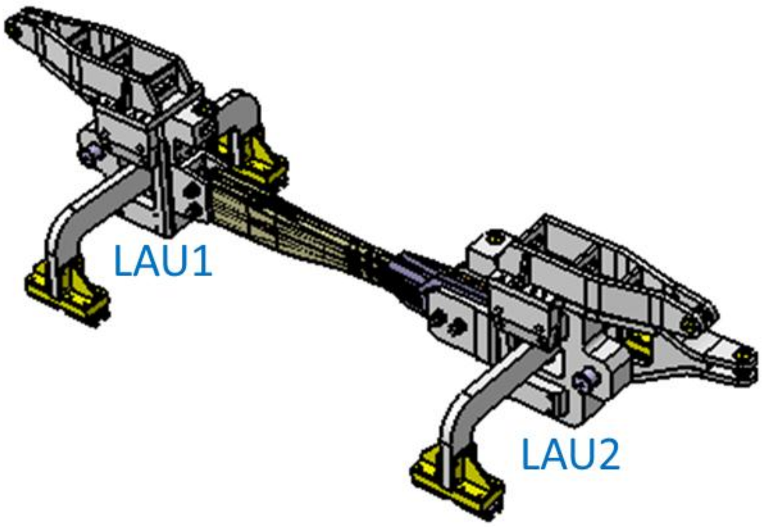

Figure 4: Load Application Units (LAU1 and LAU2) [3]

Load application units as seen in Figure 4 were designed to apply CF, BB, CB and TQ loads on defined sections. These load application units can translate only linearly in centrifugal force direction with the help of underlying linear guides. These linearly moving legs are connected a special gimbal structure to make it freely movable in all rotational directions at the center. Load application units can also move freely around the central axis with the two pin joints below and above of the gimbal structure.

After talking about load application units, load introduction structures will be defined step by step. Centrifugal force load is applied via a hydraulic actuator located in the spanwise direction, and a reaction rod keeps the assembly fixed in CF direction, as seen in Figure 5. Due to the linear guides which the cars are move on, loading axis of the CF load cannot change.

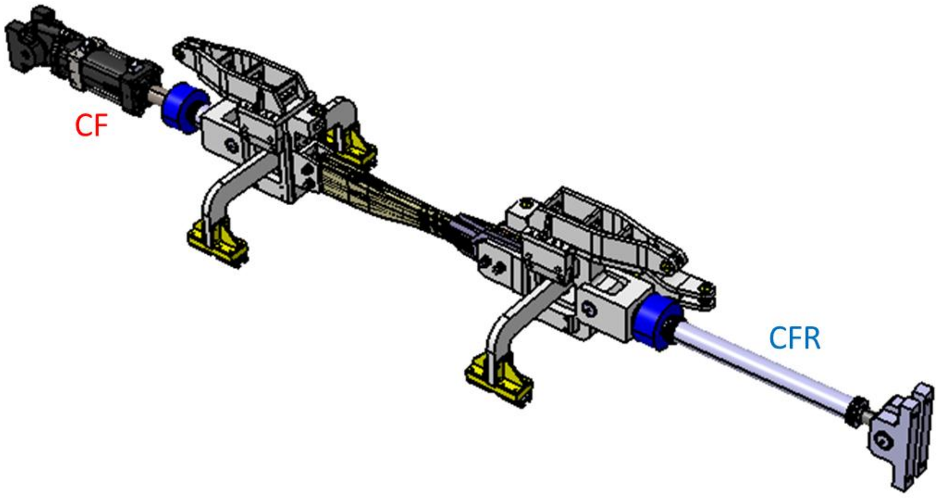

Figure 5: Centrifugal Force Actuator and Reaction Rod (CF and CFR) [3]

Beam bending loads, which bends the helicopter blade into the page and out of the page directions, are applied by two hydraulic actuators connected to two load application units as seen in Figure 6.

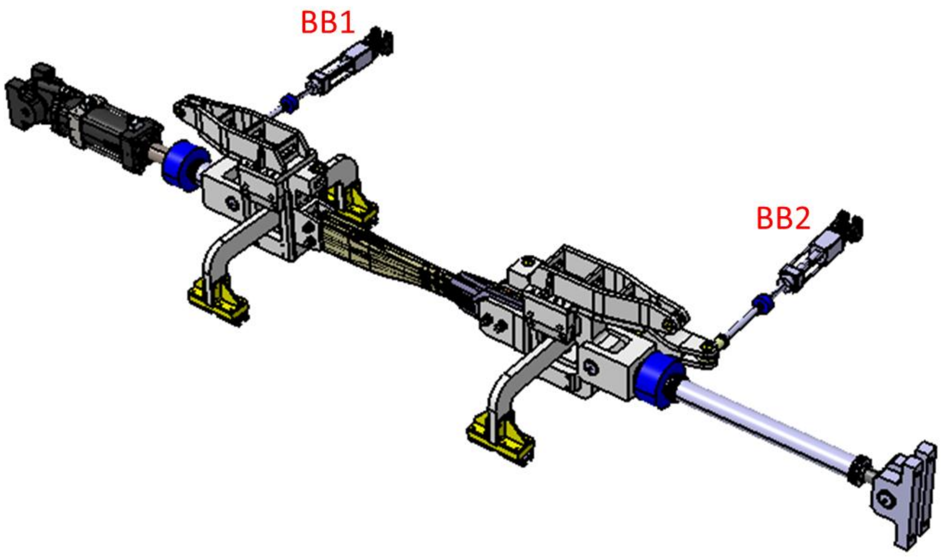

Figure 6: Beam Bending Actuators (BB1 and BB2) [3]

Torque load is transferred to the test article via one of the cars with a hydraulic actuator while another car is kept fixed in torque direction with a reaction rod as seen in Figure 7.

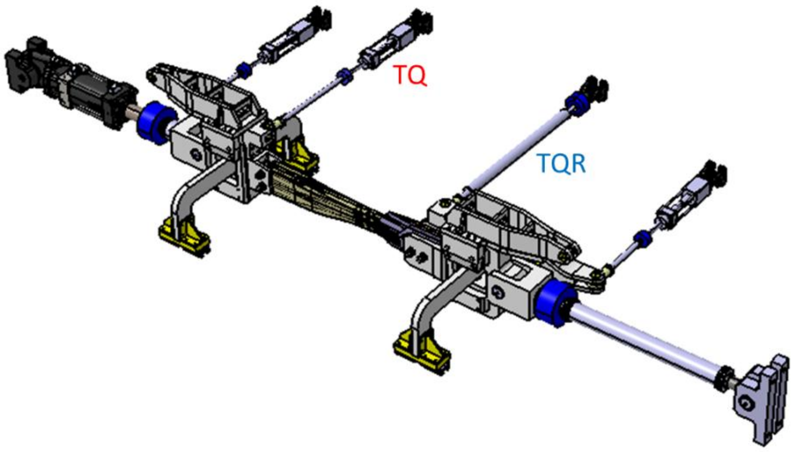

Figure 7: Torque Actuator and Reaction Rod (TQ and TQR) [3]

Chord bending loads, which bends the helicopter blade parallel to page plane, are applied by two hydraulic actuators connected to the two load application units as seen in Figure 8.

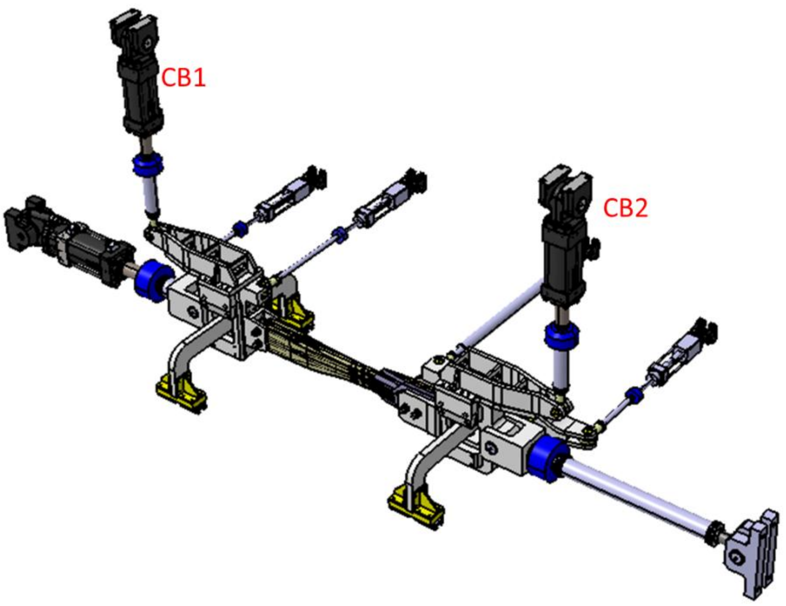

Figure 8: Chord Bending Actuators (CB1 and CB2) [3]

After investigating the load introduction structures, test setup infrastructure introduced briefly. During the test, sensor data is collected continuously from the sensors; including displacement transducers, strain gages, and load cells; with the help of a data acquisition system. It is connected to a controller to give feedback for controlling the test system. This controller is also used to command hydraulic actuators by controlling the hydraulic pump units and hydraulic service manifolds. A schematic of the test control can be seen in Figure 9.

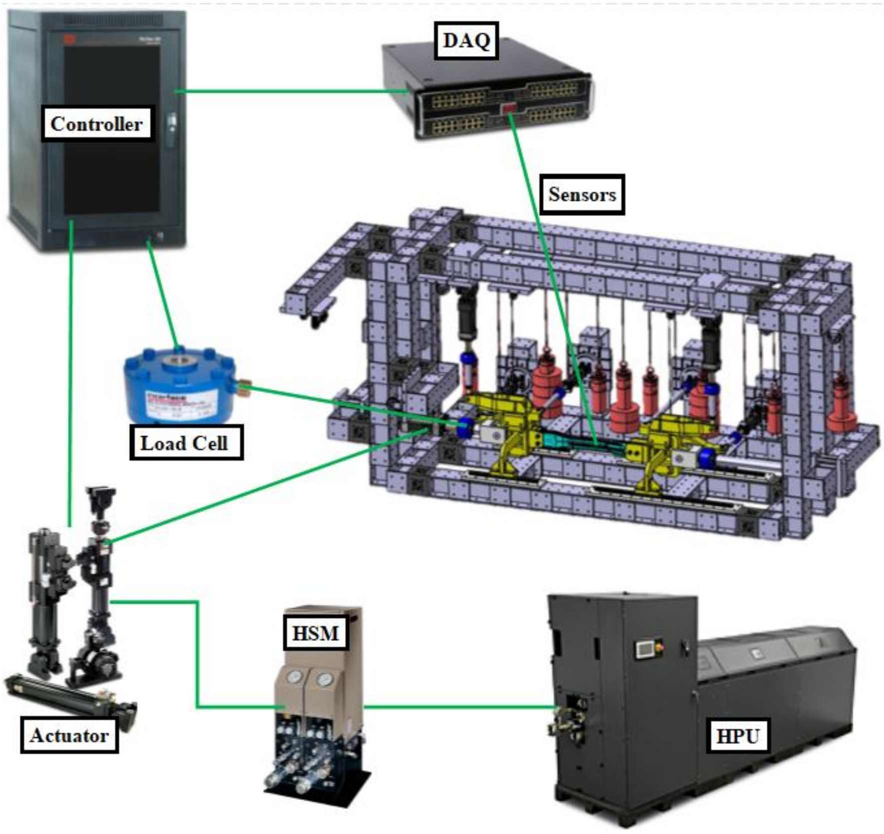

Figure 9: Schematic of the Test Control System [3][4][5][6][7][8][9]

1.3 Reasons for Actuator Load Calculation Tool Development

During the design phases of helicopter blade structural test system, helicopter structural test team calculated the actuator loads according to the test loads given by the test requester. In the calculations, it is assumed that the helicopter blade under huge CF loading is rigid. Nonlinear motion of the actuators is also neglected due to the rigidity assumption. Under these circumstances, the system is assumed to be statically determinate. There are six actuator forces (red ones on the figure), and six reaction forces (blue ones on the figure) in the system as seen in the Figure 10. Two reaction points on both cars (LAU1 and LAU2) acting on the linear guides are assumed to be one, which decreases the number of reaction forces to four.

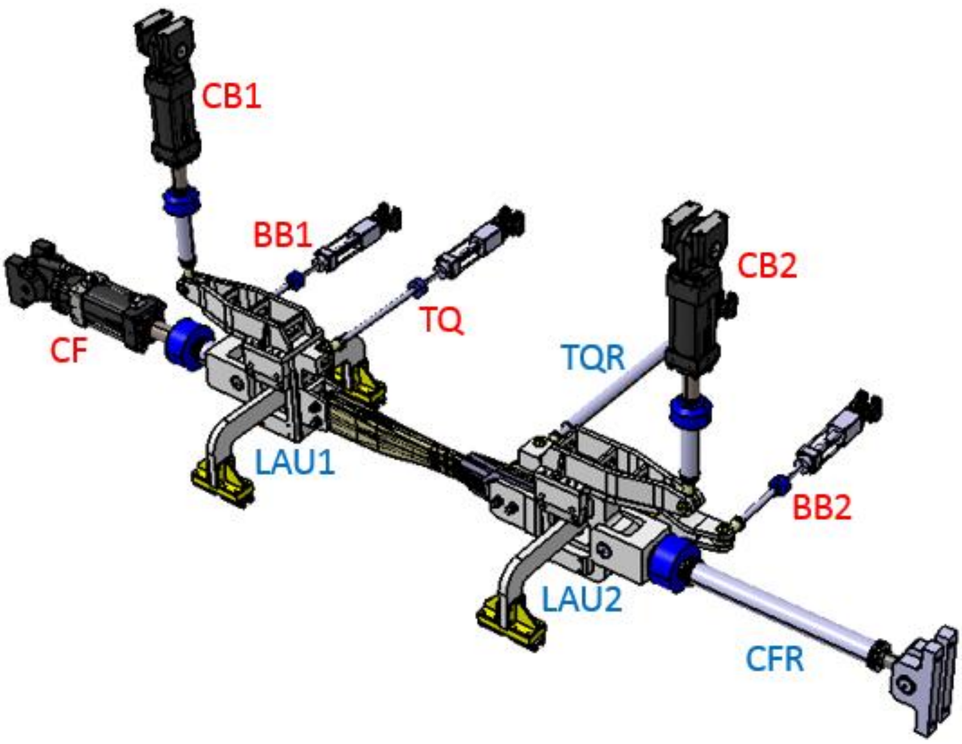

Figure 10: Load Introduction Structures and Naming

By knowing the locations of the forces and predetermined section loads on the test article, an excel sheet created. By defining actuator loads as variable input loads and section loads as constraints to the solver tool of excel, all the actuator loads were calculated.

However; after the commissioning of the helicopter blade test system, it is seen that the calculated actuator loads cannot create the expected section loads on the instrumented and calibrated helicopter blade. The reasons for this situation are the followings:

- The blade is not rigid under even the huge CF loading, so the rigidity assumption does not hold.
- Assumed load application and reaction point locations changed due to the highly elastic behavior of the test blade and the complex motions of the gimbal system during the loading.
- The motion of the actuators is also nonlinear due to the complex movement of the connection points on the cars.

Under these conditions, the need for accurate actuator loads is obvious. So, a study for an actuator load calculation tool development is started.

1.4 Reasons for Using a Dummy Component

For the development of actuator load calculation tool for a rotating beam like aerospace structure, it is not feasible to use an original helicopter blade due to the reasons listed below:

- Helicopter blade is expensive.
- Manufacturing time of a helicopter blade is high.
- The motion of the helicopter blade under even single axis loading is highly complex.
- Expected internal load calculations cannot be calculated with simple hand calculation methods.
- Finite element analysis process of a helicopter blade is troublesome.
- The final product is highly dependent on manufacturing conditions and environmental conditions.
- Finally sharing information about the original helicopter blade is commercially improper.

Under these circumstances, using a dummy component is more feasible than using an original helicopter blade. Thus, the development of actuator load calculation tool is carried out with a dummy component.

1.5 Layout of Thesis Work

After seeing the need for an actuator load calculation algorithm for multiaxial loading, a study is started in order to develop an actuator load calculation tool for helicopter blade structural test system.

A flowchart describing the structure of the thesis is shown in Figure 11. A dummy structural component is designed in CATIA environment and analyzed with using Patran and Nastran. Created finite element analysis model is used to both check the strength of the dummy component and to create an input file to dynamic analysis model. These steps are presented in CHAPTER 4.

Actuator load calculation algorithm generation steps are described in CHAPTER 5. A dynamic analysis model of the helicopter blade structural test system is conducted using MSC Adams software. The model is used to find the strain data on the dummy component using the ADAMS Flex and Durability modules. Calibration dynamic analysis model is created for the calculation of calibration coefficients of the dummy component. By using calibration coefficients and strain data found from dynamic analysis model of the test setup, section loads on the dummy component are calculated.

A multiaxial test on the dummy component is conducted to verify the generated algorithm and explained in CHAPTER 6. A dummy component is manufactured, and is wired with strain gages, after which calibration and crosstalk compensation operations are accomplished, and the section loads on the dummy component are measured from the multiaxial test. Using measurements of six strain bridges, chord bending, beam bending, torque, and centrifugal force, on two different sections are calculated. The developed methodology is validated by executing a multiaxial test on the dummy component with a combined loading of chord bending, beam bending, torsion, and centrifugal force loading. Found section loads from the test and estimated section loads using generated algorithm are compared to verify the actuator load calculation tool for multiaxial test system of a rotating beam like aerostructure.

Finally, conclusions of the study and the future work for this study are presented in CHAPTER 7.

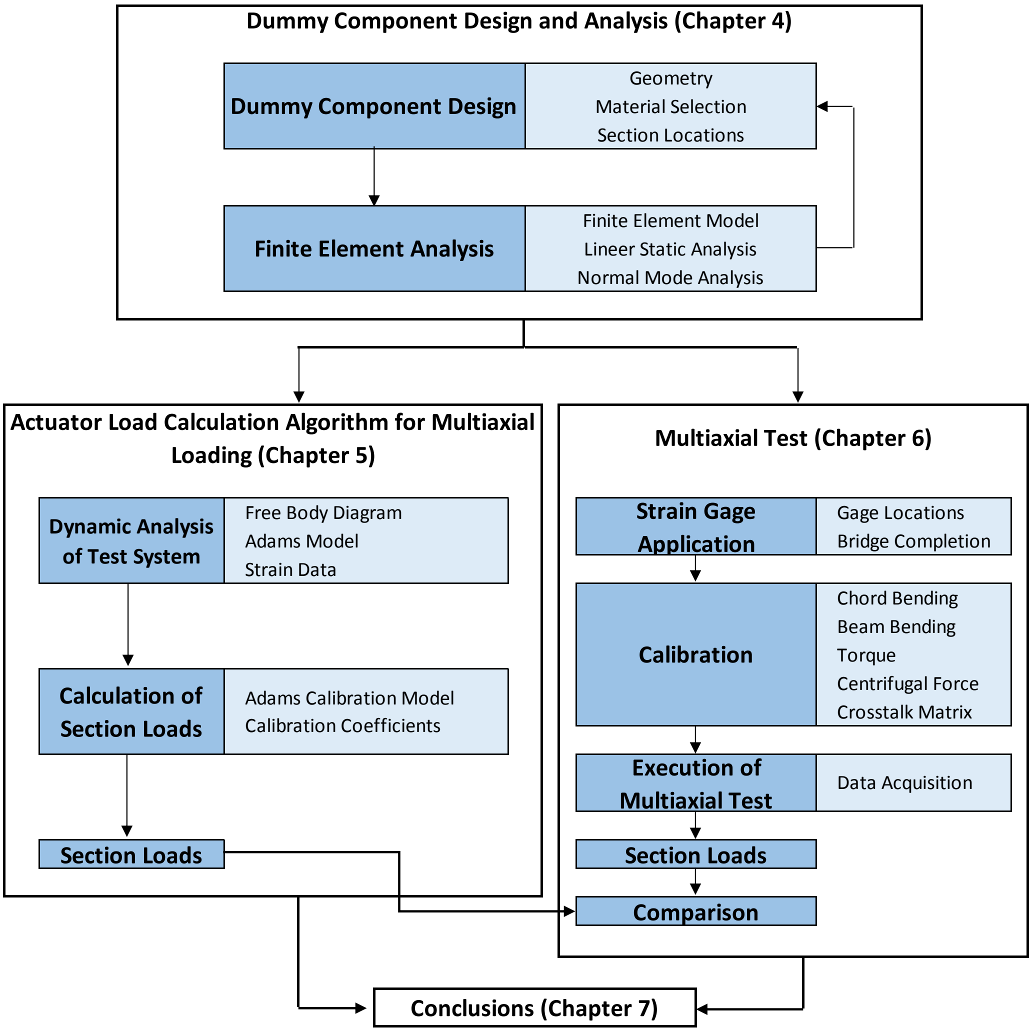

Figure 11: Flowchart of the Methodology for Actuator Load Calculation Tool and Verification with Multiaxial Testing

CHAPTER 2

LITERATURE SURVEY

Literature survey was conducted on previous helicopter blade test system work and previous applications of MSC Adams in similar processes. Brief information is given about helicopter blade structural test systems in order of increasing complexity. MSC Adams, which is used for nonlinear dynamic analysis, and its application to some sample projects are summarised.

2.1 Helicopter Blade Structural Test Systems

Helicopter blade structural test systems have been used for design verification purposes for years. With the historical development of engineering, helicopter blade structural test systems and test methods also improved. Helicopter blade structural test systems are discussed in historical order.

Anusonti-Inthra and Liu [10] used a non-destructive procedure to measure the structural properties of the helicopter blade for verification of calculations. This non-destructive method is used to estimate mass distribution and stiffness of the rotor blade. Blade mass distribution is calculated by determining the total weight, CG location and mass moment of inertia of the blade. The used methods are simple. CG location is determined by putting the blade on a wedge and finding its balance point. The mass moment of inertia about the CG in pitch, lead-lag and flap directions is determined by connecting it on an oscillating platform in different configurations and measuring the period of the blade response under a known oscillatory torque as seen in Figure 12. The flap bending stiffness of the rotor blade is found by merely fixing the blade from the root and applying dead weight from the tip as seen in Figure 13. Flap bending, lead-lag bending, and torsional stiffness of the blade are also estimated by fixing the blade from the root and exciting it in the proper direction with the help of a shaker. While shaker excites the blade, tri-axial accelerometers on the blade measure the response, and a commercial software calculates its stiffness properties from the frequency response function of the blade. Illustration of the described test setup can be seen in Figure 14. Measured stiffness values are compared with the stiffness values calculated from finite element analysis, and the calculations are verified.

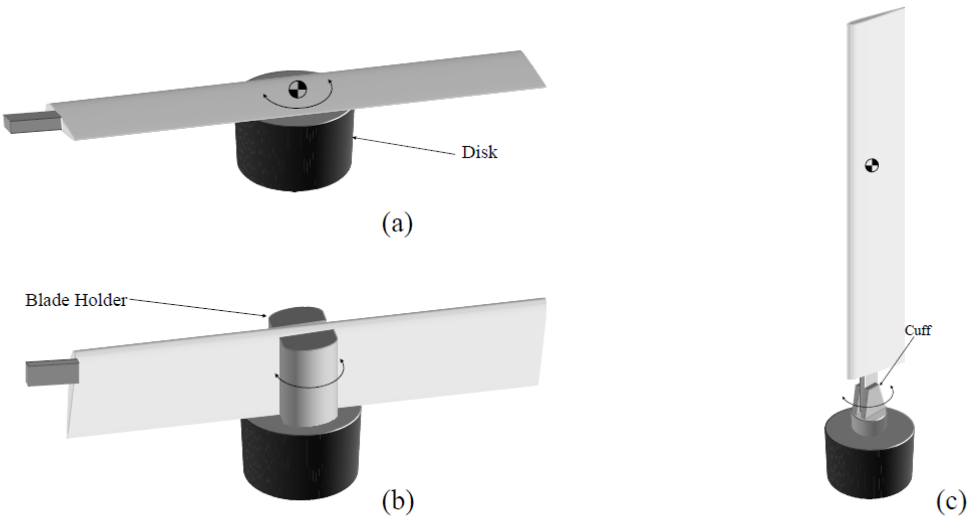

Figure 12: Mass Moment of Inertia Measurement System in (a) Lead-lag, (b) Flap and (c) Pitch Directions [10]

Figure 13: Flap Bending Stiffness Determination Test System [10]

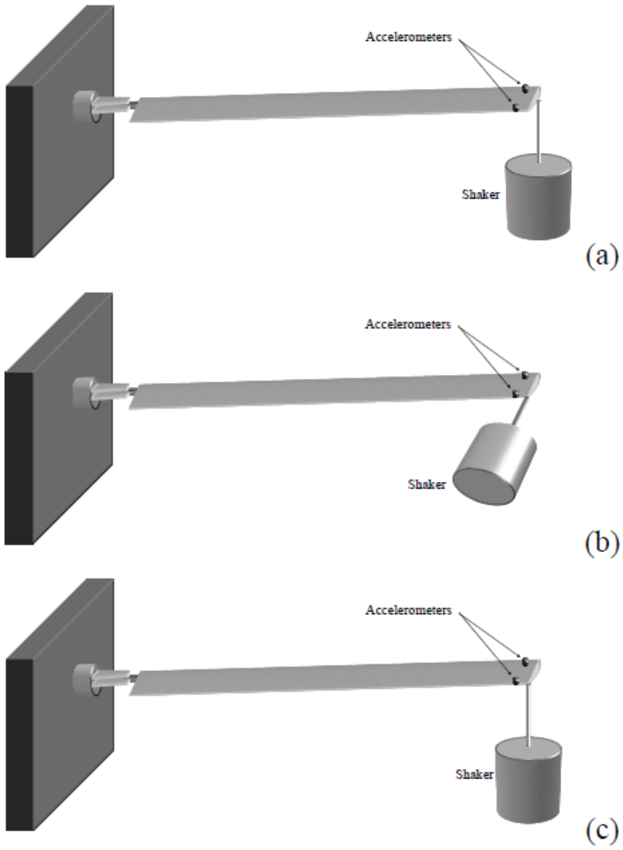

Figure 14: Test System for (a) Flap Bending, (b) Lead-lag Bending and (c) Torsional Stiffness Determination [10]

Shin [11] used a load frame to conduct a uniaxial static test on a rotor blade for verification of the designed rotor blade. An interface structure simulating the hub attachment is designed to conduct this test. Additionally, the tip of the rotor blade is modified as a metal fixture which is gripped to the moving side of the load frame. An equivalent load calculated from the maximum centrifugal force and the highest aerodynamic loading is applied to the test article. During the test, elongation of the test article and the load on it is monitored. After the test, by comparing the failure load and the estimated failure load, the verification of the designed rotor blade is completed.

Need for the multiaxial loading and the importance of fatigue are seen by Rasuo, and a system that can apply steady centrifugal force and vibratory chordwise bending, vibratory flapwise bending and vibratory torsional pitch loads are started to use. The main rotor blade of a light multipurpose helicopter and a tail rotor blade of a heavy transport helicopter tested in this system. The test article is connected from an attachment fitting that simulates hub of the helicopter while holding the blade at a specific angle. Holding at a constant angle ensures that an excitation arm can apply flapwise bending, chordwise bending and torsional pitch loads at the same time. These three vibratory loads are given with the help of a crank arm connected to an electric motor with a reduction gearbox. Vibratory speed controlled by changing the transmission ratio to hold the blade in resonance. Steady centrifugal force is given from the root of the blade with the help of a hydraulic actuator and pulley system with steel cables. Described the test system and the details of it can be seen in Figure 15.[12][13][14]

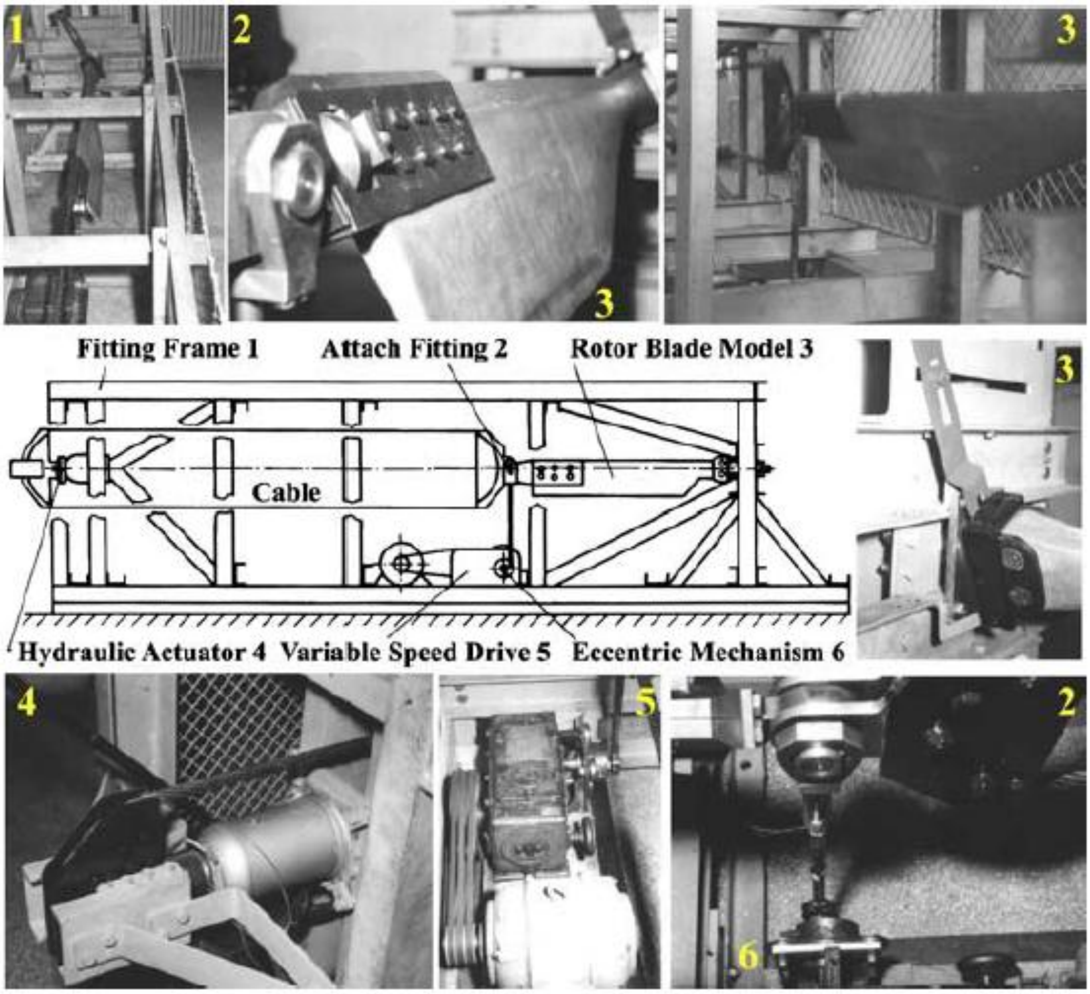

Figure 15: Helicopter Rotor Blade Test System [14]

A modern version of the Rasuo's test system used by the Korean Aerospace Research Institute [15] is shown in Figure 16, which is another version of resonant fatigue helicopter blade test system. The working principle of the test systems is the same. The test system can apply steady centrifugal force and vibratory flap moment and vibratory drag moment. This system introduces the steady centrifugal force from the root of the rotor blade with the help of a hydraulic actuator and cable system as seen on the top left of the figure. Additionally, vibratory flap moment and vibratory drag moment is applied with an electric motor and eccentric disk system. Moment ratio is set from the connection angle of the attachment lug. Applied centrifugal force is measured with a load cell. Flap and drag moments are measured by using full bridge strain gage circuits.

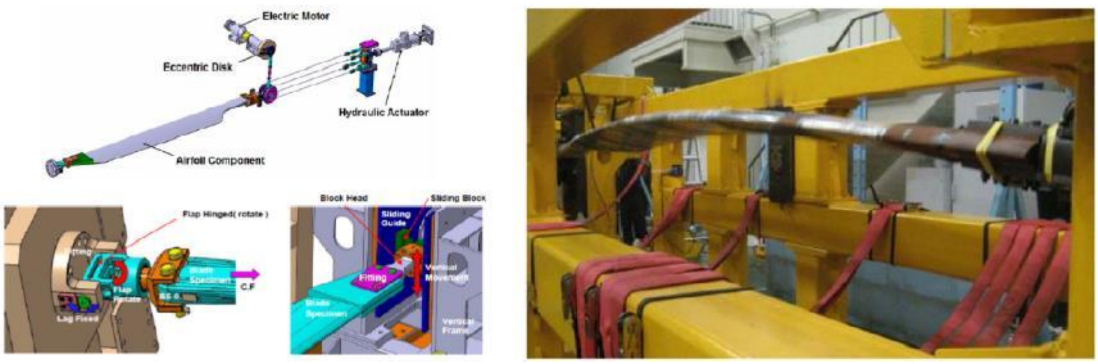

Figure 16: Resonant Fatigue Helicopter Rotor Blade Test System [15]: (left) schematic of the vibratory and centrifugal loading, (right) photograph of the test system with a blade.

Lischer [16] developed a test system that can apply steady centrifugal force, steady in-plane moment, alternating out-of-plane moment, alternating in-plane moment and alternating torque. Steady centrifugal force is applied from the tip of the blade with the help of a hydraulic actuator. To apply it from the tip of the blade a special fitting was designed. By giving a proper angle to the centrifugal force actuator, the steady in-plane moment is also achieved. An alternating in-plane moment was applied from the tip attachment's leading-edge side by a hydraulic actuator. It is applied by alternating the force in a proper frequency. Alternating out-of-plane moments and torque were given by vibrating the blade in resonance with the first mode out-of-plane bending frequency from the root end of the blade with the help of a hydraulic actuator. All moments were measured from calibrated strain gages mounted on the surface of the test rotor blade at six stations. The described test system can be seen in Figure 17.

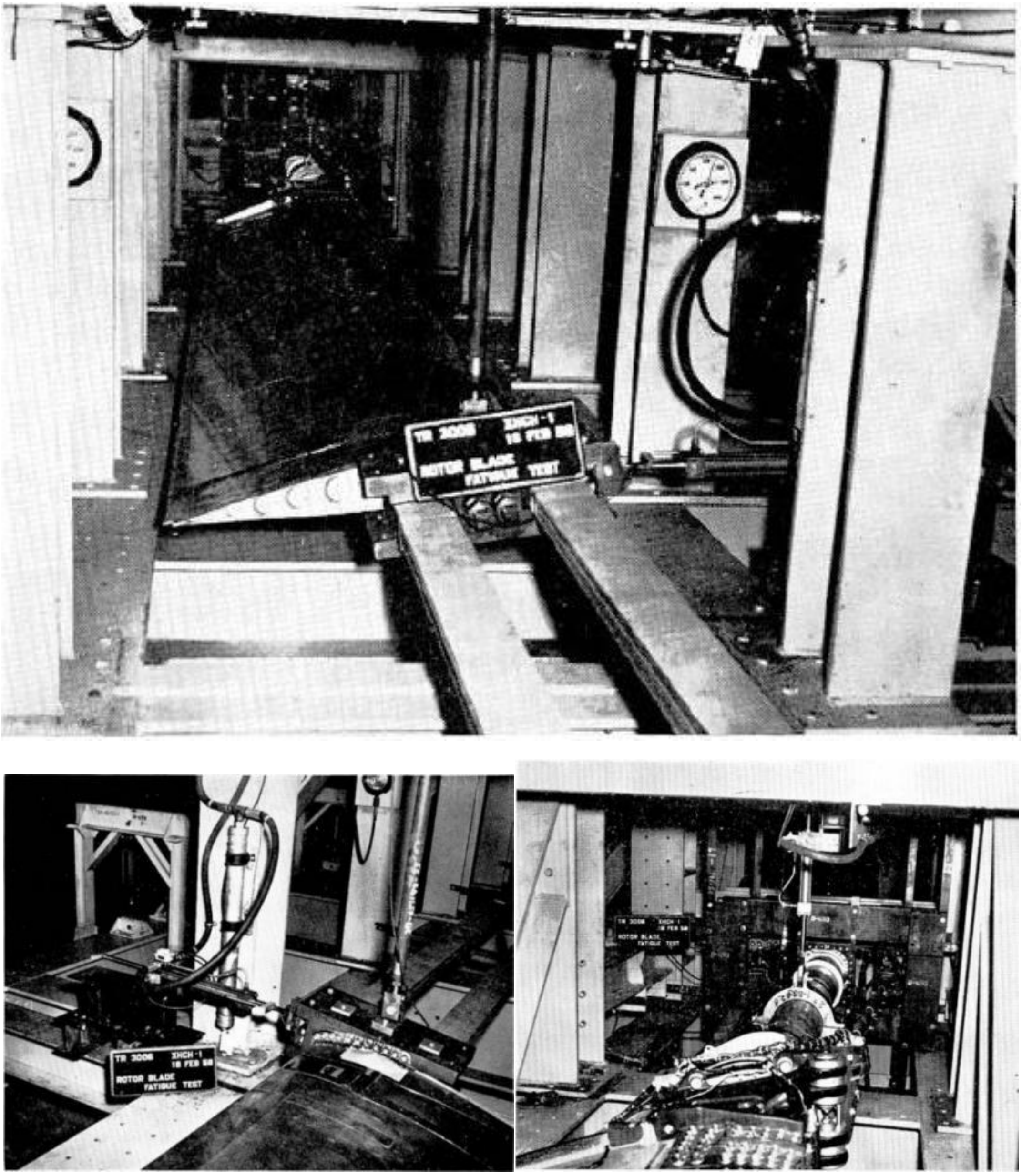

Figure 17: Large Helicopter Rotor Blade Fatigue Test System [16]

In the BERP IV (British Experimental Rotor Programme) project [17], the designed test system can apply alternating centrifugal, alternating bending and alternating torsion loads, independent of each other. Centrifugal force loading is applied from the root end of the test specimen with a hydraulic actuator. Torsion loads are applied from the specimen interface fitting again with the help of a hydraulic actuator. Flap and lag loads are applied from the tip of the test specimen with hydraulic actuators. Gimbal mechanism at the tip side of the test rig and reaction struts at proper points are used to keep the rotor blade in alignment to minimize cross-coupling between the different loads. Helicopter rotor blade structural test system designed for BERP IV project can be seen in Figure 18.

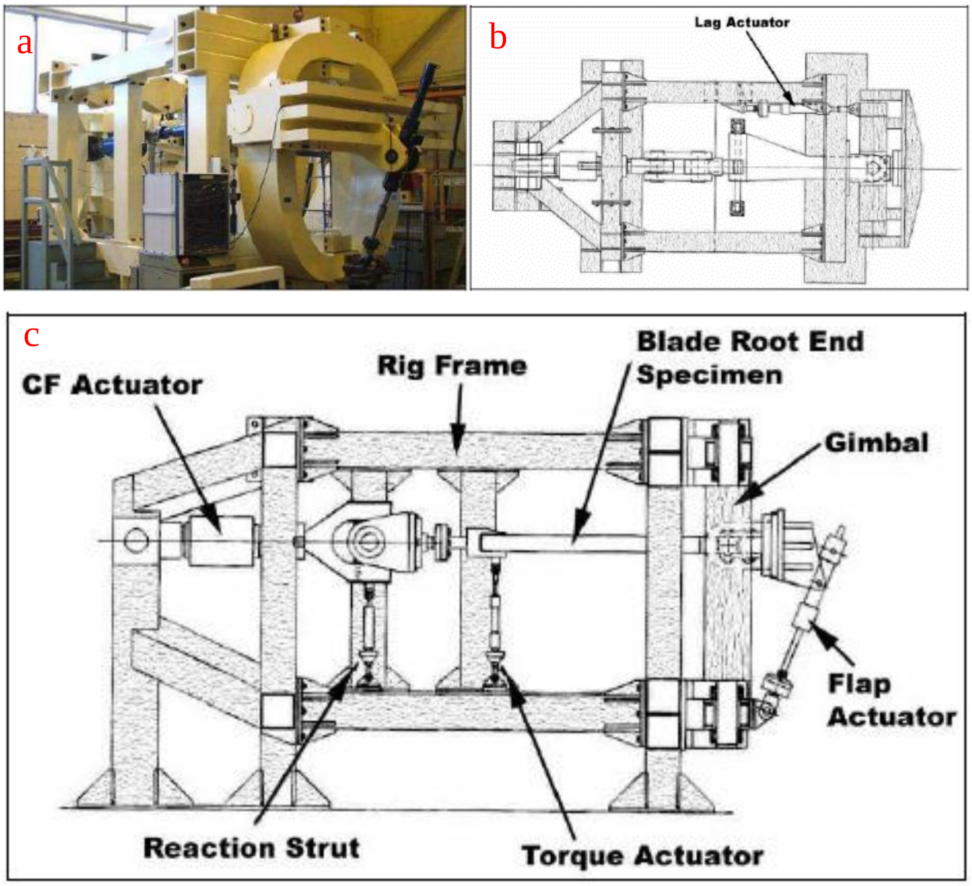

Figure 18: (a) BERP IV Helicopter Rotor Blade Structural Test System [17], showing (b) top view, and (c) side view.

2.2 MSC Adams Sample Projects

Adams is a multibody dynamic simulation software. Adams is used to observing the dynamics of moving parts and to see how loads and forces spread throughout mechanical systems. Two papers, among lots of papers, are selected to show sample works done in MSC Adams and summarized below.

Ewanochko [18] describes an integrated durability analysis process by using CAE software including Adams on a John Deere rotary cutter. A CAD model of the rotary cutter is modified for both a meshing software and Adams software. Meshed geometries are turned into MNF files by using ANSYS FEA software and then imported into Adams model. After the creation of a dynamic analysis model with flexible properties in Adams, which simulates a rotating drum test conditions, stress/time histories at every node were calculated. Available stress data imported into a fatigue tool to perform durability analysis and calculated results are imported into ANSYS for post-processing. After completing the post process, the approach can predict crack locations and the life of the rotary cutter. Details of the procedure and a sample photo of a rotary cutter can be seen in Figure 19.

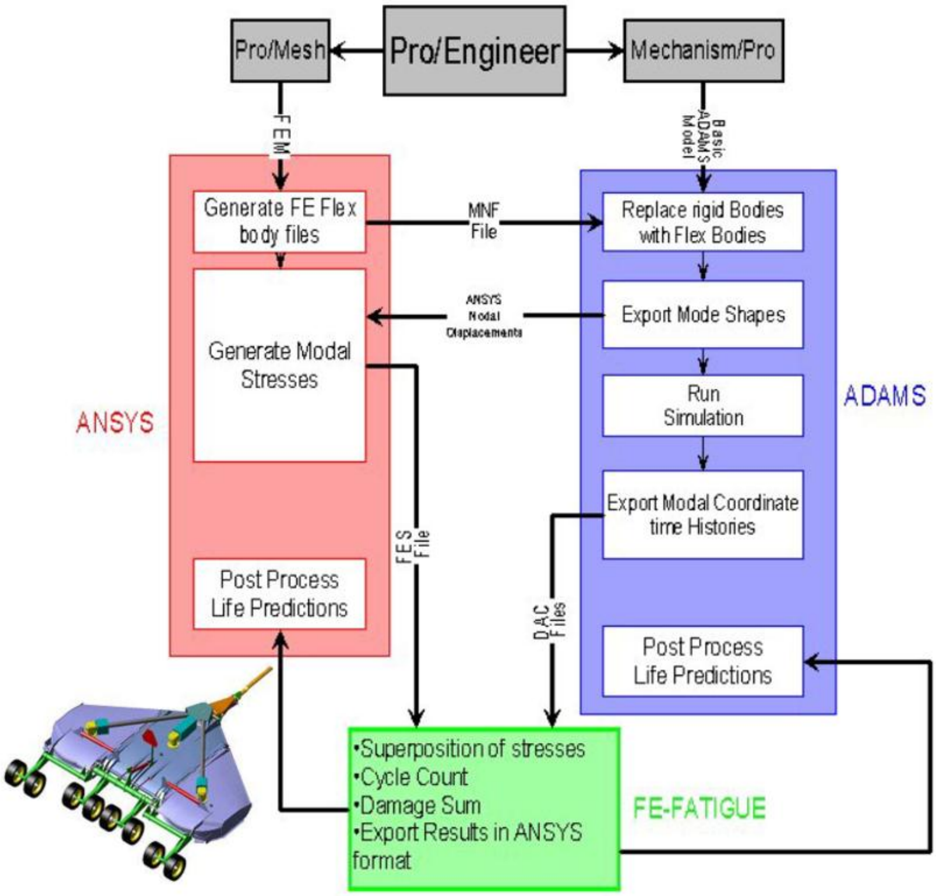

Figure 19: John Deere 15ft Rotary Cutter Integrated Durability Analysis Flowchart [18]

Gang [19] presents a method implementation to simulate the concrete pump truck boom system with flexible elements in MWorks software. Both rigid and flexible system models are investigated and compared in this paper. Beforehand, a rigid model created and simulated; which shows small and linear deformations on the boom system and takes too long to complete calculations. Then, MNF files created in Nastran were imported into a rigid model to turn it into a flexible model as imitating Adams Flex module's flex theory. The flexible model was also simulated. Finally, it is seen that the flexible model is more accurate and faster than the rigid model. Concrete pump truck and the details of the workflow of modeling and simulation can be seen in Figure 20.

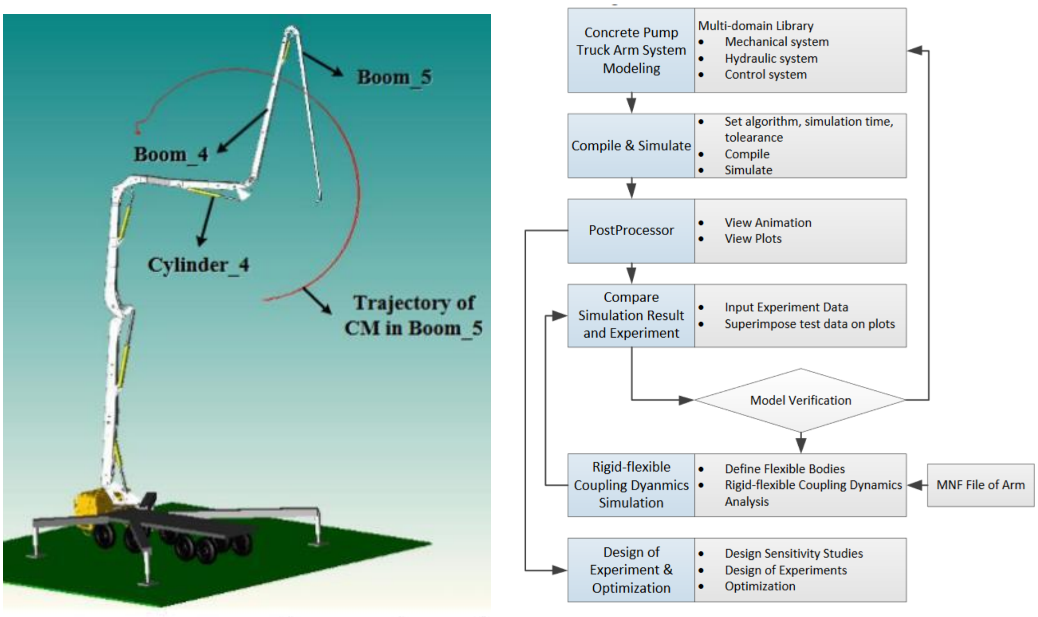

Figure 20: Concrete Pump Truck Boom System Simulation Workflow [19]

CHAPTER 3

METHOD

Methodology used in background of MSC Adams, strain gages, strain calibration and crosstalk phenomena are discussed in this section. Brief information is given on the background of MSC Adams and its plug-ins, which is used for nonlinear dynamic analysis. Strain gage theory and bridge creation procedures are discussed. Strain calibration and crosstalk effects on strain measurements are also discussed in this section. Methodology and the road map followed during the study is explained in this section.

3.1 Background of MSC Adams

Adams is multibody dynamic simulation software. Adams is the acronym for Automated Dynamic Analysis of Mechanical Systems. Adams is used to observing the dynamics of moving parts and to see how loads and forces spread throughout mechanical systems. [20] [21]

Adams runs nonlinear dynamic analysis solver which is very faster than FEA solver solutions; which is a great advantage against FE tools. Adams is designed for large-scale problems and suitable for high-performance computing environments. [21]

Adams is also a multidisciplinary software including motion, structures, actuation, and controls. Adams can integrate mechanical parts, hydraulics, electronics, pneumatics, and control systems. By integrating them, it optimizes product design and reduces spent time and cost. [21]

Adams has many plug-ins; however, Adams Flex and Durability modules are used in this work. So, these two modules are shortly described in this part.

Adams Flex module provides including component's flexibility characteristics. It is done by importing FEA-based flexible bodies into Adams environment. This operation gives user advantage of transforming a rigid part into an MNF-based flexible body. Additionally, it gives better structural conformity and better accuracy for load and displacement predictions. [21] [22]

Flex theory uses modal superposition, component mode synthesis (Craig-Bampton method) and mode shape orthonormalization to derive significantly simplified stiffness matrix and mass matrix, which can be used to improve the governing system of equations of motion. [23] [24]

Adams Durability module provides users for evaluating stress and strain data of components within mechanical systems. This module can export loads to FEA software for detailed stress analysis, and this makes FE analysis more accurate and faster. Additionally, it can be integrated with MSC Fatigue to make fatigue life predictions. [21] [22]

3.2 Strain Gages & Bridges

Strain gages and bridges is an extensive topic. One can give a tremendous amount of knowledge even it can easily be longer than this thesis study. This part is introduced short and direct knowledge for one have no idea about strain gages to understand topics covered during this work efficiently.

The strain gage is simply a resistance used for strain measurement. A strain gage converts force, pressure, weight, strain, and others into a change in electrical resistance. Different kinds of strain gages can be found in the market. However; the most common one is bonded metallic foil grid resistance strain gage. It is shown in Figure 21, and it includes general nomenclature about a strain gage. [25][26][27]

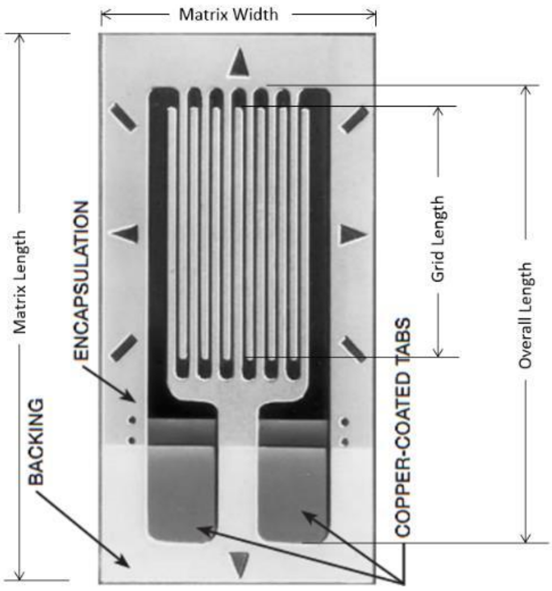

Figure 21: Strain Gage Nomenclature [27]

Strain gages use geometric dependence of the electrical conductance. Strain gages change resistance when they are stretched or compressed. This resistance change is measured using a Wheatstone bridge circuit. Wheatstone bridge, shown in Figure 22, is a circuit of four resistive arms with an input voltage, V_i, that is applied across the bridge. Wheatstone bridge consists of two parallel voltage divider circuit. The output of the Wheatstone bridge, V_o, is measured between the middle nodes of two voltage divider circuits. [25][28][29]

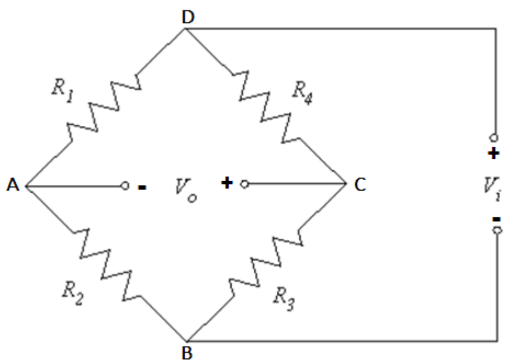

Figure 22: Wheatstone Bridge

V_o can be calculated as

$$V_o = V_C - V_A \tag{1}$$

$$V_o = V_i \left[\frac{R_3}{R_3 + R_4} - \frac{R_2}{R_1 + R_2}\right] \tag{2}$$

By applying strain on the Wheatstone bridge causing ΔR amount of change in corresponding resistance, the equation becomes

$$V_o = V_i \left[\frac{R_3 + \Delta R_3}{R_3 + \Delta R_3 + R_4 + \Delta R_4} - \frac{R_2 + \Delta R_2}{R_1 + \Delta R_1 + R_2 + \Delta R_2}\right] \tag{3}$$

By knowing two arms of the bridge balanced (R_1=R_2 and R_3=R_4) and ΔR<<R.

$$\frac{V_o}{V_i} = \left[\frac{\Delta R_1}{R_1} - \frac{\Delta R_2}{R_2} + \frac{\Delta R_3}{R_3} - \frac{\Delta R_4}{R_4}\right] \tag{4}$$

$$\frac{\Delta R}{R} = k\varepsilon \tag{5}$$

By inserting equation 5, where k is gage factor, into equation 4

$$\frac{V_o}{V_i} = \frac{k}{4}[\varepsilon_1 - \varepsilon_2 + \varepsilon_3 - \varepsilon_4] \tag{6}$$

Above equation is the strain and voltage relation equation.

Wheatstone bridge circuit always has four resistors. 1, 2 or 4 of them could be strain gauges. Largest output signal or voltage can be taken with four active strain gages. Modern amplifiers have special cards on them to complete missing resistors in the Wheatstone bridge circuit.

3.3 Calibration and Crosstalk

Calibration is the process of turning a strain-based measuring instrument output to a known reference input like force. Calibration is required to ensure that the force measurement meets the needs of the test requester and achieves the required degree of uncertainty. It is advised that to calibrate the system with deadweight applications to keep the uncertainty low. [30]

Multi-axis calibration is conducted twice per axis by considering positive and negative loading. Loads should be applied from predetermined points, and each position must be loaded and unloaded incrementally. These loading and unloading must be repeated to see the repeatability of the calibration results. Calibration curves of the strain-based measuring instrument should be found by following described steps. [31]

Strain gage load calibration is done widely to measure the in-flight loads of the aircraft and rotorcraft. Because, aerodynamic loads, inertia effects and maneuvering loads are all calculated theoretically, and these have to be verified in real case scenarios. [32]

Crosstalk is the effect of a calibration force applied along one axis on a different axis rather than desired, for example, an output on the y-axis transducer caused by applied force in the x-axis. It may be necessary to construct unique calibration algorithms to determine the magnitude of crosstalk effects. [30]

In theory, a pure loading in a measurement channel like F_x, F_y, F_z, M_x, M_y and M_z will not produce an output on any other measurement channel. Unfortunately, it does not happen in the real world. Efects of the pure loading on an unintended loading direction is called crosstalk, and it is generally between 1 and 5% for each channel. For one channel, it is a low value; however, by considering the remaining five channels, crosstalk could be high as 5% to 25%. [33]

Inverse matrix method can be used to compensate crosstalk mathematically. While applying a known external load in line with one axis during the calibration, the response of all channels should be recorded to use this method. This data is channel output O, and it is equal to the sensitivity (mV/V per unit load), K, times the applied load, F. By knowing these, all transfer functions can be written as;

$$
\begin{aligned}
O_{F_x} &= K_1 \cdot F_x \\
O_{F_y} &= K_7 \cdot F_x \\
O_{F_z} &= K_{13} \cdot F_x \\
O_{M_x} &= K_{19} \cdot F_x \\
O_{M_y} &= K_{25} \cdot F_x \\
O_{M_z} &= K_{31} \cdot F_x
\end{aligned} \tag{7}
$$

From equation 7, transfer functions, K, can be found by dividing the sensors outputs to the applied load. The same procedure should be done to calibrate the remaining five axes of the sensor. Using the superposition, they can be combined and written as follows;

$$
\begin{aligned}
O_{F_x} &= K_1 \cdot F_x + K_2 \cdot F_y + K_3 \cdot F_z + K_4 \cdot M_x + K_5 \cdot M_y + K_6 \cdot M_z \\
O_{F_y} &= K_7 \cdot F_x + K_8 \cdot F_y + K_9 \cdot F_z + K_{10} \cdot M_x + K_{11} \cdot M_y + K_{12} \cdot M_z \\
O_{F_z} &= K_{13} \cdot F_x + K_{14} \cdot F_y + K_{15} \cdot F_z + K_{16} \cdot M_x + K_{17} \cdot M_y + K_{18} \cdot M_z \\
O_{M_x} &= K_{19} \cdot F_x + K_{20} \cdot F_y + K_{21} \cdot F_z + K_{22} \cdot M_x + K_{23} \cdot M_y + K_{24} \cdot M_z \\
O_{M_y} &= K_{25} \cdot F_x + K_{26} \cdot F_y + K_{27} \cdot F_z + K_{28} \cdot M_x + K_{29} \cdot M_y + K_{30} \cdot M_z \\
O_{M_z} &= K_{31} \cdot F_x + K_{32} \cdot F_y + K_{33} \cdot F_z + K_{34} \cdot M_x + K_{35} \cdot M_y + K_{36} \cdot M_z
\end{aligned} \tag{8}
$$

With these six equations and six unknowns, it will be possible to solve for the unknown test loads. By applying the inverse matrix method, this equation set can be solved.

$$O = K \cdot F \tag{9}$$

By multiplying both sides of the equation with the inverse of “K,” the equation becomes;

$$F = K^{-1} \cdot O \tag{10}$$

By merely dividing applied loads to the outputs, crosstalk matrix K^{-1} can be found.

3.4 Road Map of the Study

Linear static or hand calculation methods do not meet the load calculation needs for actuator load calculation tool. Therefore, nonlinear calculation methods should be employed. Because, hand calculations with nonlinear methods are laborious and time-consuming, calculations are done with nonlinear dynamic analysis software. By investigating the literature and considering software in TAI, MSC Adams is selected.

An algorithm, as shown in Figure 23, for this purpose is developed and verified with a test executed in a real test system. Main points of the algorithm are as follows:

- A test component need is seen, and a dummy component that fits the test system is designed. To show that the dummy component withstands multiaxial test loads, FE analysis is carried out.

- Adams Flex and Adams Durability modules are used to increase the efficiency of the dynamic analysis model. The dummy component is then modeled with flex properties to use these tools. MNF file is needed to import flex properties into MSC Adams. MNF file is created by the finite element analysis software. By modifying the FE strength model, an FEM for MNF file creation is generated.
- MNF file is imported into the MSC Adams software, and movement mechanisms are modeled for the test system in a software environment.
- Created dynamic analysis model gives strain results on the node locations of meshed dummy blade. These strain values are turned into section loads. Calibration coefficients are required for these calculations. A calibration dynamic analysis model in Adams is created and under known pure loading calibration coefficients are detected.
- Section loads are calculated by using strain data and calibration coefficients found from Adams software.
- To verify the developed algorithm, results are compared with test results. Dummy blade is instrumented to collect strain data in predetermined regions. Collected strain gage data are calibrated to compare with section loads found in Adams.
- Dummy blade is calibrated in a calibration test system under known loads. During calibrations in order to eliminate the undesirable effects of pure loading on another loading, cross-talk compensation operations are also done.
- After completing all required preparations, the multiaxial test is executed. Section loads from the multiaxial test and Adams dynamic analysis are compared and discussed.

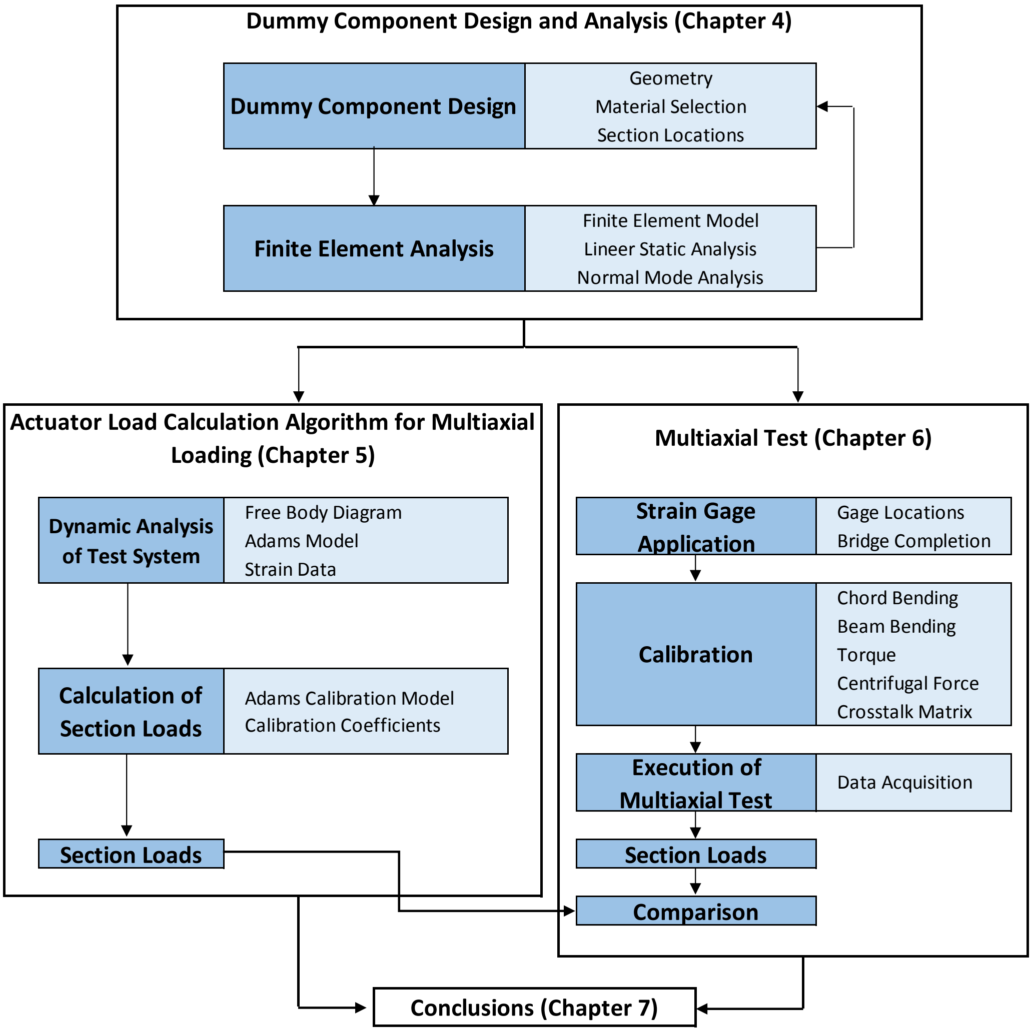

Figure 23: Flowchart of the Methodology for Actuator Load Calculation Tool and Verification with Multiaxial Testing

CHAPTER 4

DUMMY COMPONENT DESIGN AND ANALYSIS

4.1 Introduction

Design and structural analysis steps of dummy component are introduced in this chapter. The dummy component that will be used in the test system to simulate the helicopter blade, is designed, and its design phases are explained. The applicability of the dummy component is then checked using finite element analysis tools.

4.2 Design of the Dummy Component

Design steps of the dummy component which stands instead of an original helicopter component and make more straightforward to the tool creation are explained in this part.

4.2.1 Introduction

Due to the reasons mentioned in section 1.4, a dummy component designed for the development of actuator load calculation tool. In the following sections, firstly the geometric property determination of the dummy component is explained. During the geometric property determination section, selection procedure of the section locations; which are internal load calculation locations, is described. Finally, the material selection of the dummy component and properties of it are given.

4.2.2 Geometric Properties of the Dummy Component

Geometric properties of the dummy component are driven by the dimensional properties of the helicopter blade structural test system. Dimensions of the holes and the distances between them are dedicated according to the existing test system. With these criteria and the original test article's circumference length knowledge, width and length of the dummy component are defined approximately.

With this approximate dimensional information, to manufacture it as cheap as possible scrap yard of TAI is investigated. During the investigations, an aluminum part with dimensional properties of 1605x246x32 mm (Length x Width x Thickness) is found.

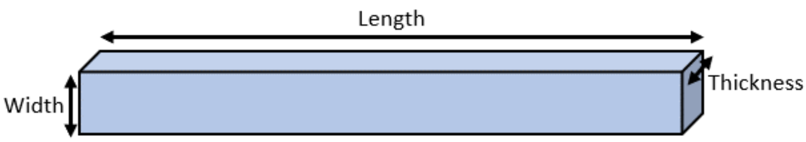

Figure 24: Schema of Dimension Terminology

By knowing the circumferential dimensions of the scrap material, the hole locations are defined on the dummy part, and the final geometric dimensions of the dummy component are decided as shown in Figure 25. Dummy Component is manufactured in TAI manufacturing facilities with the drawing created by this information.

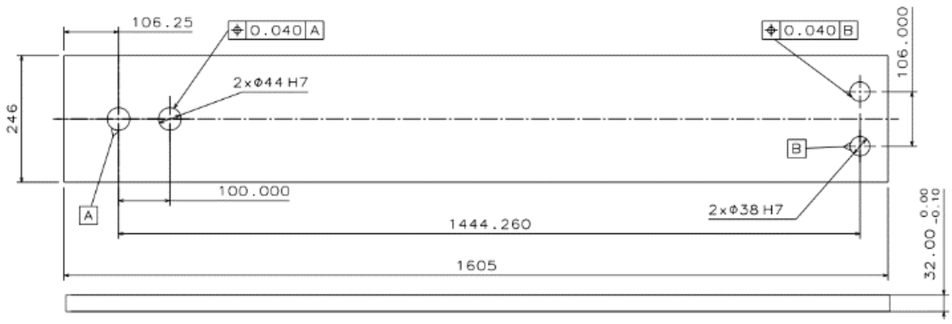

Figure 25: Drawing of Dummy Component (All dimensions are in mm.)

Due to the low thickness of the dummy component, there is a need for fillers to keep stationary the dummy article inside the lugs of the structural test system. Bushings are cut from the scrap tubes to fill these gaps. Bushings outer diameter and thickness is defined according to found scrap tube. The outer diameter of the bushings is 60 mm, and the thickness of the tube is 10 mm. The length of the bushings is defined by the gaps of the lugs. Holes are in the column formation is connected to the root clevis, and the internal gap of the root clevis is 115 mm, so the length of the root bushings is 42.50 mm. The other end of the dummy component is connected to the tip clevis, and the gap between the internal sides of clevis is 159.92 mm, so the length of the tip bushings is 64.96 mm. With this dimensional information, four bushings in each kind are manufactured in TAI facilities.

Figure 26: Photograph during the Manufacturing of Dummy Component

In total, a dummy component, four tip bushings, and four root bushings are manufactured in TAI facilities and the final products can be seen Figure 27.

Figure 27: Dummy Component and Bushings

4.2.2.1 Determination of Section Locations

Structural test of a helicopter blade is done to establish the predefined section loads defined by test requester. Test requesters are demanded to see distributed real-life loads on the test blade; however, this is not possible in a test environment. Loads are applied to reach the critical loads at critical sections to represent the real-life loads according to strength analyses done by the test requester. Test requesters generally demand more than two sections because of the complex loading on the test article. By considering this and making the tool development less complicated while keeping the cost low, the number of internal load control locations is set to two.

After deciding the number of internal load control locations, it is time to decide the locations of the sections. Two sections should have selected far from the whole effects and load application locations by considering Saint-Venant's Principle. Under these circumstances, stations are randomly defined as 400 mm and 900 mm far from the root end of the dummy component, which is the side closer to the column like hole formation. From now on, 400 mm distant station is named as STA400 or section 1, and 900 mm distant station is named as STA900 or section 2.

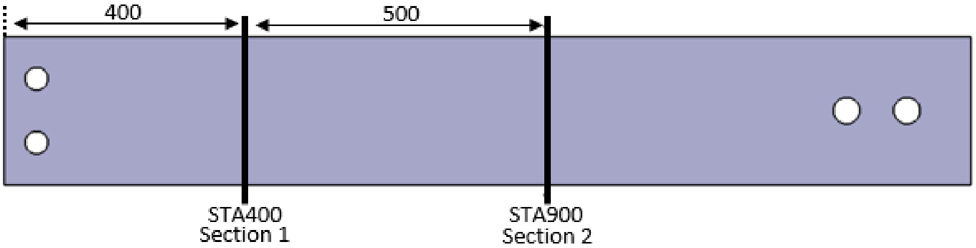

Figure 28: Representation of Section Locations on Dummy Component

4.2.3 Material Properties of the Dummy Component

An exceptional material selection is not made for the dummy component, because it is taken from the scrap yard according to its dimensional properties. It is aluminum alloy coded as Al2024 T351, and its properties are shown Table 1.

Table 1: Material Properties of Al2024 T351 [34]

Density, ρ:	2.70 [g/cm^3]
Young's Modulus, E:	70 [GPa]
Shear Modulus, G:	26 [GPa]
Poisson's Ratio, ν:	0.35
Tensile Yield Strength:	344.74 [MPa]
Tensile Ultimate Strength:	441.26 [MPa]

4.3 Finite Element Analysis of the Dummy Component

Finite element analysis of dummy component and its conformability investigated in this part.

4.3.1 Introduction

Finite element analysis of dummy component is done for two purposes. These are to see the dummy component strength against test conditions and to implement the dummy component properly into the dynamic analysis model of the helicopter blade test system.

First, the finite element model creation steps of the dummy component in MSC Patran software is described. Then, finite element model is solved with MSC Nastran software. Finally, found results are displayed and discussed.

4.3.2 Finite Element Modelling of the Dummy Component

Finite element model of the dummy component is created in MSC Patran software with two different loading and boundary conditions cases.

Before creating the base FEM of the dummy component, geometry preparations should be done. First, the CAD model of the dummy component imported into the Patran. Then; it is split up according to section and strain gage locations (Details of strain gage locations can be found in section 6.2.1) and hole locations. Splitting lines are intersected at strain gage locations to put there nodes to take strain data. Splitting of the hole locations is done to create a better mesh around the holes.

After completing the geometric preparations, the model is meshed with HEX8 hexahedral solid elements to get more accurate results. [35] Total number of HEX8 elements in the created model is 97716. Material properties of the dummy component are also integrated according to given data in Table 1. After conducting all these steps, FEM of the dummy component without BC and loads can be seen Figure 29.

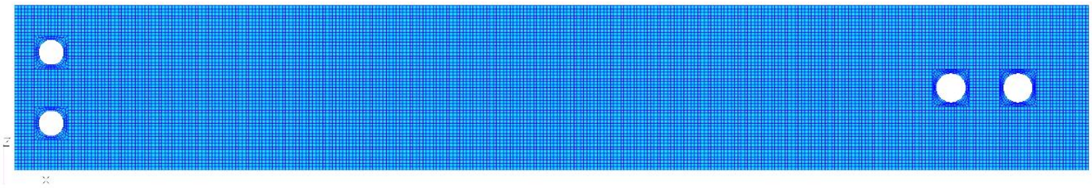

Figure 29: Finite Element Model of Dummy Blade without BC and Loads

Test loads and boundary conditions are applied to check the strength of the dummy component. FEM is held from the pin locations with the help of RBE2 elements. At the left side of the dummy component, the model is held in y and z translations and rotations. At the right side, the model is held in x translation and rotation. Actuator loads are applied from car joint location to middle hole regions with the help of RBE2 elements. Applied moments are calculated by merely carrying the actuator loads from their exact locations to the car joint locations. Applied loads can be seen in Table 2. Strength FEM of the Dummy Blade can be seen in Figure 30.

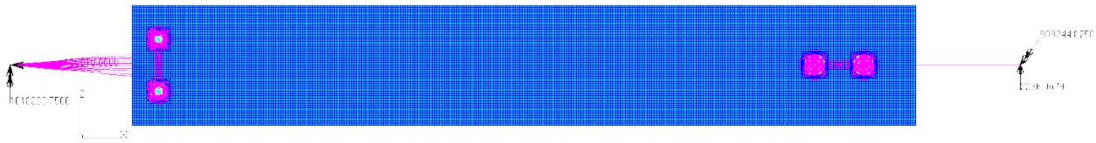

Figure 30: Strength FEM of the Dummy Blade

Table 2: Applied Loads on the Strength FEM of the Dummy Component

Actuator Name	**Force [N]**			**Moment [Nmm]**		
	x	**y**	**z**	**x**	**y**	**z**
Chord Bending 1	0	0	1000	0	720000	
Chord Bending 2	0	0	1000	0	-720000	0
Beam Bending 1	0	-1000	0	0	0	720000
Beam Bending 2	0	-1000	0	0	0	-720000
Torsion	0	-1000	0	-326000	0	270500
Centrifugal Force	-100000	0	0	0	0	0

MNF file should be created to create an input file to the dynamic analysis model of the test system. In this MNF file, connections point should be created as a node. So, the pin connection locations are modeled with RBE2 elements to put a node on every connection location. Free-free boundary conditions and no loading are demanded by the MSC Adams. So, the FEM, which can be seen in Figure 31, is created.

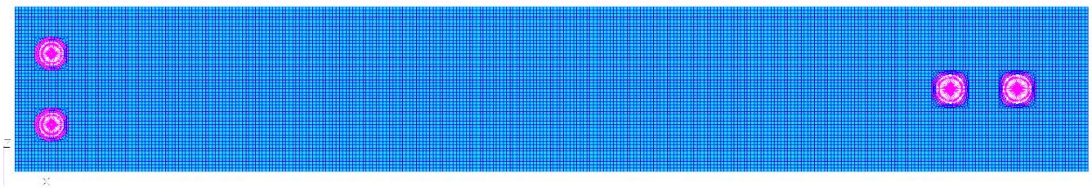

Figure 31: FEM of Dummy Blade with Free-Free BC

4.3.3 Finite Element Analysis Results of the Dummy Component

Created finite element models are solved by using MSC Nastran software. Found results are visualized by using MSC Patran software.

Strength FEM is solved by using linear static mode of MSC Nastran. Strength FEM of the dummy blade is done to show that dummy blade has enough strength to survive from test conditions. So, the found Von-Mises stress results of the strength FEM can be seen in Figure 32. Stress plot of the dummy component is visualized by ignoring the stress concentration around the holes. So, the primary object in the plot is dummy blade without hole regions, and the stress results on the right belong to this configuration. This elimination also represents a better stress distribution visualization. On the bottom left of the figure, the stress plot of the whole dummy blade can be seen. Von-Mises stress results on a deformed dummy blade without hole region can be seen on the upper right side of the figure.

According to finite element results, maximum Von-Mises stress is 158 MPa. By considering Al2024 T351, dummy blade material has a yield strength value of 344.74 MPa, the strength of the dummy blade is enough to survive under test conditions. With a simple reserve factor calculation, the dummy blade has an RF value of 2.18. The reason for using yield strength value for the calculation, plastic deformation of the dummy blade is not desirable. Because plastic deformation is an obstacle to the repeatability. Repeatability is desired to make lots of trials. Additionally, high RF value gives us a chance of ignoring modeling errors. In the light of these results, dummy blade can withstand the test conditions even under unexpected situations.

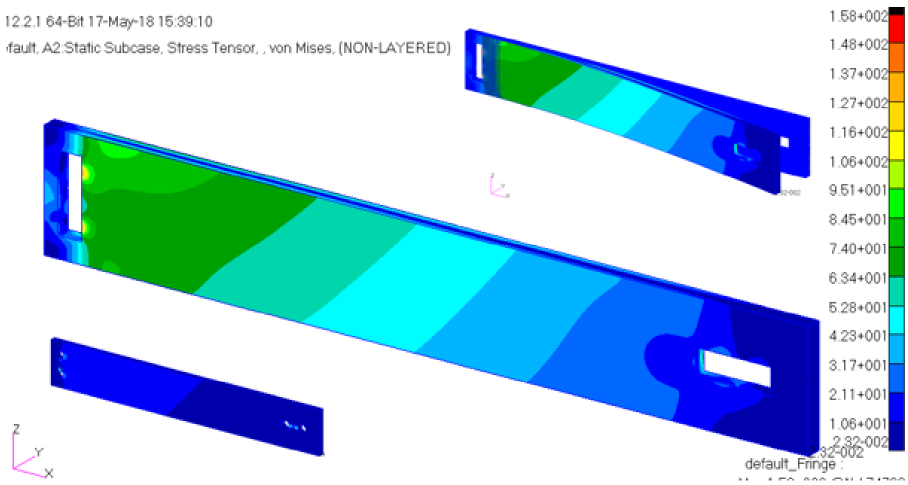

Figure 32: Von-Mises Stress Plot of the Strength FEM of the Dummy Blade

Displacement results of the dummy blade found by FEA of the Strength FEM can be seen in Figure 33. In the main view, displacement results are shown on the undeformed dummy blade and on the upper right, displacement results are shown on the deformed dummy blade. Maximum displacement value is 73.2 mm; which is a high value. This value is also proof of complex motions seen in the test system as mentioned in section 1.3.

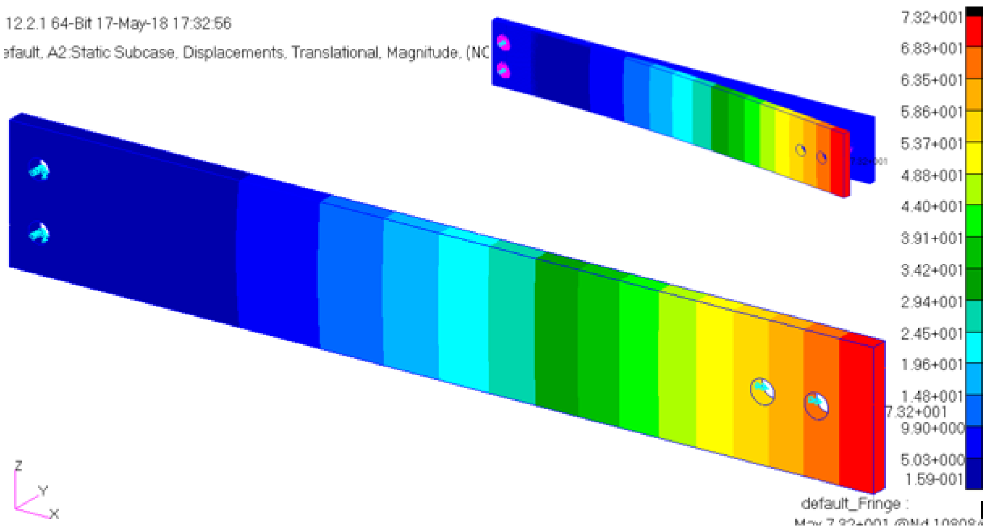

Figure 33: Displacement Plot of the Strength FEM of the Dummy Blade

FEM with the free-free BC is solved by using normal modes mode of MSC Nastran. The primary purpose of normal modes analysis is creating MNF file. MNF file is created beside the natural frequencies of the dummy blade are found. First three mode shapes can be seen in Figure 34.

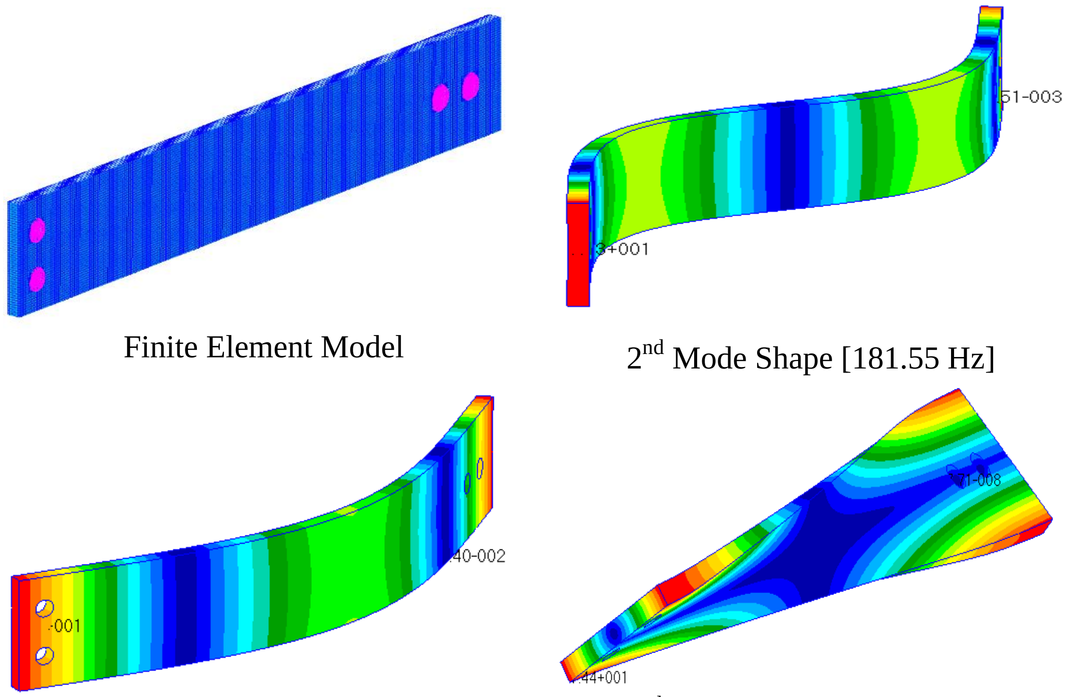

Finite Element Model

2nd Mode Shape [181.55 Hz]

1st Mode Shape [65.95 Hz]

3rd Mode Shape [250.85 Hz]

Figure 34: Finite Element Normal Modes Analysis Results

CHAPTER 5

ACTUATOR LOAD CALCULATION TOOL

5.1 Introduction

Generation steps of actuator load calculation tool are introduced in this chapter. Dynamic model of the test system is created around the dummy component with MSC Adams software using the information taken from the modal analysis of the dummy component. Calculated strain results from the dynamic analysis model of the test system are converted into section loads on the specific locations of the dummy component.

5.2 Dynamic Analysis of the Helicopter Blade Structural Test System

Dynamic analysis of the helicopter blade test system and model creation phases are investigated in this part.

5.2.1 Introduction

A kinematic model of the helicopter blade test system should be created to develop the actuator load calculation tool. Before starting the model creation, a free body diagram of the test system is drawn to understand the test system details. Then, a dynamic analysis model of the helicopter blade test system as close to reality as possible is created in MSC ADAMS environment. Finally; the model is solved by the solver of the software, and the calculated strain results on the dummy component; which will be converted into section loads; are investigated.

5.2.2 Free Body Diagram of the Test System

Before creating the dynamic analysis model of the test system, to simplify the test system, it is decided that drawing a free body diagram of the test system.

To clean up the CAD model of the test system, unrequired parts of the test system is hidden. These unrequired parts are support structures, counterbalance system, and interface parts, which are connecting actuators and cars to the support structure. After completing the hiding of unnecessary parts, obtained CAD model can be seen in Figure 35.

After simplifying the CAD model, there is still complicated members in the loading system, which are load application units. Load application unit is also simplified around the central joint by preserving the load paths of applied loads and reaction forces. Dummy component connection points on the load application units are clarified as midpoints of the two pins on both sides. Without changing the application points, actuator and constraints forces are drawn on the simplified load application units. By following these policies, drawn free body diagram of the helicopter blade structural test system can be seen in Figure 36.

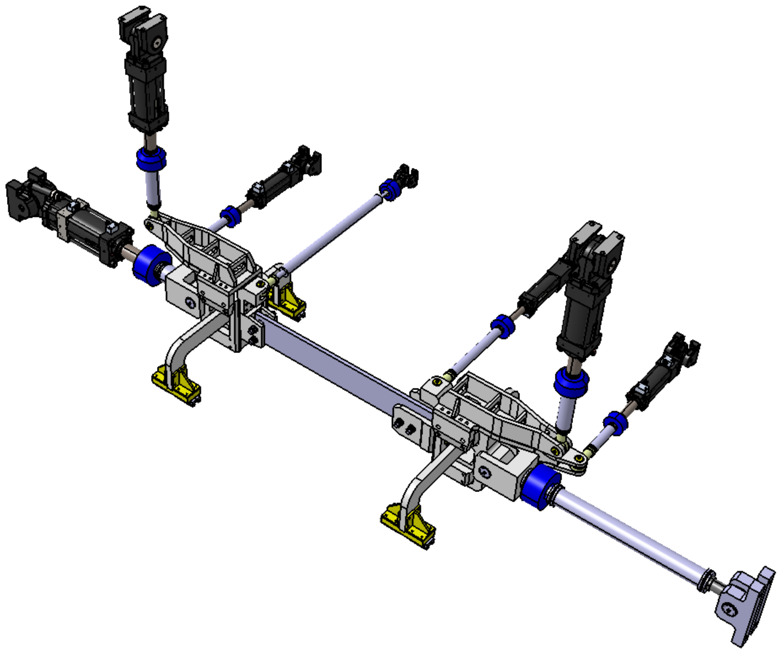

Figure 35: Loading System of the Helicopter Blade Test System

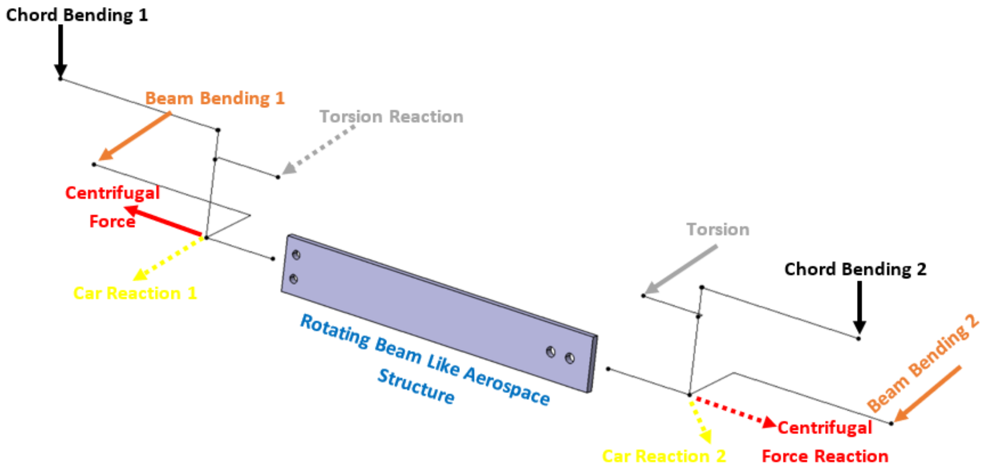

Figure 36: Free Body Diagram of the Test System

5.2.3 ADAMS Dynamic Analysis Model of the Test System

ADAMS dynamic analysis model of the test system as close to reality as possible is created. Model is created around the MNF file created from the FEM of the dummy component.

Section loads desired to applied on the dummy blade; chord bending, beam bending, torque, and centrifugal force; are applied with external loads throughout gimbal like load application units standing both right and left of the dummy component. Gimbal structures are centered between the cars moving linear on rails. External loads are applied from dedicated points on the load application units by simulating the hydraulic cylinders.

Crawl, walk, run philosophy is used during the model creation process.

After completing the import process of all solid geometries in the model, by removing all connections between the dummy blade and load application units, kinematic motion capabilities of load application units are investigated.

The basic kinematic model is created by using solid geometries for all the components in the model, frictionless joints for all the constraints and motion elements to simulate load application units.

After investigating all components and elements are moving in proper kinematic relation, the kinematic model is converted into a dynamic model step by step.

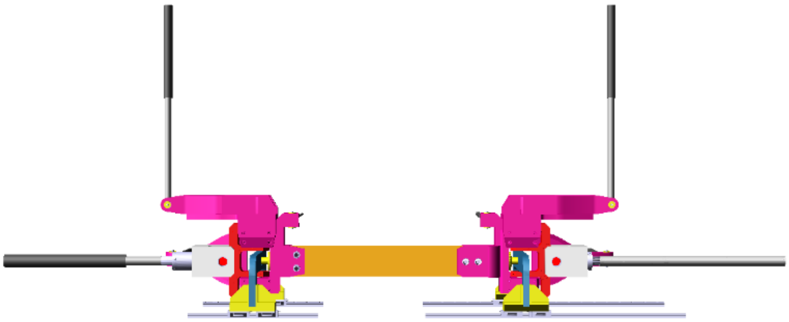

Figure 37: Front View of Dynamic Analysis Model

To reach the final dynamic analysis model in MSC Adams; firstly, the connection between the dummy blade and load application units are established. Necessary parts are turned into flex parts. Then, joint frictions are defined by considering dimensional and material properties. Finally, motion elements change to force elements. With these steps, the Adams dynamic analysis model of helicopter blade structural test system is finalized. Dynamic analysis model can be seen in Figure 37 and Figure 38.

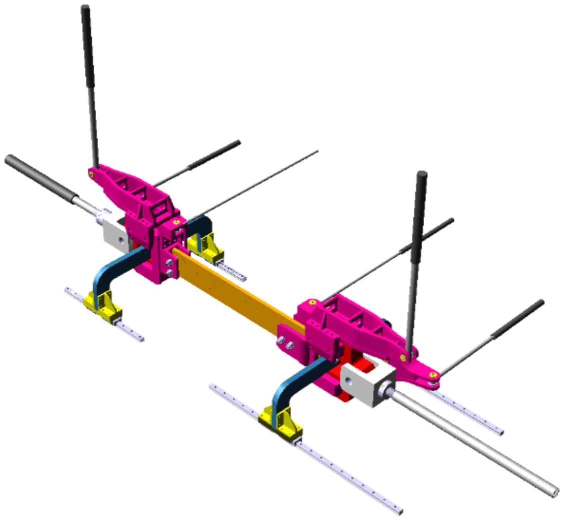

Figure 38: Isometric View of Dynamic Analysis Model

While creating dynamic analysis model, linear cars, which are positioned at the legs of load application units, are simulated by using inline, and orientation joint primitive elements, which only give motion permission in the global x-direction. In general, linear guides are modeled in MSC Adams with translational joints. However, in exceptional cases, like this model, to escape from redundant constraint phenomenon, using inline and orientation joint primitive elements combination instead of translational joint elements is a preferred method. These joint primitive elements can be seen in Figure 39.

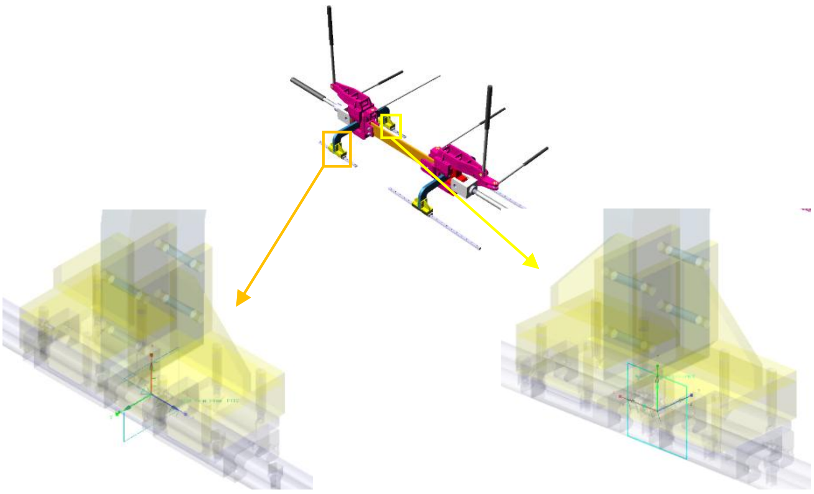

Figure 39: Inline Joint Primitive (Left) and Orientation Joint Primitive (Right)

Redundant constraint phenomenon occurs when one degree of freedom is controlled with more than one joint. In this condition, there is an extra equation for a degree of freedom, which is unnecessary to the solution of the model.

Cars moving on linear guides are self-lubricated; so, their friction values are negligibly low. Because of this, used connection elements are modeled as frictionless.

Load application unit is designed as two parts, which are pivoted on two points on the same vertical axis. These pivot points are modeled with revolute joints which only give motion permission in the global y-axis. The parts closer to the dummy blade are centered to interspace of linear guides. This part is connected to the legs of the load application unit with spherical joint element, which gives motion permission of rotation in 3 axes. All three joint elements are positioned parallel in the global y-axis and can be seen in Figure 40. This spherical joint element is the fulcrum point of a load application unit, and it is working under high and complex loading. Under these circumstances, joint friction would be affecting the results of the dynamic analysis model. So, friction effects are included in the spherical joint and two revolute joints.

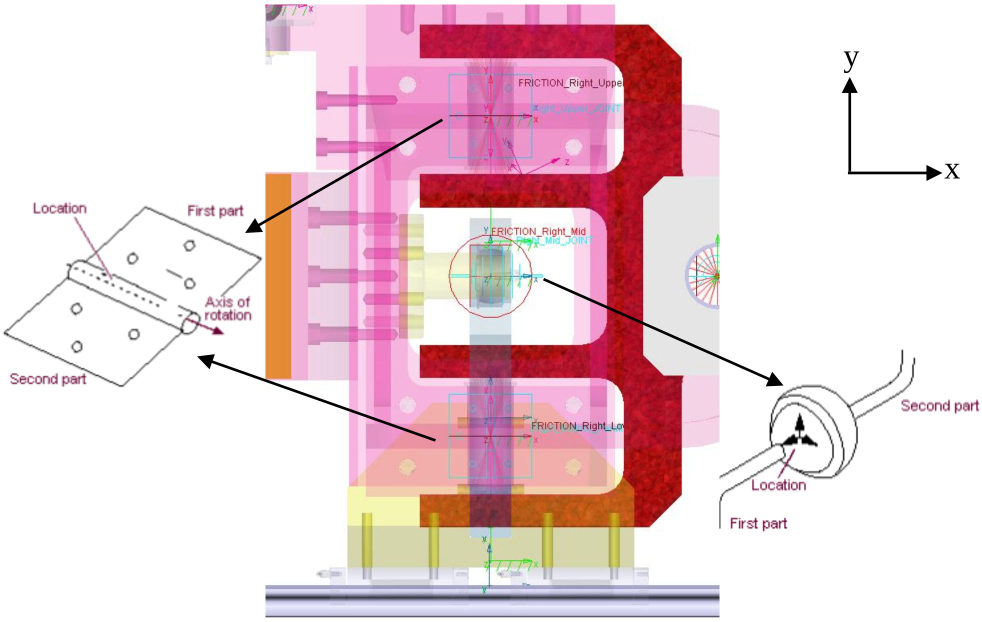

Figure 40: Central Joints on Load Application Unit

Modeling details of both load application units are the same except one location. That difference occurred due to the connection location geometry variation of the dummy blade. These joints are modeled with revolute joint elements which give motion permission in only global z-axis. These revolute joint elements are simulating dummy blade connection pins. While connecting the dummy blade to the test system, these pins are connected as close fit due to the low tolerance values. Because of these reasons, high and imponderable amount of preload is seen on the part, and it would be affecting the friction mechanisms on the joints. These unpredictable friction forces were not added to joints to not cause undesirable effects on the dynamic analysis model. So, the revolute joints are modeled as frictionless. These joints can be seen in Figure 41.

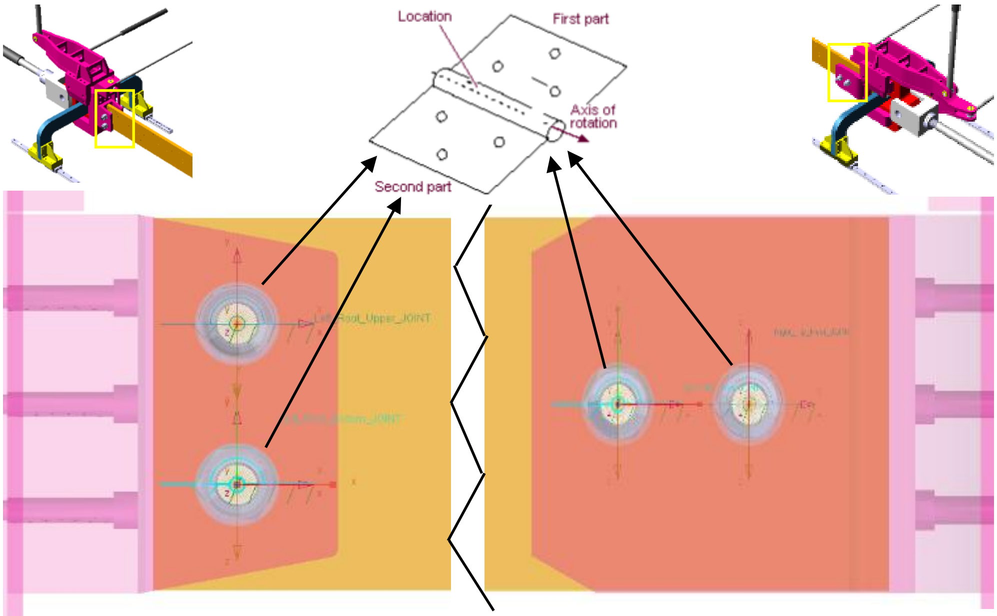

Figure 41: Revolute Joints on Dummy Component Connection Locations

Hydraulic actuators on the test system, which are consist of cylinders and pistons, are modeled with cylindrical geometries in Adams. Pistons are guided throughout the cylinders, and this is modeled with cylindrical joint elements. Cylindrical joint element permits one translational motion and rotational motion on the same axis. These guides are self-lubricated systems, so they have low friction values. Because of this, revolute joints are modeled without friction.

Actuators are connected to support structure from their cylinder side, in Adams ground, with spherical joints. Additionally, actuators are connected to the load application units from their piston side also with spherical joints. On both sides, by considering material properties, frictions are included in the Adams model. Actuator modeling details can be seen in Figure 42.

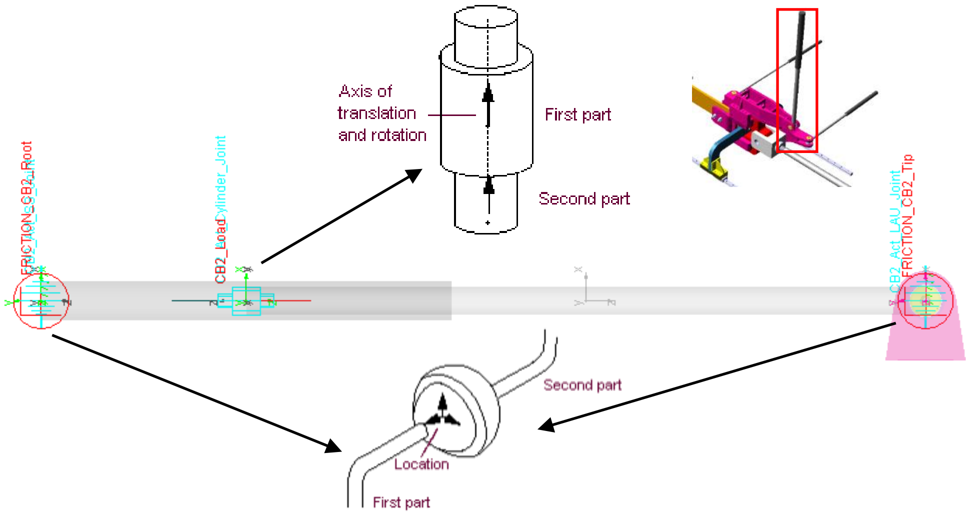

Figure 42: Actuator Modelling in Adams

Predetermined test loads, also given in Table 2, are applied from the cylinder side ends of the actuator pistons. Applied load values can be seen in Table 3. Positive loads mean actuator pistons are moving outside of the cylinders, and negative loads mean actuator pistons are moving inside of the cylinders.

Table 3: Actuator Loads Applied in Adams Model

Actuator Name	Force [N]
Chord Bending 1	1000
Chord Bending 2	1000
Beam Bending 1	1000
Beam Bending 2	1000
Torsion	-1000
Centrifugal Force	-100000

5.2.4 Results of the Dynamic Analysis Model

Dynamic analysis model of the helicopter blade structural test system described in section 5.2.3 is solved to get strain values by using Adams Durability and Flex modules.

Strain values at strain gage locations must be determined to get the strain values from the strain bridges. While creating FEM of the dummy blade, a node is created for every strain gage location as seen in Figure 43. Corresponding node numbers according to strain bridges can be found in Table 4. Details of the strain gages and bridges including positioning, gage type and gage sensing direction are explained in section 6.2.1.

By using strain gage numbers and strain gage sensing directions, strain plots of the node locations can be drawn in MSC Adams software. Strain values belong to the strain gages of the chord bending 1 bridge plot can be seen in Figure 44.

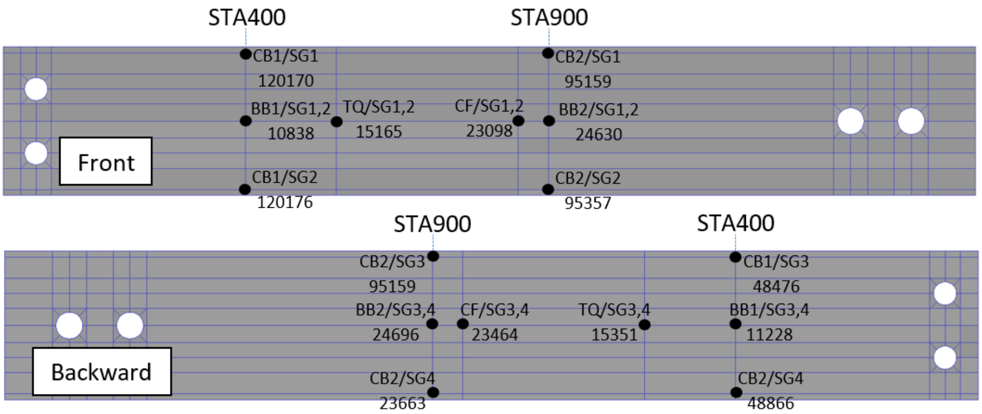

Figure 43: Strain Gage Node Locations

Table 4: Strain Gage Node Numbers

Bridge Name	Strain Gage Node #
Chord Bending 1	120170, 120176, 48476, 48866
Chord Bending 2	95159, 95357, 23465, 23663
Beam Bending 1	10838, 11228
Beam Bending 2	24630, 24696
Torsion	15165, 15351
Centrifugal Force	23098, 23464

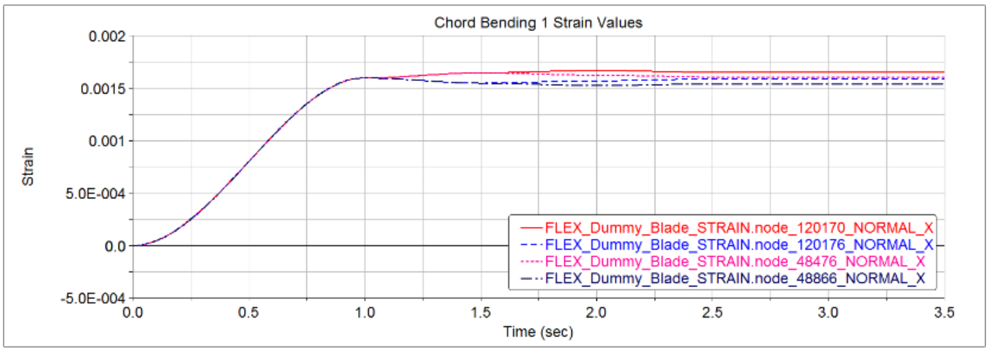

Figure 44: Strain Plot of Strain Gages belongs to Chord Bending 1 Bridge

Strain values of the strain bridges are calculated by using equation 6 in section 3.2. These calculations are done in MSC Adams environment by using its graphical calculation tools. First, the strain value of the first node corresponding to the first strain gage and third node corresponding to the third strain gage result is added. The same calculation is also done among strain results of second and fourth nodes. Sum of strain value of second and fourth nodes are subtracted from the sum of strain value of first and third nodes. Handheld value is scaled with 0.25, or in other words, it is divided by 4 and the found result is the strain value would be read from corresponding strain bridge. By following these steps, sample calculation done for chord bending 1 bridge can be seen in Figure 45.

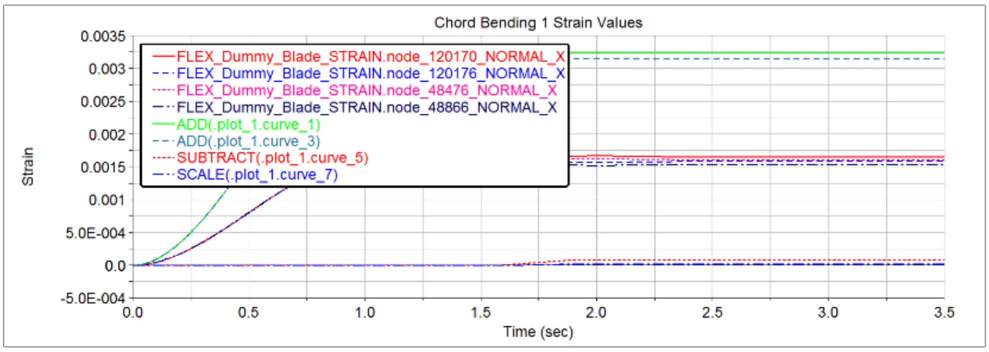

Figure 45: Strain Plot of Chord Bending 1 Bridge

Calculated strain results for all the bridges can be seen in Table 5. All calculations are following the procedure explained above.

Table 5: Strain Results of Strain Bridges

Bridge Name	**Strain [με]**
Chord Bending 1	26
Chord Bending 2	26
Beam Bending 1	-81
Beam Bending 2	-77
Torsion	65
Centrifugal Force	159

Exaggerated views of the simulation results found in Adams can be seen in Figure 46 and Figure 47.

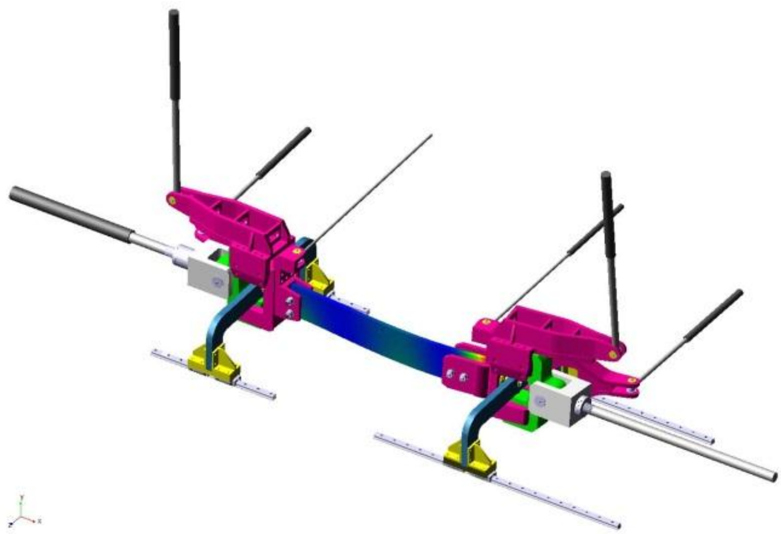

Figure 46: Simulation Result of Dynamic Analysis Model (Isometric View)

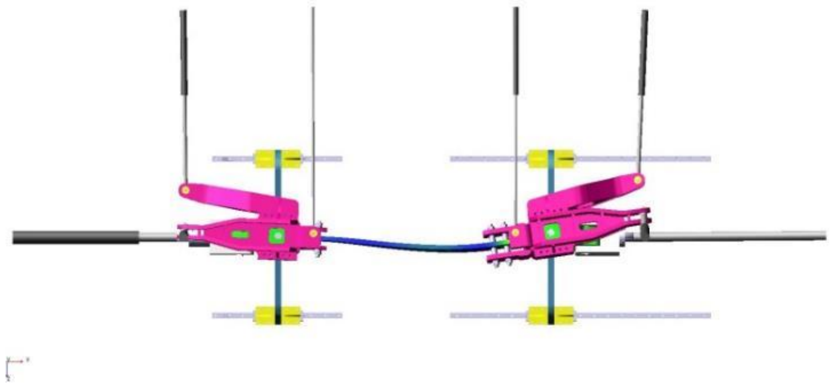

Figure 47: Simulation Result of Dynamic Analysis Model (Top View)

5.3 Calculation of the Section Loads on the Dummy Component

Calculation of the section loads on the dummy component from dynamic analysis results is described in this part.

5.3.1 Introduction

Strain data taken from Adams dynamic analysis model is used to calculate section loads of the dummy component. Load calibration of the dummy blade in Adams should be done to use that strain data. An Adams calibration dynamic analysis model is created, and strain data under known loading is found. With this information, calibration curves are drawn, and calibration coefficients are calculated. By multiplying found strain data from dynamic analysis model with calibration coefficients, section loads can be calculated.

5.3.2 ADAMS Calibration Dynamic Analysis Model

Adams calibration dynamic analysis model is created as close as possible to the real-world conditions. Built calibration dynamic analysis model can be seen in Figure 48. While creating calibration dynamic analysis model same procedures explained in section 5.2.3 are followed.

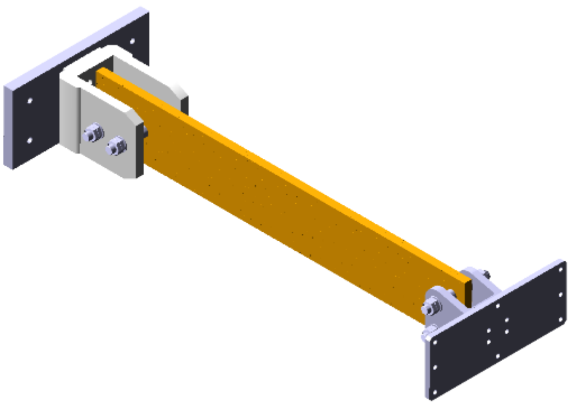

Figure 48: Adams Calibration Dynamic Analysis Model

At both sides of the dummy blade, pin and lug connection points are modeled with revolute joint elements which give motion permission in only rotation around pin central axis. At these joint elements, due to the geometric complexity of close fit connections, these joints are modeled as frictionless. Additionally, at the tip side lug in which pin holes are side by side, the model is held in all direction by using a fixed joint element on the outer surface of the lug. Details of the joint elements on calibration dynamic analysis model can be seen in Figure 49.

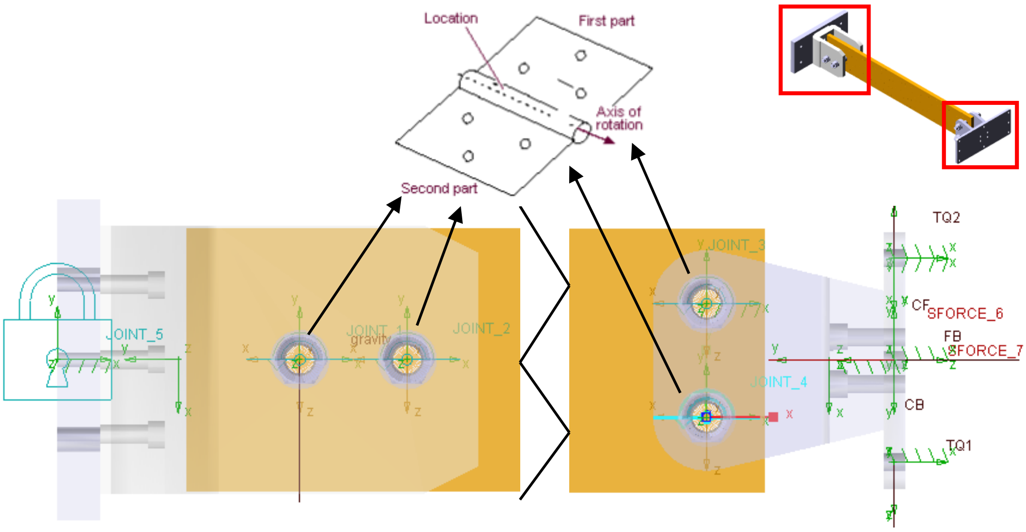

Figure 49: Joint Elements of Calibration Dynamic Analysis Model

At the root side of the dummy blade in which pin holes are in column-like formation, calibration loads are applied. Calibration loads for chord bending, beam bending, and torsion calibrations are applied step by step starting from 0 to 500 N by known locations on the load application lug. By changing the load directions, negative and positive calibration cases are done. Additionally, centrifugal force calibration is applied through the middle of the load application lug with an increment of 10000 N from 0 to 50000 N.

5.3.3 Results of the Calibration Dynamic Analysis Model

Calibration dynamic analysis model of the dummy component described in section 5.3.2 is solved to get strain values by using Adams Durability and Flex modules.

Strain values at strain gage locations should be determined to get the strain values from the strain bridges. By using strain gage numbers given in Table 4, strain plots of the node locations can be drawn in MSC Adams software. Strain values belong to strain gages of the chord bending bridges in both under positive and negative loading conditions can be seen in Figure 50.

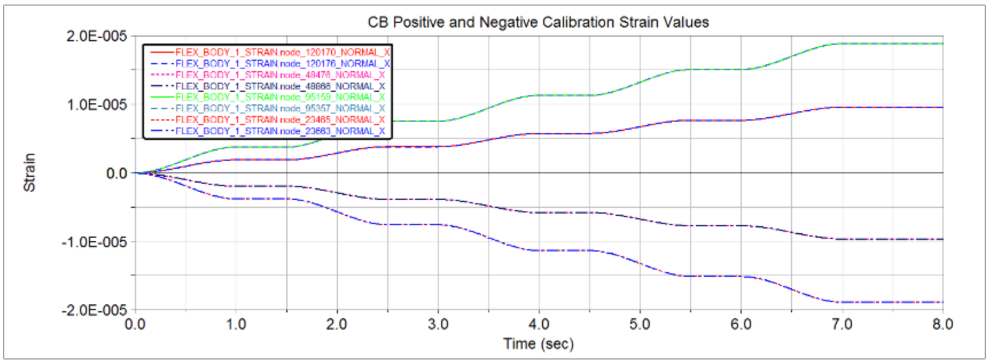

Figure 50: Strain Values of CB Gages on Positive & Negative Loading

Strain values of the strain bridges under calibration loading are calculated by using equation 6 in section 3.2. First, the strain value of the first node corresponding to the first strain gage and third node corresponding to the third strain gage result is added. The same calculation is also done among strain results of second and fourth nodes. Sum of strain value of second and fourth nodes are subtracted from the sum of strain value of first and third nodes. Handheld value is scaled with 0.25, or in other words, it is divided by 4 and the result found is the strain value would be read from corresponding strain bridge. Explained calculations are done in MSC Adams environment by using its graphical calculation tools. Found strain results are written in a table form as one column is loading and the other is the strain value in the Microsoft Excel software to find the calibration coefficients.

5.3.4 Calculation of the Calibration Coefficients

Strain values should be known under pure loading to calculate calibration coefficients. The known loads applied in Adams calibration dynamic analysis model are turned into moments by knowing the moment arms.

As described in section 5.2.4, strain results at gage locations are turned into strain results at strain bridges.

Load or moment vs. strain graph is drawn by knowing the strain results of strain bridge and corresponding applied loading. Calibration curves for chord bending 1, chord bending 2, beam bending 1, beam bending 2, torsion and centrifugal force are drawn with the information of applied loading and strain results. After drawing the graphs, trend lines are created with the help of Excel software. Finally, by displaying a trendline equation on the graph, calibration coefficients are found for each strain bridge. The slope value of the moment or load versus strain curve is the calibration coefficient. Moment vs. strain plot belongs to chord bending 1 strain bridge can be seen in Figure 51 as a sample calibration curve.

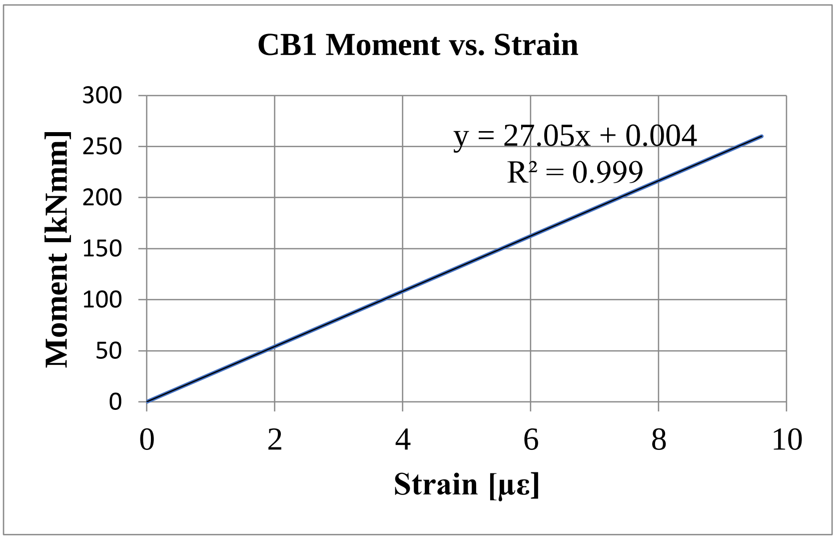

Figure 51: CB1 Moment vs. Strain Plot

In Adams, due to the perfect loading and theoretically ideal environment, positive and negative calibration coefficients are the same, and there is no crosstalk effect. So, there is only one calibration coefficient value for all bridges. Found calibration coefficients of all strain bridges are tabulated in Table 6.

Table 6: Calibration Coefficients

Bridge Name	**Calibration Coefficient**
Chord Bending 1	27.05 kNmm/με
Chord Bending 2	27.05 kNmm/με
Beam Bending 1	3.25 kNmm/με
Beam Bending 2	3.25 kNmm/με
Torsion	2.24 kNmm/με
Centrifugal Force	0.61 kN/με

5.3.5 Estimated Section Loads on the Dummy Component

In order to calculate section loads, section strain values and calibration coefficients are needed. All these variables are found in the preceding sections. By merely multiplying calibration coefficients with strain values, section loads can be found. Estimated section loads are tabulated in Table 7.

Table 7: Estimated Section Loads

Bridge Name	**Strain [με]**	**Calibration Coefficient**	**Section Load**
Chord Bending 1	26	27.05 kNmm/με	703 kNmm
Chord Bending 2	26	27.05 kNmm/με	703 kNmm
Beam Bending 1	-81	3.25 kNmm/με	-262 kNmm
Beam Bending 2	-77	3.25 kNmm/με	-250 kNmm
Torsion	65	2.24 kNmm/με	146 kNmm
Centrifugal Force	159	0.61 kN/με	96.97 kN

Above results are the outputs of the dynamic analysis model of the helicopter blade structural test system. Found results are illustrated on the section locations of the dummy component as in Figure 52. These results will be verified by executing multiaxial testing on a dummy component including chord bending, beam bending, torsion, and centrifugal loading.

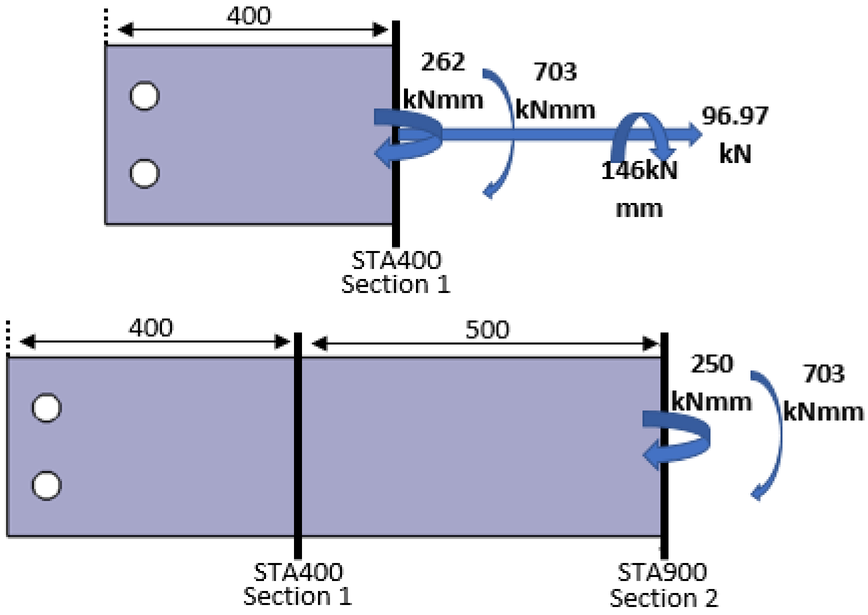

Figure 52: Illustration of Estimated Section Loads

CHAPTER 6

MULTIAXIAL TEST

6.1 Introduction

The multiaxial test is done merely to verify the actuator load calculation tool for a rotating beam like aerospace structure structural test system. The work done in the computer environment during the development phases of actuator load calculation tool is simulated in the real world.

First, strain bridges installation details on the dummy component will be explained. After explaining gage location selections and bridge completion procedures, load calibration of the dummy component in positive and negative chord bending, positive and negative beam bending, positive and negative torsion and positive centrifugal force calibrations are done. Then, the crosstalk matrix of the dummy component is calculated. Finally, the execution of the test is completed, and the results of the test are shared.

6.2 Strain Bridges on the Dummy Component

For calculating the section loads, two chord bending strain bridges and two beam bending strain bridges are installed on the two predetermined section locations. Additionally, a torsion bridge in one of the sections and a centrifugal force bridge on another section are installed on the dummy component. In total, six strain bridges are installed on the dummy component.

To increase voltage output, in other words, strain output, full bridge configuration with four strain gages in all the strain bridges are used. Beam bending bridges are constructed from four uniaxial gages. These gages are glued parallel to corresponding bending main strain directions. Highest possible strain output location of beam bending bridges is selected as midline of the dummy component. Because maximum beam bending displacement occurs at the midline of the dummy component Chord bending bridges are also constructed from four uniaxial gages. These gages are glued parallel to corresponding bending main strain directions. Highest possible strain output location of chord bending bridges is selected as close as possible to upper and lower end of the dummy component. Even tough, Maximum chord bending occurs at the upper and lower sides of the dummy component, strain gages are positioned on front and back surface, due to the lack of enough space and handling problems. V shape rosettes, including two gages with 45^{o} alignment, which is the internal angle between two legs, are used for the torsion bridges and glued parallel to expected highest torsional strain direction. For the centrifugal force bridge, T rosettes are used to eliminate bending strain effects on the centrifugal strains and one side of the T glued parallel to the centrifugal force direction.

Covers of the used strain gages can be seen in Figure 53. Type of the selected strain gages are determined considering the loading type and directions. All the properties of the used gages can be found from back covers. Additionally, gage factors of the used strain gages are tabulated in Table 8.

Figure 53: Covers of the Used Strain Gages

Table 8: Gage Factors of Used Strain Gages

Bridge Name	Gage Type	Gage Factor
Chord Bending 1	CEA-13-250UN-350	2.130
Chord Bending 2	CEA-13-250UN-350	2.130
Beam Bending 1	CEA-13-250UN-350	2.130
Beam Bending 2	CEA-13-250UN-350	2.130
Torsion	CEA-00-187UV-350	2.030
Centrifugal Force	CEA-00-125UT-350	2.075 2.090

Strain gage positioning and the bridge completion procedures are discussed in the following sections.

6.2.1 Locations of the Strain Gages

Strain gages should be located to possible maximum output locations. So, bending bridges should be located as far from the neutral axis to maximize bending outputs. In the same manner, torsion bridges should be located as far from the shear center of the structure and near to the neutral axis plane to maximize torsional output and minimize bending response. [36]

In the light of these variables, strain gage positions are determined as chord bending gages are near the upper and lower ends of the dummy blade, and beam bending, torsion, and centrifugal bridge gages are located into the middle of the upper and lower end of the dummy blade. Positioning diagram of the strain gages can be seen in Figure 54.

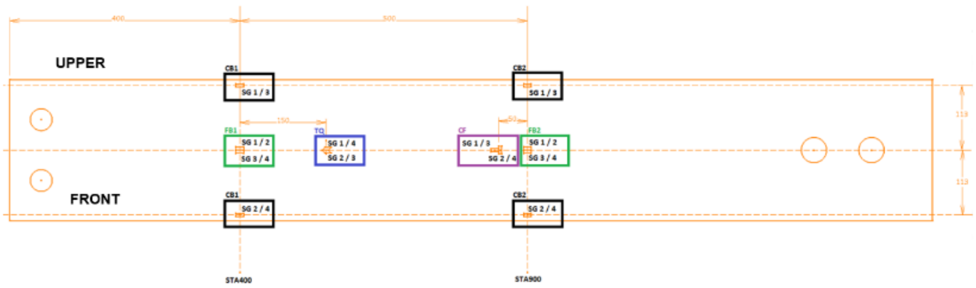

Figure 54: Positioning Diagram of the Strain Gages

Sample photos during the application of strain gages according to defined positioning can be seen in Figure 55.

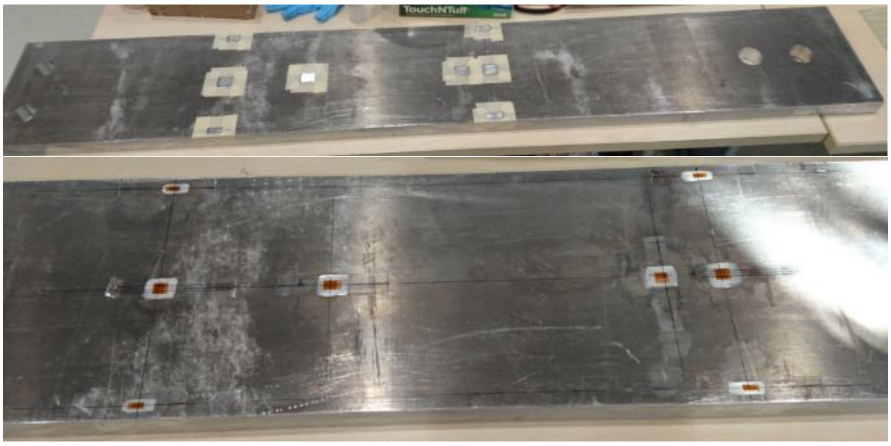

Figure 55: Sample Photos during Strain Gage Application

6.2.2 Strain Bridge Completion

After completing gluing part of the strain gage application, wiring of the strain gages should be done. Strain gages are named according to the Wheatstone bridge scheme given in Figure 22. By using a terminal corresponding to a, b, c and d points on the same plot, strain gages are turned into strain bridges by soldering the wires between taps on the gages and the taps on the terminals.

Numbering of the gages in the strain bridges are done to achieve maximum strain output. Gage one and three of beam bending bridges are put on the positive elongation side of the dummy component and gage two and four put on the opposite side of dummy component. Gage one and three of chord bending bridges are also put on the positive elongation side of the dummy component and gage two and four put on the opposite side of dummy component. Strain bridge completion diagram for chord bending and beam bending bridges can be seen in Figure 56.

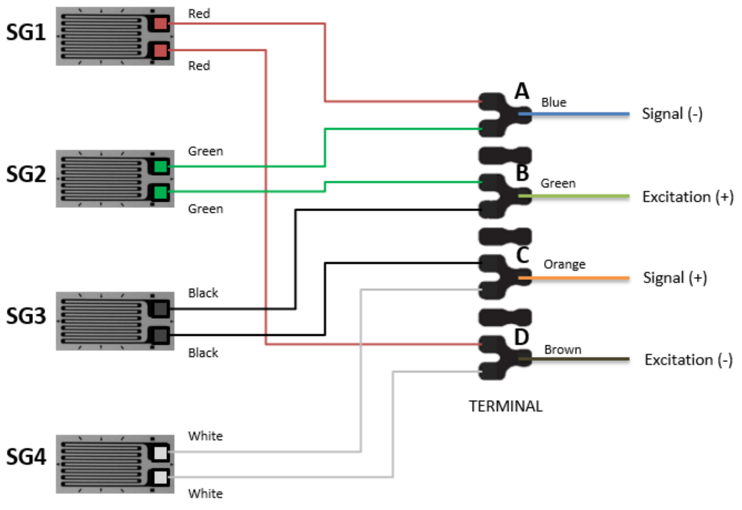

Figure 56: Chord & Beam Bending Bridges Completion Diagram

Torsion bridge completion is done by putting gage one and three in the positive elongation side of the dummy component, which is the upper half portion of the dummy component. Gage two and four are glued to negative torsion elongation side of the dummy component. Strain bridge completion diagram for torsion bridge can be seen in Figure 57.

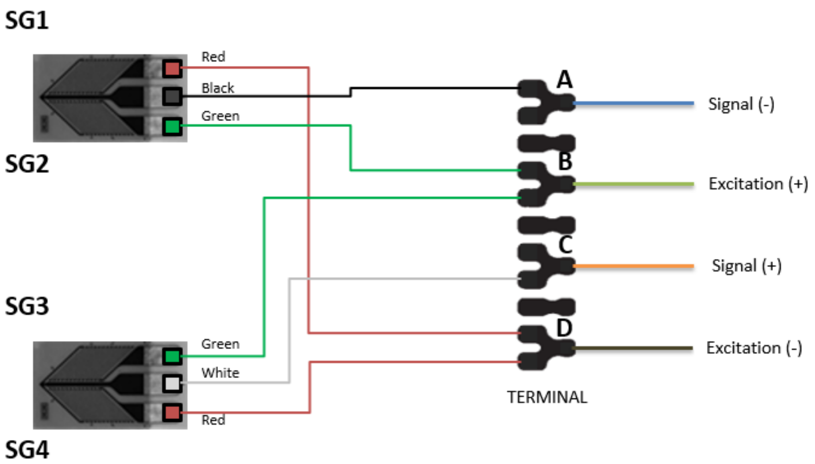

Figure 57: Torsion Bridge Completion Diagram

Strain bridge completion diagram for centrifugal force bridge can be seen in Figure 58.

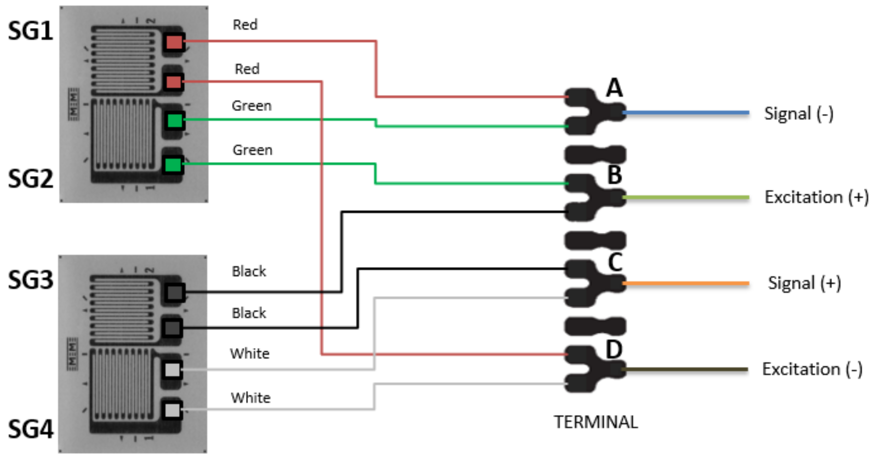

Figure 58: Centrifugal Force Bridge Completion Diagram

Sample photos of instrumented dummy blade can be seen in Figure 59.

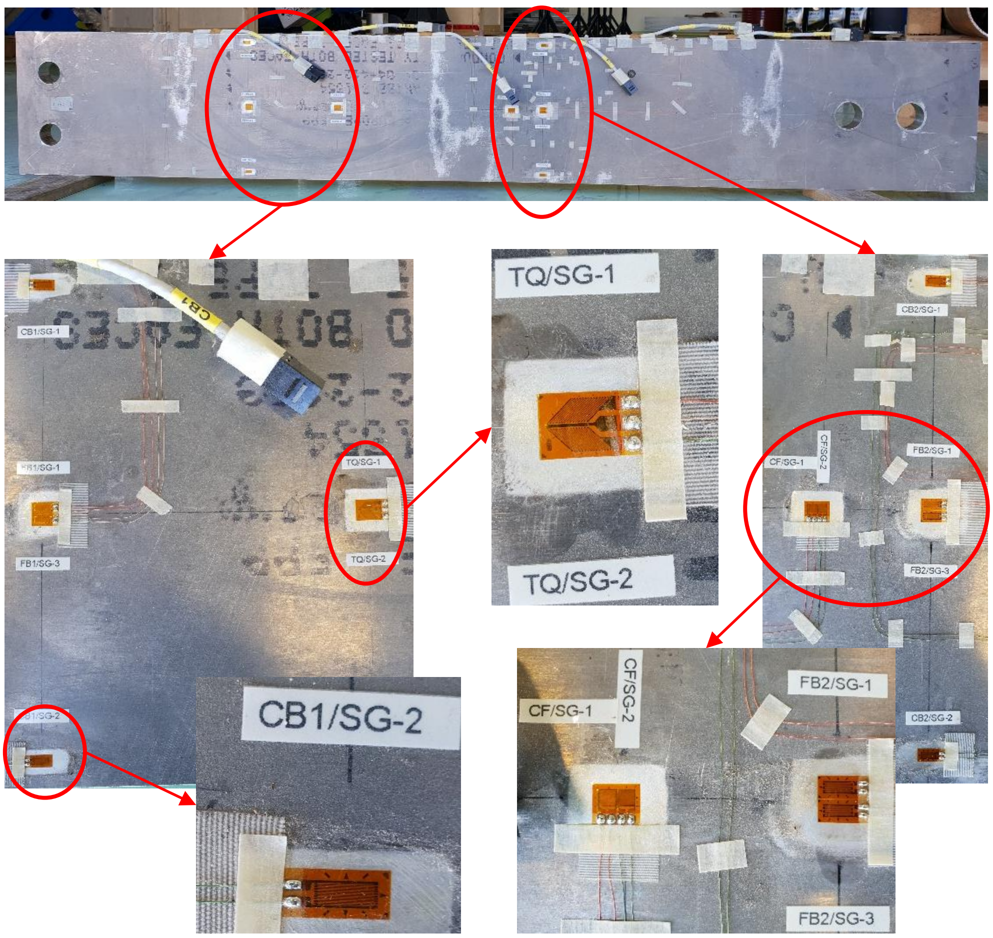

Figure 59: Instrumented Dummy Component

6.3 Calibration of the Dummy Component

Calibration of the dummy component to calculate calibration coefficients and the crosstalk matrix is explained in this part.

6.3.1 Introduction

Calibration of the dummy blade is the process of turning its strain-based measuring outputs to known reference inputs. In other words, the instrumented dummy blade is turned into a load cell at the section locations.

Calibration procedure of the dummy blade is run in an exclusive calibration test system. Calibration of all bridges under known loading is done in this calibration setup, which is on the left of the test system. Crosstalk effects during these loadings are also investigated, and crosstalk compensation operations are applied to the calibration data.

6.3.1.1 Calibration Test System

The calibration test setup is located on the left of the helicopter blade structural test system. It is manufactured to apply pure chord bending, beam bending and torsion loading to the dummy component. Calibration test setup can be seen in Figure 60.

Figure 60: Calibration Test Setup

Dummy component is fixed from the tip side to the calibration test setup and from the root side of the dummy component load application lug is connected. Load application lug has unique connection locations for applying pure calibration loads. Middle upper and lower holes are created for chord bending loading. Middle left, and right holes are drilled for beam bending loading. Additionally, the holes on the corners are drilled for torsion calibration loading. From these locations, deadweights are applied with the help of cable and pulley system. Load application lug can be seen in Figure 61.

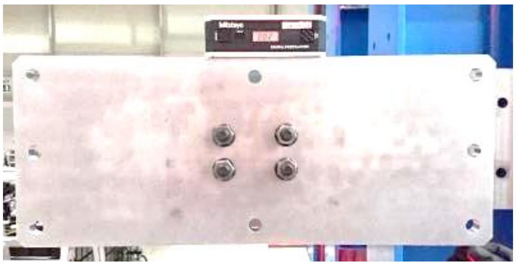

Figure 61: Load Application Lug

While applying known load with the deadweights to the dummy component, the weight of the deadweights is checked from the connected load cells on the cables that are connecting the deadweights and the load application lug. During calibration, applied data is recorded from these load cells, and the strain data is collected from the strain bridges with the help of the data acquisition system and the computers.

All positive and negative calibrations are done in this setup by applying known deadweights except the centrifugal force calibration. Centrifugal force calibration is done in the helicopter blade structural test setup due to the loading configuration and high loading requirement.

6.3.1.2 General Procedure of Calibration

Before starting the calibration, all strain gages and load cells used to control applied deadweight force, are connected to the data acquisition system. All of them are set to the zero values before loading. The orientation of the load application unit is controlled and set as its upper side is parallel to the ground. Cable and pulley system is connected to proper locations according to which calibration sequence is followed.

After setting the test system, a data point at zero loading is taken, and the load is incremented to the highest corresponding calibration load in 4 or 5 steps. In every step, a data point is also taken. After reaching the highest point, unloading is done in again in the same number of steps while taking data in every step. With these data points, all calibration curves are drawn. Crosstalk effects are investigated from these calibration graphs, and the requirement for crosstalk compensation operations are decided. Additionally, calibration procedures are done three times to check the repeatability of the procedure.

A sample photo from chord bending positive calibration can be seen in Figure 62.

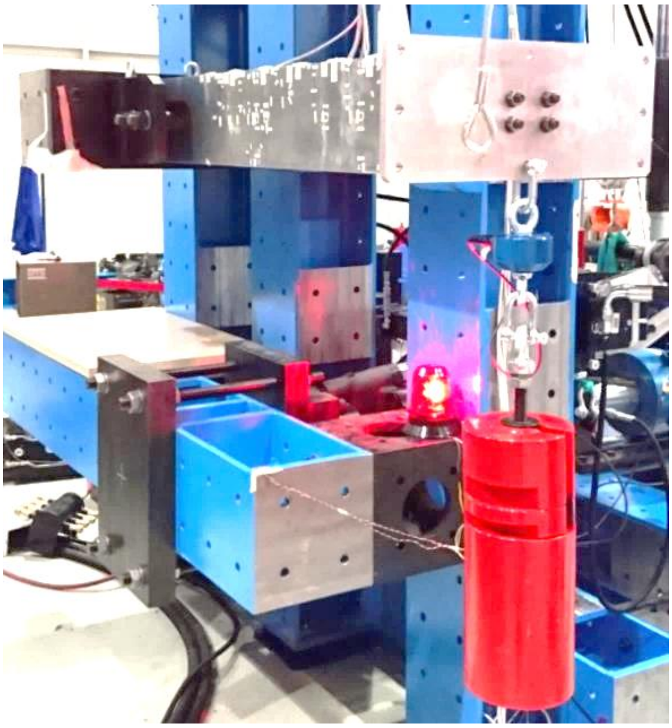

Figure 62: Positive Chord Bending Calibration

Another sample photo from centrifugal force calibration can be seen in Figure 63. As seen from the figures, positive centrifugal force calibration is done in the helicopter blade structural test system, due to the high loading requirement and loading configuration.

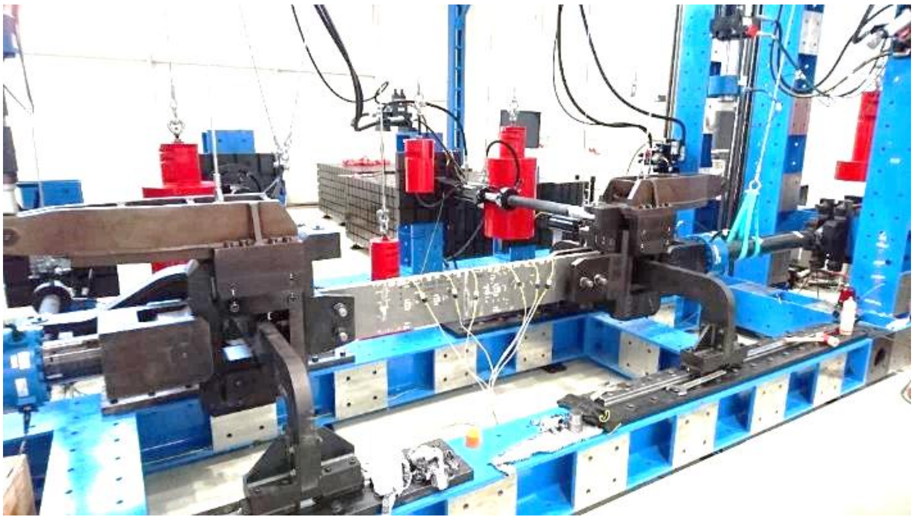

Figure 63: Positive Centrifugal Force Calibration

Centrifugal load calibration is also done with a similar procedure, but the loading is applied with the centrifugal force hydraulic actuator, and the applied load data is recorded from the load cell connected between centrifugal force hydraulic actuator and the load application unit. Centrifugal force actuator is located on the left side of the helicopter blade structural test system.

6.3.2 Chord Bending Calibration

Chord bending calibration is done under pure positive and negative chord bending loading in the calibration test system, and details of it explained below.

6.3.2.1 Positive Chord Bending Calibration

Positive chord bending calibration load is applied from the middle bottom hole of the load application lug. It is applied from there because the hole is stationed at the neutral plane of the dummy component in chord bending loading. Positive chord bending loading illustration can be seen in Figure 64.

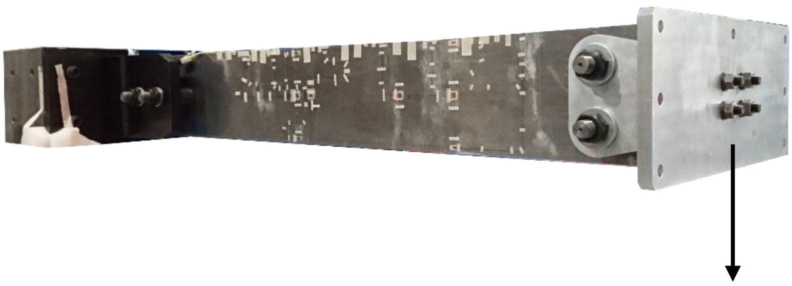

Figure 64: Positive Chord Bending Loading Illustration

The deadweight application is enforced in 5 steps starting from zero loading, and it is unloaded with the same steps to zero loading. At every step, load cell and strain gage data are recorded. Recorded calibration results under positive chord bending loading can be seen in Figure 65, Figure 66 and, Table 9.

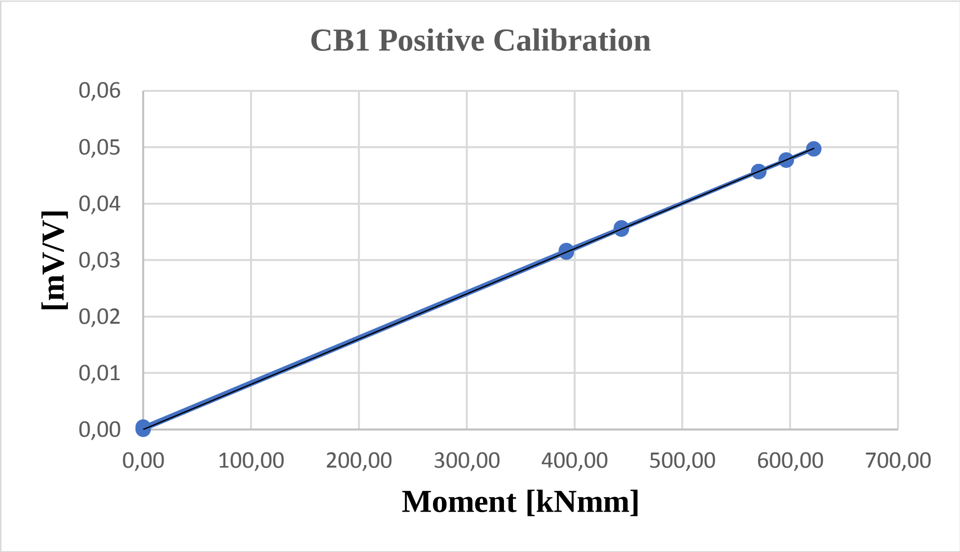

Figure 65: CB1 Strain Bridge Positive Calibration Results

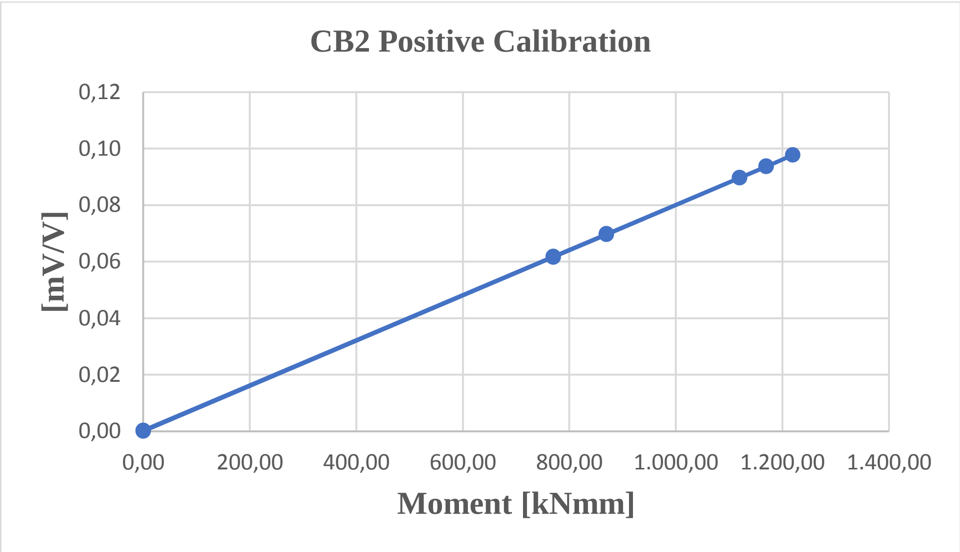

Figure 66: CB2 Strain Bridge Positive Calibration Results

Table 9: Calibration Results under Positive Chord Bending Loading

Load [kN]	**CB1 Moment [kNmm]**	**CB2 Moment [kNmm]**	**CB1 [mV/V]**	**CB2 [mV/V]**	**CF [mV/V]**	**BB1 [mV/V]**	**BB2 [mV/V]**	**TQ [mV/V]**
0.000	0.00	0.00	0.0000	0.0000	0.0000	0.0000	0.0001	0.0000
0.755	392.60	770.10	0.0314	0.0616	0.0001	0.0027	0.0052	-0.0001
0.853	443.56	870.06	0.0355	0.0696	0.0001	0.0031	0.0060	-0.0001
1.098	570.96	1119.96	0.0457	0.0896	0.0003	0.0040	0.0079	-0.0001
1.147	596.44	1169.94	0.0477	0.0936	0.0003	0.0043	0.0085	-0.0001
1.196	621.92	1219.92	0.0497	0.0977	0.0003	0.0046	0.0088	-0.0002
1.147	596.44	1169.94	0.0477	0.0937	0.0004	0.0042	0.0082	-0.0002
1.098	570.96	1119.96	0.0457	0.0897	0.0003	0.0041	0.0079	-0.0002
0.853	443.56	870.06	0.0357	0.0698	0.0003	0.0031	0.0062	-0.0002
0.755	392.60	770.10	0.0317	0.0618	0.0004	0.0029	0.0054	-0.0002
0.000	0.00	0.00	0.0004	0.0003	0.0004	0.0004	0.0005	-0.0003

6.3.2.2 Negative Chord Bending Calibration

Negative chord bending calibration load is applied from the middle upper hole of load application lug with the help of cable and pulley system. It is applied from there because the hole is stationed at the neutral plane of the dummy component in chord bending loading. Negative chord bending loading illustration can be seen in Figure 67.

Figure 67: Negative Chord Bending Loading Illustration

The deadweight application is enforced in 5 steps starting from zero loading, and it is unloaded with the same steps to zero loading. At every step, load cell and strain gage data are recorded. Recorded calibration results under negative chord bending loading illustration can be seen in Figure 68, Figure 69 and, Table 10.

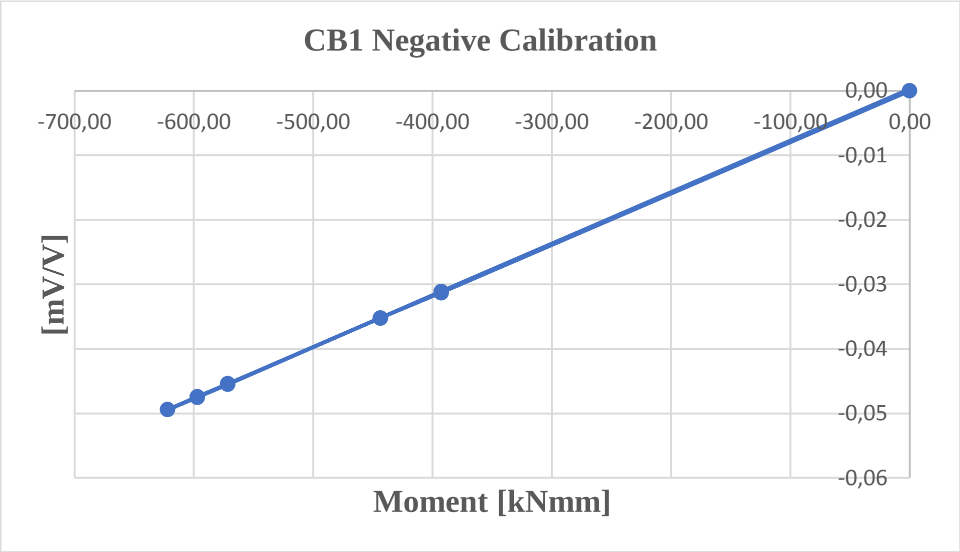

Figure 68: CB1 Strain Bridge Negative Calibration Results

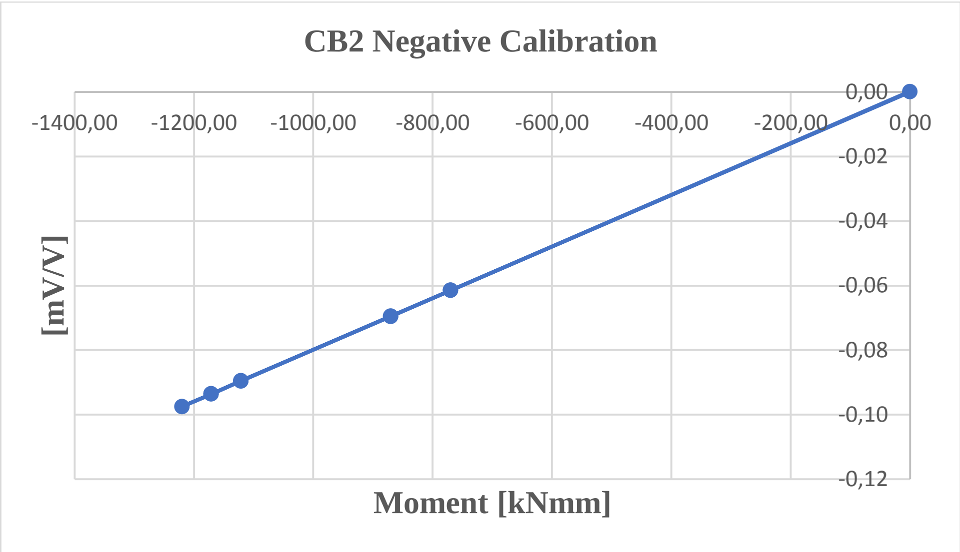

Figure 69: CB2 Strain Bridge Negative Calibration Results

Table 10: Calibration Results under Negative Chord Bending Loading

Load [kN]	CB1 Moment [kNmm]	CB2 Moment [kNmm]	CB1 [mV/V]	CB2 [mV/V]	CF [mV/V]	BB1 [mV/V]	BB2 [mV/V]	TQ [mV/V]
0.000	0.00	0.00	0.0000	0.0000	0.0000	0.0001	0.0002	0.0000
-0.755	-392.60	-770.10	-0.0313	-0.0615	0.0002	-0.0023	-0.0051	-0.0006
-0.853	-443.56	-870.06	-0.0352	-0.0696	0.0002	-0.0027	-0.0059	-0.0007
-1.099	-571.48	-1120.98	-0.0455	-0.0895	0.0002	-0.0034	-0.0074	-0.0008
-1.148	-596.96	-1170.96	-0.0475	-0.0936	0.0003	-0.0035	-0.0077	-0.0008
-1.196	-621.92	-1219.92	-0.0494	-0.0975	0.0003	-0.0038	-0.0081	-0.0009
-1.148	-596.96	-1170.96	-0.0474	-0.0936	0.0003	-0.0036	-0.0080	-0.0008
-1.099	-571.48	-1120.98	-0.0454	-0.0896	0.0003	-0.0033	-0.0074	-0.0008
-0.853	-443.56	-870.06	-0.0352	-0.0695	0.0003	-0.0026	-0.0056	-0.0007
-0.755	-392.60	-770.10	-0.0311	-0.0615	0.0003	-0.0021	-0.0048	-0.0005
0.000	0.00	0.00	0.0003	0.0002	0.0003	0.0003	0.0002	-0.0002

6.3.3 Beam Bending Calibration

Beam bending calibration is done under pure positive and negative beam bending loading in the calibration test system, and details of it explained below.

6.3.3.1 Positive Beam Bending Calibration

Positive beam bending calibration load is applied from the middle right hole of load application lug with the help of cable and pulley system. It is applied from there because the hole is stationed at the neutral plane of the dummy component in beam bending loading. Positive beam bending loading illustration can be seen in Figure 70.

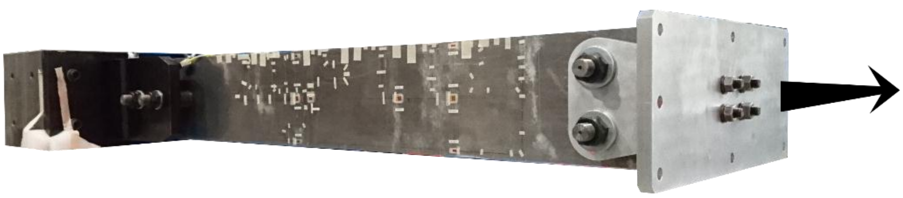

Figure 70: Positive Beam Bending Loading Illustration

The deadweight application is enforced in 4 steps starting from zero loading, and it is unloaded with the same steps to zero loading. At every step, load cell and strain gage data are recorded. Recorded calibration results under positive beam bending loading can be seen in Figure 71, Figure 72 and, Table 11.

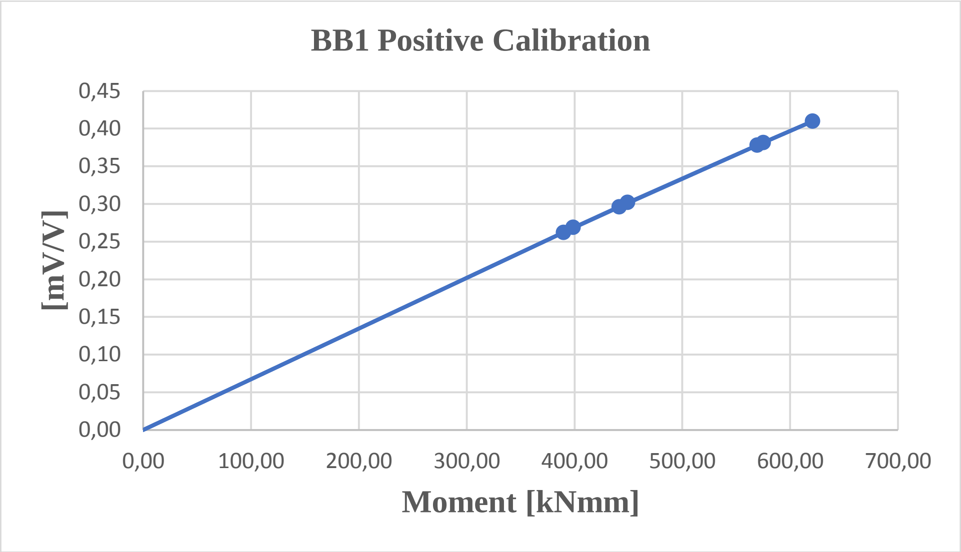

Figure 71: BB1 Strain Bridge Positive Calibration Results

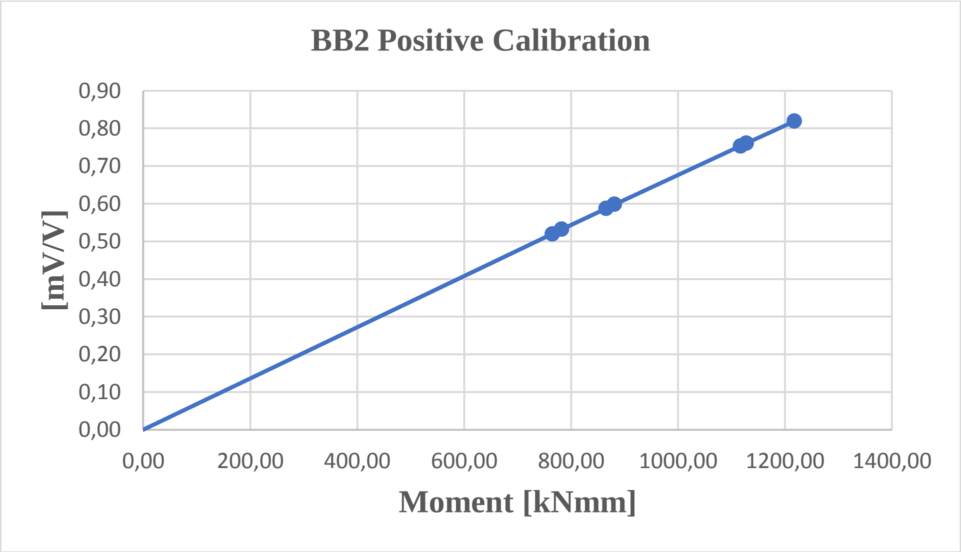

Figure 72: BB2 Strain Bridge Positive Calibration Results

Table 11: Calibration Results under Positive Beam Bending Loading

Load [kN]	BB1 Moment [kNmm]	BB2 Moment [kNmm]	CB1 [mV/V]	CB2 [mV/V]	CF [mV/V]	BB1 [mV/V]	BB2 [mV/V]	TQ [mV/V]
0.000	0.00	0.00	0.0000	-0.0001	0.0000	-0.0001	-0.0002	0.0000
0.750	390.00	765.00	-0.0002	-0.0007	-0.0002	0.2622	0.5197	0.0004
0.849	441.48	865.98	-0.0002	-0.0006	-0.0002	0.2959	0.5873	0.0007
1.095	569.40	1116.90	-0.0001	-0.0006	-0.0003	0.3777	0.7535	0.0013
1.194	620.88	1217.88	-0.0002	-0.0005	-0.0004	0.4099	0.8194	0.0016
1.106	575.12	1128.12	-0.0001	-0.0006	-0.0003	0.3815	0.7607	0.0014
0.864	449.28	881.28	-0.0001	-0.0005	-0.0002	0.3018	0.5987	0.0010
0.767	398.84	782.34	0.0000	-0.0004	-0.0002	0.2687	0.5321	0.0009
-0.001	-0.52	-1.02	0.0000	-0.0001	0.0000	-0.0001	-0.0005	0.0000

6.3.3.2 Negative Beam Bending Calibration

Before negative beam bending calibration, the specimen is rotated 180^{o} from its mid-axis. Because there is no connection location for the pulley system on the left of the test calibration test setup. Negative beam bending calibration load is also applied from the middle right hole of load application lug with the help of cable and pulley system. However, it is the middle-left hole if it is not turned. It is applied from there because the hole is stationed at the neutral plane of the dummy component in beam bending loading. Negative chord bending loading illustration can be seen in Figure 73.

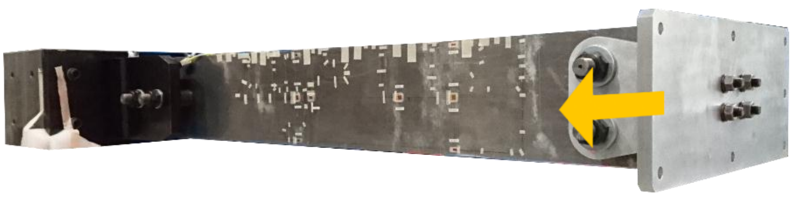

Figure 73: Negative Beam Bending Loading Illustration

The deadweight application is enforced in 5 steps starting from zero loading, and it is unloaded with the same steps to zero loading. At every step, load cell and strain gage data are recorded. Recorded calibration results under negative beam bending loading can be seen in Figure 74, Figure 75 and, Table 12.

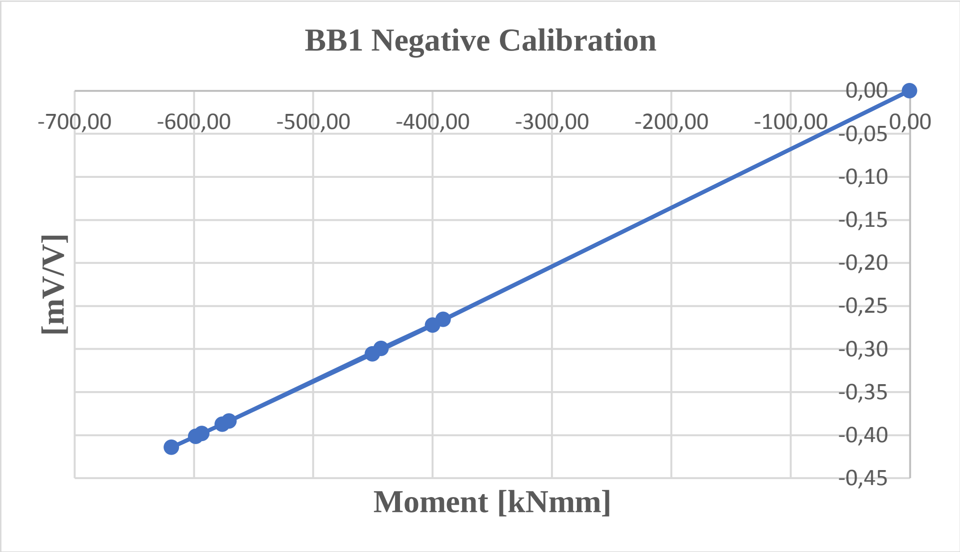

Figure 74: BB1 Strain Bridge Negative Calibration Results

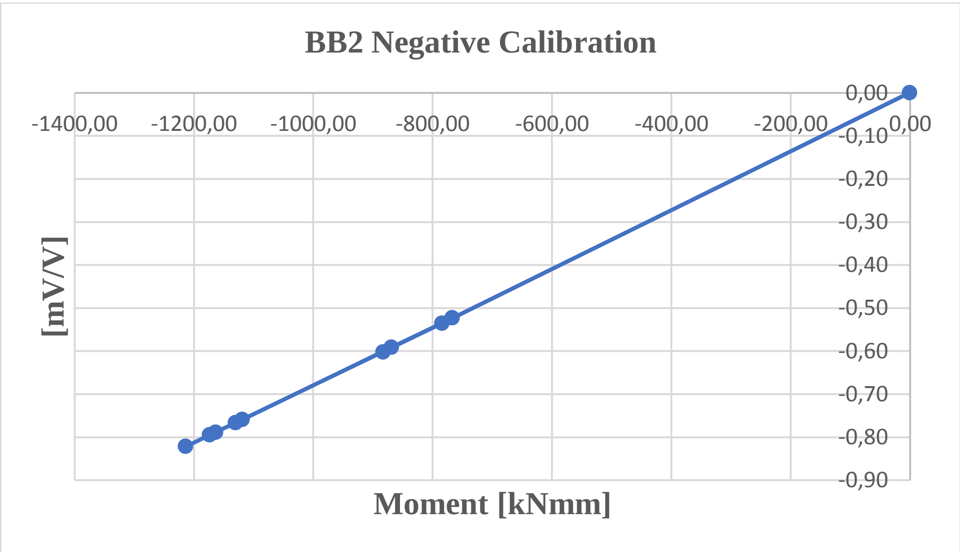

Figure 75: BB2 Strain Bridge Negative Calibration Results

Table 12: Calibration Results under Negative Beam Bending Loading

Load [kN]	BB1 Moment [kNmm]	BB2 Moment [kNmm]	CB1 [mV/V]	CB2 [mV/V]	CF [mV/V]	BB1 [mV/V]	BB2 [mV/V]	TQ [mV/V]
-0.001	-0.52	-1.02	0.0001	0.0000	0.0000	0.0000	0.0000	0.0001
-0.752	-391.04	-767.04	-0.0001	-0.0001	0.0000	-0.2656	-0.5231	-0.0019
-0.852	-443.04	-869.04	-0.0001	-0.0001	0.0000	-0.2992	-0.5909	-0.0021
-1.097	-570.44	-1118.94	-0.0002	-0.0002	-0.0001	-0.3835	-0.7592	-0.0021
-1.141	-593.32	-1163.82	-0.0002	-0.0003	-0.0001	-0.3981	-0.7887	-0.0022
-1.190	-618.80	-1213.80	-0.0002	-0.0003	-0.0001	-0.4141	-0.8214	-0.0023
-1.151	-598.52	-1174.02	-0.0002	-0.0002	-0.0001	-0.4013	-0.7950	-0.0023
-1.108	-576.16	-1130.16	-0.0002	-0.0002	-0.0001	-0.3873	-0.7664	-0.0023
-0.866	-450.32	-883.32	-0.0001	-0.0003	0.0000	-0.3056	-0.6022	-0.0017
-0.769	-399.88	-784.38	0.0000	-0.0001	0.0000	-0.2722	-0.5355	-0.0016
-0.001	-0.52	-1.02	0.0001	0.0000	0.0001	0.0002	0.0004	-0.0001

6.3.4 Torque Calibration

Torque calibration is done under pure positive and negative torsional loading in the calibration test system, and details of it explained below.

6.3.4.1 Positive Torque Calibration

Positive torsion calibration load is applied from the upper right hole, and lower left hole of load application lug with the help of cable and pulley system. It is applied from there because the holes are stationed at maximum torsion load creation location. Positive torsion calibration illustration can be seen in Figure 76.

Figure 76: Positive Torsion Calibration Illustration

The deadweight application is enforced in 4 steps starting from zero loading, and it is unloaded with the same steps to zero loading. At every step, load cell and strain gage data are recorded. Recorded calibration results under positive torsion loading can be seen in Figure 77 and Table 13.

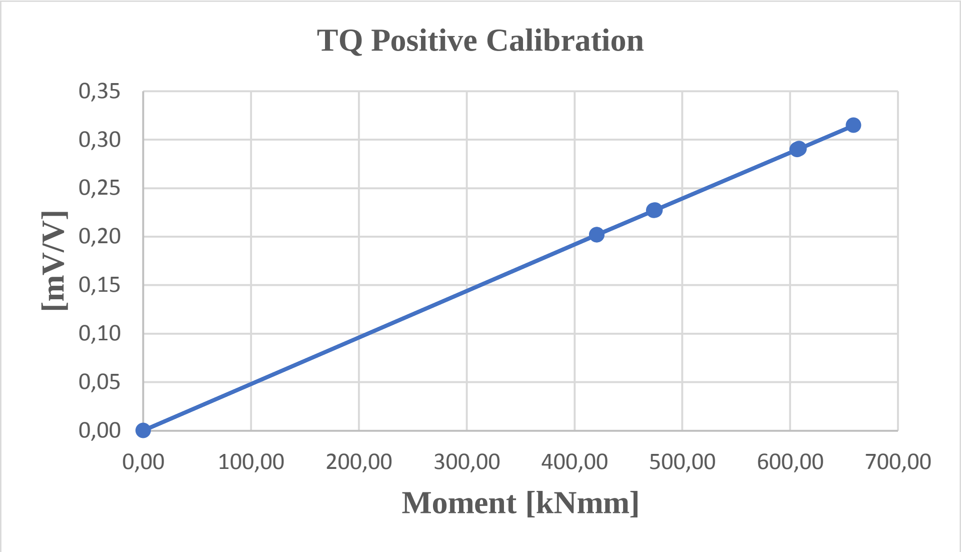

Figure 77: TQ Strain Bridge Positive Calibration Results

Table 13: Calibration Results under Positive Torsion Loading

Load 1 [kN]	**Load 2 [kN]**	**Torque [kNmm]**	**CB1 [mV/V]**	**CB2 [mV/V]**	**CF [mV/V]**	**BB1 [mV/V]**	**BB2 [mV/V]**	**TQ [mV/V]**
0.001	0.000	0.55	0.0000	0.0000	-0.0001	0.0000	0.0000	0.0000
-0.765	0.765	-420.75	-0.0018	-0.0001	-0.0058	0.0008	-0.0021	0.2019
-0.861	0.861	-473.55	-0.0020	-0.0001	-0.0066	0.0010	-0.0021	0.2268
-1.103	1.102	-606.65	-0.0026	-0.0003	-0.0085	0.0015	-0.0025	0.2897
-1.198	1.198	-658.90	-0.0030	-0.0002	-0.0093	0.0016	-0.0024	0.3146
-1.106	1.106	-608.30	-0.0027	-0.0002	-0.0086	0.0015	-0.0023	0.2906
-0.863	0.863	-474.65	-0.0020	0.0000	-0.0067	0.0010	-0.0024	0.2273
-0.765	0.765	-420.75	-0.0018	0.0000	-0.0060	0.0009	-0.0023	0.2018
0.000	0.001	0.00	-0.0001	-0.0001	-0.0002	0.0001	-0.0003	0.0001

6.3.4.2 Negative Torque Calibration

Negative torsion calibration load is applied from the upper left hole and the lower right hole of load application lug with the help of cable and pulley system. It is applied from there because the holes are stationed at maximum torsion load creation location. Negative torsion calibration illustration can be seen in Figure 78.

Figure 78: Negative Torsion Calibration Illustration

The deadweight application is enforced in 4 steps starting from zero loading, and it is unloaded with the same steps to zero loading. At every step, load cell and strain gage data are recorded. Recorded calibration results under negative torsion loading can be seen in Figure 79 and Table 14.

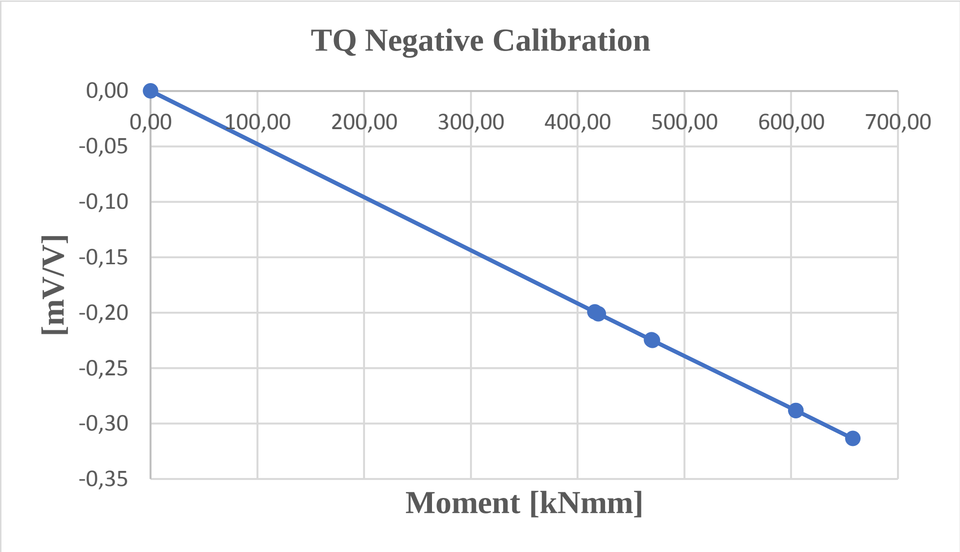

Figure 79: TQ Strain Bridge Negative Calibration Results

Table 14: Calibration Results under Negative Torsion Loading

Load 1 [kN]	**Load 2 [kN]**	**Torque [kNmm]**	**CB1 [mV/V]**	**CB2 [mV/V]**	**CF [mV/V]**	**BB1 [mV/V]**	**BB2 [mV/V]**	**TQ [mV/V]**
0.000	0.000	0.00	0.0000	-0.0001	0.0000	-0.0001	0.0000	0.0000
-0.763	-0.763	-419.65	0.0012	-0.0009	0.0055	-0.0028	-0.0024	-0.2010
-0.853	-0.853	-469.15	0.0014	-0.0009	0.0062	-0.0030	-0.0026	-0.2244
-1.099	-1.098	-604.45	0.0017	-0.0013	0.0079	-0.0039	-0.0037	-0.2882
-1.196	-1.195	-657.80	0.0018	-0.0015	0.0085	-0.0045	-0.0045	-0.3134
-1.099	-1.098	-604.45	0.0017	-0.0013	0.0079	-0.0041	-0.0038	-0.2882
-0.855	-0.855	-470.25	0.0013	-0.0010	0.0062	-0.0032	-0.0026	-0.2251
-0.757	-0.758	-416.35	0.0012	-0.0008	0.0055	-0.0028	-0.0022	-0.1994
0.000	0.001	0.00	-0.0001	-0.0001	0.0000	-0.0004	0.0000	0.0003

6.3.5 Centrifugal Force Calibration

Centrifugal force calibration is done only under pure positive centrifugal loading in helicopter blade structural test system, and details of it explained below.

6.3.5.1 Positive Centrifugal Force Calibration

Positive centrifugal force calibration is done under the effect of centrifugal force actuator in the helicopter blade test system. The whole setup is set but to give free motion in other loading axes all constraints and actuators are disconnected. Centrifugal load is applied incrementally in 5 steps with the help of hydraulic actuator. At every step, load cell and strain gage data are recorded. Recorded calibration results under positive centrifugal loading can be seen in Figure 80 and Table 15.

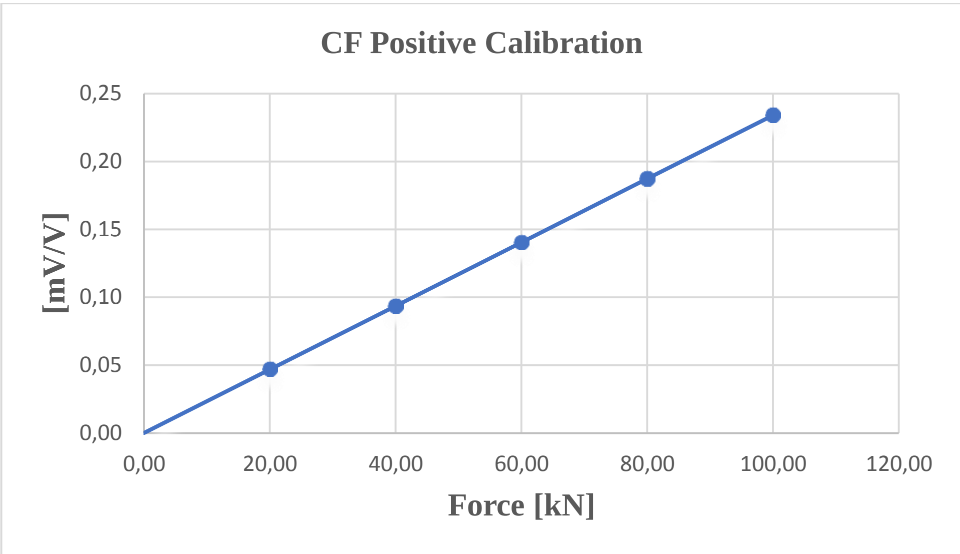

Figure 80: CF Strain Bridge Positive Calibration Results

Table 15: Calibration Results under Positive Centrifugal Loading

Load [kN]	**CB1 [mV/V]**	**CB2 [mV/V]**	**CF [mV/V]**	**BB1 [mV/V]**	**BB2 [mV/V]**	**TQ [mV/V]**
-0.032	0.0001	0.0000	0.0000	-0.0001	0.0000	0.0001
20.009	0.0187	0.0150	0.0469	-0.0346	-0.0224	0.0093
40.021	0.0172	0.0141	0.0935	-0.0357	-0.0298	0.0120
60.008	0.0170	0.0144	0.1403	-0.0344	-0.0336	0.0125
80.012	0.0173	0.0149	0.1872	-0.0326	-0.0368	0.0123
100.008	0.0168	0.0150	0.2340	-0.0316	-0.0398	0.0118

6.3.6 Calculation of Cross-Talk Matrix

By investigating the calibration results above, need for crosstalk compensation can be easily seen. Calculation of cross-talk matrices can be done with handheld calibration results by following the procedure explained in section 3.3.

Crosstalk matrices are built according to sections and considering section load directions. Section locations and naming can be seen in Figure 81. In order to build the matrix, maximum applied calibration loads are written in the first row and below of them are filled with the corresponding strain output found from the calibration procedure.

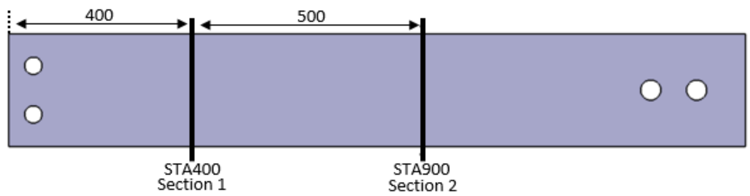

Figure 81: Dummy Component Section Locations and Naming

In all sections, chord bending, beam bending, torsion, and centrifugal force is recorded. With the addition of the maximum calibration loads, 5x4 matrices are built. For both sections positive and negative output matrices created can be seen below.

Positive Section 1

$$\text{Output Matrix [mV/V]}\quad \begin{array}{cc} & \begin{array}{cccc} CB1\,[kNmm] & BB1\,[kNmm] & CF\,[kN] & TQ\,[kNmm] \end{array} \\ \begin{array}{c} Eng\ Unit \\ CB1 \\ FB1 \\ CF \\ TQ \end{array} & \left[\begin{array}{cccc} 621.92 & 620.88 & 100.023 & 658.90 \\ 0.0497 & 0.0046 & 0.0003 & -0.0002 \\ -0.0002 & 0.4099 & -0.0004 & 0.0016 \\ -0.0089 & -0.0201 & 0.2333 & 0.0169 \\ -0.0030 & 0.0016 & -0.0093 & 0.3146 \end{array}\right] \end{array}$$

Positive Section 2

$$\text{Output Matrix [mV/V]}\quad \begin{array}{cc} & \begin{array}{cccc} CB1\,[kNmm] & BB1\,[kNmm] & CF\,[kN] & TQ\,[kNmm] \end{array} \\ \begin{array}{c} Eng\ Unit \\ CB1 \\ FB1 \\ CF \\ TQ \end{array} & \left[\begin{array}{cccc} 1219.92 & 1217.88 & 100.023 & 658.90 \\ 0.0977 & 0.0088 & 0.0003 & -0.0002 \\ -0.0005 & 0.8194 & -0.0004 & 0.0016 \\ -0.0024 & -0.0349 & 0.2333 & 0.0169 \\ -0.0002 & -0.0024 & -0.0093 & 0.3146 \end{array}\right] \end{array} \quad (11)$$

Negative Section 1

Output Matrix [mV/V]

$$\begin{bmatrix} & CB1\ [kNmm] & BB1\ [kNmm] & CF\ [kN] & TQ\ [kNmm] \\ Eng\ Unit & -621.92 & -618.8 & -100.023 & -657.80 \\ CB1 & -0.0494 & -0.0038 & 0.0003 & -0.0009 \\ FB1 & -0.0002 & -0.4141 & -0.0001 & -0.0023 \\ CF & 0.0089 & 0.0201 & -0.2333 & -0.0169 \\ TQ & 0.0018 & -0.0045 & 0.0085 & -0.3134 \end{bmatrix}$$

Negative Section 2

Output Matrix [mV/V]

$$\begin{bmatrix} & CB1\ [kNmm] & BB1\ [kNmm] & CF\ [kN] & TQ\ [kNmm] \\ Eng\ Unit & -1219.92 & -1213.8 & -100.023 & -657.80 \\ CB1 & -0.0975 & -0.0081 & 0.0003 & -0.0009 \\ FB1 & -0.0003 & -0.8214 & -0.0001 & -0.0023 \\ CF & 0.0024 & 0.0349 & -0.2333 & -0.0169 \\ TQ & -0.0015 & -0.0045 & 0.0085 & -0.3134 \end{bmatrix}$$

Every row of output matrix is divided by the first-row value or maximum calibration load to find sensitivity matrices. The first row is removed, and a handheld 4x4 matrix is the sensitivity matrix. Sensitivity or transfer function, K, matrices can be seen below.

Positive Section 1

K Matrix [mV/V/EU]

$$\begin{bmatrix} 7.991E-05 & 7.409E-06 & 2.999E-06 & -3.035E-07 \\ -3.216E-07 & 6.602E-04 & -3.999E-06 & 2.428E-06 \\ -1.431E-05 & -3.237E-05 & 2.332E-03 & 2.565E-05 \\ -4.824E-06 & 2.577E-06 & -9.298E-05 & 4.775E-04 \end{bmatrix}$$

Positive Section 2

K Matrix [mV/V/EU]

$$\begin{bmatrix} 8.009E-05 & 7.226E-06 & 2.999E-06 & -3.035E-07 \\ -4.099E-07 & 6.728E-04 & -3.999E-06 & 2.428E-06 \\ -1.967E-06 & -2.866E-05 & 2.332E-03 & 2.565E-05 \\ -1.639E-07 & -1.971E-06 & -9.298E-05 & 4.775E-04 \end{bmatrix} \tag{12}$$

Negative Section 1

K Matrix [mV/V/EU]

$$\begin{bmatrix} 7.943E-05 & 6.141E-06 & -2.999E-06 & 1.368E-06 \\ 3.216E-07 & 6.692E-04 & 9.998E-07 & 3.497E-06 \\ -1.431E-05 & -3.248E-05 & 2.332E-03 & 2.569E-05 \\ -2.894E-06 & 7.272E-06 & -8.498E-05 & 4.764E-04 \end{bmatrix}$$

Negative Section 2

K Matrix [mV/V/EU]

$$\begin{bmatrix} 7.992E-05 & 6.673E-06 & -2.999E-06 & 1.368E-06 \\ 2.459E-07 & 6.767E-04 & 9.998E-07 & 3.497E-05 \\ -1.967E-06 & -2.875E-05 & 2.332E-03 & 2.569E-05 \\ 1.230E-06 & 3.707E-06 & -8.498E-05 & 4.764E-04 \end{bmatrix}$$

Unit of sensitivity matrices is mV/V/Engineering Unit. During testing, mV/V data is collected from strain bridges. To turn strain bridge data into section loads inverse of the sensitivity matrices are needed. The inverse of the sensitivity matrices is called crosstalk matrices. Crosstalk compensation, K^{-1}, matrices calculated from sensitivity matrices can be seen below.

Positive Section 1

$$\begin{array}{c} K^{-1}\ \text{Matrix} \\ [EU/\ mV/V] \end{array} \quad \begin{array}{cccc} CB1\ [kNmm] & BB1\ [kNmm] & CF\ [kN] & TQ\ [kNmm] \end{array} \\ \begin{bmatrix} 12510.63 & -141.22 & -15.95 & 9.53 \\ 6.03 & 1514.79 & 2.28 & -7.82 \\ 75.29 & 20.22 & 427.75 & -23.03 \\ 141.02 & -5.66 & 83.12 & 2090.06 \end{bmatrix}$$

Positive Section 2

$$\begin{array}{c} K^{-1}\ \text{Matrix} \\ [EU/\ mV/V] \end{array} \quad \begin{array}{cccc} CB1\ [kNmm] & BB1\ [kNmm] & CF\ [kN] & TQ\ [kNmm] \end{array} \\ \begin{bmatrix} 12485.33 & -134.74 & -15.91 & 9.48 \\ 7.65 & 1486.30 & 2.23 & -7.67 \\ 10.55 & 18.04 & 427.83 & -23.07 \\ 6.37 & 9.60 & 83.32 & 2089.89 \end{bmatrix}$$

Negative Section 1

$$\begin{array}{c} K^{-1}\ \text{Matrix} \\ [EU/\ mV/V] \end{array} \quad \begin{array}{cccc} CB1\ [kNmm] & BB1\ [kNmm] & CF\ [kN] & TQ\ [kNmm] \end{array} \\ \begin{bmatrix} 12591.31 & -114.43 & 14.92 & -36.12 \\ -6.64 & 1494.45 & -1.05 & -10.89 \\ 76.17 & 20.33 & 427.97 & -23.45 \\ 90.18 & -19.88 & 76.44 & 2094.68 \end{bmatrix}$$

Negative Section 2

$$\begin{array}{c} K^{-1}\ \text{Matrix} \\ [EU/\ mV/V] \end{array} \quad \begin{array}{cccc} CB1\ [kNmm] & BB1\ [kNmm] & CF\ [kN] & TQ\ [kNmm] \end{array} \\ \begin{bmatrix} 12513.29 & -122.57 & 14.84 & -35.84 \\ -4.41 & 1477.78 & -1.03 & -10.78 \\ 10.83 & 18.20 & 427.89 & -23.24 \\ -30.33 & -7.94 & 76.29 & 2094.95 \end{bmatrix} \tag{13}$$

To verify matrices, inverse check ($K \cdot K^{-1}$) operation is done. It is done to check that inverse matrix operations are done truly. All results are found as identity matrices. So, the matrix inverse operations are true.

By including crosstalk compensation matrices into the controller of helicopter blade structural test system, section loads can be visualized in test monitors.

6.4 Execution of Multiaxial Test

Execution of a multiaxial test with a dummy component in a helicopter blade structural test system is explained in this part.

6.4.1 Introduction

Instrumented and calibrated dummy blade, which can be seen in Figure 82, is assembled in the helicopter blade structural test system. All the mechanical connections like the actuator load application unit, counterbalance system with load application unit and the hydraulic line connections, are checked visually. Cable connections are checked as follows:

- Cable connections of the sensors are checked.
- Load cell A and B bridges (double output for safety) and displacement transducers on the actuators are connected to the controller.
- Strain bridges are connected to the data acquisition system, and the cable between the data acquisition system and the controller is also checked.
- By checking the cables between the controller and the computer, cable checks are completed.

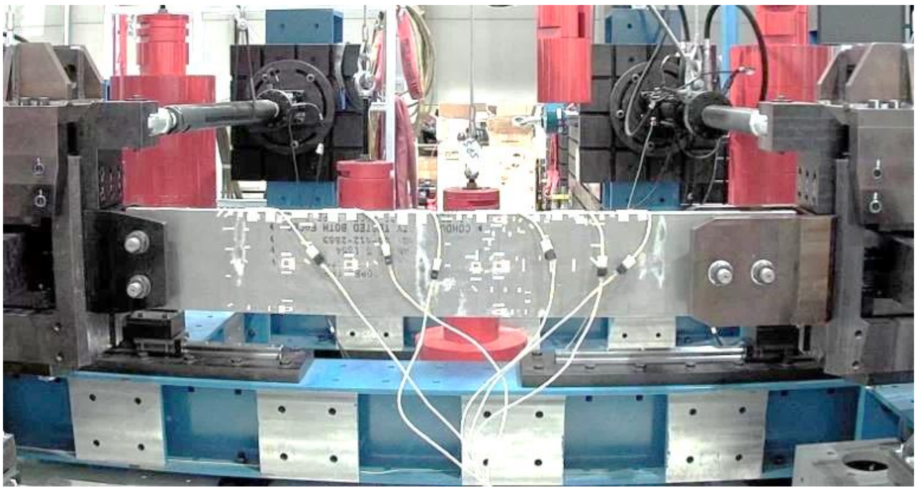

Figure 82: Instrumented Dummy Component Assembly

After completing the external checks, a test program is created in the controller software. Crosstalk compensation and calibration data of load cells and displacement transducers are implemented into the test control software. Force and display limits for the safety of equipment and personnel is defined to the controller test system.

After making some trials to check if the system is working correctly, actuator loads given in Table 16 are applied to the dummy component. Positive loading means actuator stroke is increasing or actuator is compressing the part; negative loading means actuator stroke is decreasing or actuator is pulling the part. Actuators for the helicopter blade structural test system are named in Figure 83. Centrifugal force actuator is parallel to the dummy component and positioned in the left part of the figure. Load application unit in the far side of the photo is LAU1, and the load application unit bottom right side is LAU2 with corresponding chord and beam bending actuators named accordingly. Chord bending actuators are located perpendicular to the dummy blade on top of the load application units. Beam bending actuators are positioned at the back of the load application units and closer to the support structure. Finally, the torsion actuator is in the back of LAU2 close to the dummy component.

Table 16: Actuator Loads Applied during Multiaxial Test

Actuator Name	**Force [N]**
Chord Bending 1	1000
Chord Bending 2	1000
Beam Bending 1	1000
Beam Bending 2	1000
Torsion	-1000
Centrifugal Force	-100000

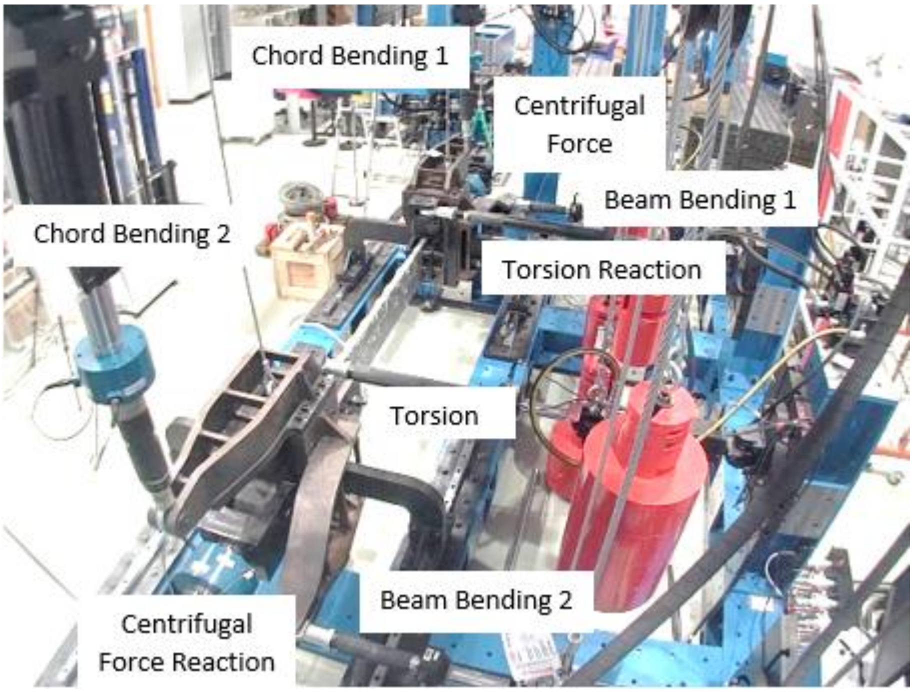

Figure 83: Actuator Naming in the Test System

With these configurations, the test is executed, and section loads are monitored and recorded from the test system.

6.4.2 Results of the Multiaxial Test

After the execution of the multiaxial test on dummy component, the section loads that are output from controller software are tabulated in Table 17.

Table 17: Section Loads found in Multiaxial Test

Bridge Name	Section Load
Chord Bending 1	645 kN mm
Chord Bending 2	699 kN mm
Beam Bending 1	-257 kN mm
Beam Bending 2	-267 kN mm
Torsion	161 kN mm
Centrifugal Force	99.004 kN

The results are the outputs of multiaxial testing of the dummy component under chord bending, beam bending, torsion centrifugal force loading and are illustrated on the section locations of the dummy component as in Figure 84. These results are used to verify dynamic analysis model of the helicopter blade test system.

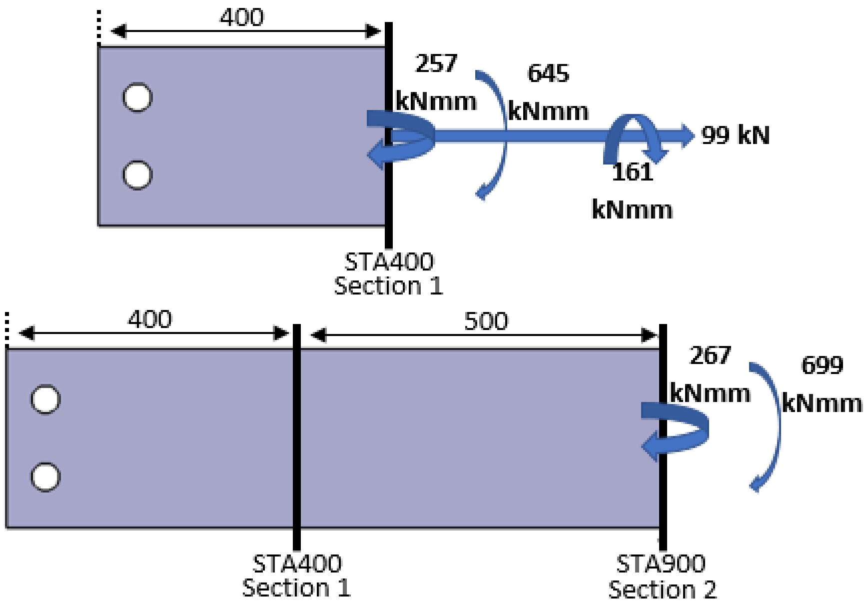

Figure 84: Illustration of Section Loads from Test Results

6.5 Comparison of Section Loads Obtained from Adams and Multiaxial Test

The section loads obtained from Adams dynamic analysis model and the multiaxial test should be compared. Compared simulation and the test results and the absolute percentage error rates are tabulated in Table 18.

Table 18: Comparison of Section Loads Obtained from Adams and Test

Bridge Name	Section Load		Absolute % Error
	Adams	Test	
Chord Bending 1	703 kNmm	645 kNmm	9.05
Chord Bending 2	703 kNmm	699 kNmm	0.63
Beam Bending 1	-262 kNmm	-257 kNmm	2.03
Beam Bending 2	-250 kNmm	-267 kNmm	6.44
Torsion	146 kNmm	161 kNmm	9.32
Centrifugal Force	96.97 kN	99.004 kN	2.05

It can be observed from absolute percentage errors that all error rates among all section loads are lower 10%. Having errors less than 10% shows that the model created in Adams is a well-formed model. Because under such a complex loading and such complex motion mechanisms, it is too low.

Maximum absolute percentage error observed is 9.32% in torsion loading. All rotational loads are applied with two hydraulic actuators, and their absolute percent error results are lower than torsional loading. So, by adding an extra actuator or modifying the torsion constraint modeling, like increasing joint frictions by making stiffer, this error might be reduced.

Minimum absolute percentage error observed is 0.63% in chord bending loading of section two. However, absolute percentage error result of chord bending 1 strain bridge is the second highest result as 9.05%. These results may also be explained by the effect of the torsion actuator. On the load application unit, torsion reaction constraint is fixed, and it may be modeled stiffer than the real.

As a result, actuator load calculation tool for a rotating beam like aerospace structure structural test is developed and it is verified by executing a multiaxial test on a dummy component under chord bending, beam bending, torsion, and centrifugal force loading, with an average absolute percentage error rate of 4.92%.

CHAPTER 7

CONCLUSIONS

7.1 General Conclusions

An actuator load calculation tool is developed that can be used to calculate the loads applied by hydraulic actuators of an existing helicopter blade multiaxial structural test system. A dummy component is designed and used to develop the load calculation tool by carrying out dynamic analysis and testing of the dummy component as follows:

1) A dummy component that can be assembled into a helicopter blade test system is designed in a computer-aided-design software. The strength of the dummy component is checked by using a finite element software. Additionally, the same finite element model is modified to create an MNF file, which is an input to create a dynamic analysis model of the test system.
2) Dynamic analysis model of the test system is created using a multibody dynamic simulation software. MNF file is imported into the model to give flexible properties to the dummy component during simulations. Strain results on the dummy component are calculated with the help of modules of multibody dynamic simulation software. Strain data on the dummy component is turned into section loads at predetermined locations of the dummy component. Calibration dynamic analysis model is used to calculate calibration coefficients belongs to dummy component. By using calibration coefficients and strain data found from dynamic analysis model of the test setup section loads on the dummy component are calculated.

3) The dummy component is manufactured at TAI facilities for testing in the helicopter blade test bench. Strain gages are applied on the component to calculate section loads on predetermined locations of the dummy component. Six strain bridges, measuring chord bending, beam bending, torque, and centrifugal force, on two different sections are established. Calibration procedures and cross-talk compensation operations are done on the dummy component. Strain-based sensor calibration is done to turn the instrumented dummy blade into a load cell like structure at predetermined section locations.
4) The tool is verified by executing a multiaxial test on a dummy component under a combined loading including chord bending, beam bending, torsion, and centrifugal force loading. An average absolute percentage error rate of 4.92% between the testing and estimated section loads is obtained and the tool is found to be successful.

The actuator load calculation tool developed in this thesis can be used in the calculation of actuator loads of multiaxial loading test of real helicopter blades, such as the composite helicopter blade of T-625 (Gökbey) helicopter, by importing the finite element model and the composite material properties of the helicopter blade.

7.2 Future Work

Development of the actuator load calculation tool can be improved by incorporating temperature effects, detailed joint friction models and more flex parts in the dynamic analysis model.

Automatization of the tool can be achieved by self-communicating the MSC Adams and Microsoft Excel software or developing a controller module which can set actuator loads according to internal calculations don with the help of Adams Controls module.

Finally, the algorithm will be used on a multiaxial test of a real composite helicopter blade with the loads calculated from actuator load calculation tool and by importing the finite element model and the material properties of the real helicopter blade.

REFERENCES

[1] J. Martin, J. Fila, and D. Reisdorfer. Helicopter Structural Integrity Program Volume 1 – Structural Test Requirements Specification. Bell Helicopter Textron Inc., Fort Worth, TX, July 1990.

[2] CS-29 EASA Certification Specifications for Large Rotorcraft. European Aviation Safety Agency.

[3] A. U. Limon, Y. Ulu and D. Çöker. Döner Kiriş Benzeri Havacılık Yapılarının Yapısal Testi için Eyleyici Yükü Hesaplama Algoritması ve Çok Eksenli Test ile Doğrulanması. VI. Ulusal Havacılık ve Uzay Konferansı, Kocaeli, 28-30 September 2016.

[4] Photo of Hydraulic Power Unit. Retrieved from https://www.mts.com/en/forceandmotion/aerospacetesting/MTS_2012975?article=2 on 8 August 2017.

[5] Photo of Hydraulic Service Manifold. Retrieved from https://www.mts.com/en/products/producttype/test-components/hydraulic-power-distribution/hydraulic-service-manifolds/index.htm on 8 August 2017.

[6] Photo of Hydraulic Actuator. Retrieved from https://www.mts.com/en/products/producttype/test-components/actuators-hydraulic-components/actuators/index.htm on 8 August 2017.

[7] Photo of Load Cell. Retrieved from http://www.interfaceforce.com/index.php?1000-Fatigue-Rated-LowProfile-Load-Cell&mod=product&show=1 on 8 August 2017.

[8] Photo of Controller. Retrieved from https://www.mts.com/cs/groups/public/documents/library/dev_003624.pdf on 8 August 2017.

[9] Photo of Data Acquisition System. Retrieved from https://www.mts.com/en/forceandmotion/aerospacetesting/MTS_006696?article=2 on 8 August 2017.

[10] P. Anusonti-Inthra and Y. Liu. Structural Property Determination for an Articulated Rotor Blade. National Institute of Aerospace, Hampton, VA, 2006

[11] S. Shin. Design, Manufacturing, and Testing of an Active Twist Rotor. MS thesis, Massachusetts Institute of Technology, USA, June 1999.

[12] B. Rasuo. An Experimental Technique for Verification Fatigue Characteristics of Laminated Constructions from Composite Materials: Full-Scale Testing of the Helicopter Rotor Blades. In ICAS2010, 27th International Congress of the Aeronautical Sciences, Nice, France, 19-24 September 2010.

[13] B. Rasuo. Design, Fabrication, and Testing of the Helicopter Tail Rotor Blade from Composite Laminated Materials. University of Belgrade, Belgrade, Serbia, 27 March 1980.

[14] B. Rasuo. Experimental Techniques for Evaluation of Fatigue Characteristics of Laminated Constructions from Composite Materials: Full-Scale Testing of the Helicopter Rotor Blades. Journal of Testing and Evaluation, Vol. 39, No. 2. Paper ID: JTE102768, 2010.

[15] Y. Kee, S. Kim, J. Han, and J. Jung. Resonant Fatigue Testing of Full Scale Composite Helicopter Rotor Blades. ECCM15, 15th European Conference on Composite Materials, Venice, Italy, 24-28 June 2012.

[16] A. A. Lischer. Development Fatigue Testing of a Large Helicopter Rotor Blade. Symposium on Fatigue of Aircraft Structures. Philadelphia, American Society for Testing Materials, Spec. Tech. Publ. No. 274, June 1960, pages 79-98.

[17] R. Harrison, S. Stacey, and B. Hansford. BERP IV the Design, Development, and Testing of an Advanced Rotor Blade. American Helicopter Society 64th Annual Forum, Montreal, Canada, 29 April-1 May 2008.

[18] T. Ewanochko, D. Nelson, M. Esaki, and E. Pesheck. Integrated Durability Analysis Using ANSYS, ADAMS and FE-Fatigue. 16th European Mechanical Dynamics User Conference, Berchtesgaden, Germany, 14-15 November 2001.

[19] X. Gang, Z. Yan, Z. Fanli and C. Liping. Modeling and Simulation of the Coupled Rigid-flexible Multibody Systems in MWorks. Proceedings of the 9th International Modelica Conference, Munich, Germany, 3-5 September 2012.

[20] MSC ADAMS. In Wikipedia. Retrieved from https://en.wikipedia.org/wiki/MSC_ADAMS on 20 May 2018.

[21] Adams: The Multibody Dynamic Simulation Solution. In MSC Software Corp. Retrieved from http://www.mscsoftware.com/product/adams on 20 May 2018.

[22] Adams: Real Dynamics for Functional Virtual Prototyping. In MSC Software Corp. Retrieved from http://media.mscsoftware.com/sites/default/files/ds_adams_ltr_w.pdf on 20 May 2018.

[23] Welcome to Adams/Flex (07/11/2014). In MSC Software Corp. Retrieved from https://simcompanion.mscsoftware.com/infocenter/index?page=content&id=DOC9304&actp=RSS on 20 May 2018.

[24] P. Häußler, D. Emmrich, O. Müller, B. Ilzhöfer, L. Nowicki and A. Albers. Automated Topology Optimization of Flexible Components in Hybrid Finite Element Multibody Systems using ADAMS/Flex and MSC.Construct. 16th European ADAMS User Conference, 2001.

[25] Strain Gauge. In Wikipedia. Retrieved from https://en.wikipedia.org/wiki/Strain_gauge on 20 May 2018.

[26] Application Note 290-1: Practical Strain Gage Measurements, Omega Engineering, Agilent Technologies Inc., 1999.

[27] Technical Note TN-505-6: Strain Gage Selection: Criteria, Procedures, Recommendations. Micro-Measurements, Vishay Precision Group, 8 March 2018.

[28] Strain Measurement. In Measurement Computing Corp. Retrieved from https://www.mccdaq.com/handbook/chapt_7.aspx on 20 May 2018.

[29] Measuring Strain with Strain Gages. In National Instruments. Retrieved from http://www.ni.com/white-paper/3642/en/ on 20 May 2018.

[30] A. Hunt (Ed.). Guide to Measurement of Force. The Institute of Measurement and Control, 2013. ISBN: 0 904457 28 1

[31] P. Hovell, D. Webber, and T. Roberts. The Use of Calibrated Strain Gauges for Flight Load Determination. Royal Aircraft Establishment, Farnborough, July 1968.

[32] T. Skopinski, W. Aiken and W. Huston. Calibration of Strain-Gage Installations in Aircraft Structures for the Measurement of Flight Loads. Report 1178, National Advisory Committee for Aeronautics, 1953.

[33] D. Schrand. Cross-Talk Compensation Using Matrix Methods. Sensors & Transducers Journal, Vol. 79, Issue 5, May 2007, pages 1157-1163.

[34] MMPDS-10: Metallic Materials Properties Development and Standardization (MMPDS). Federal Aviation Administration, Battelle Memorial Institute (distributor), April 2015.

[35] S. Benzley, E. Perry, K. Merkley, B. Clark, and G. Sjaardama. A Comparison of All Hexagonal and All Tetrahedral Finite Element Meshes for Elastic and Elasto-plastic Analysis. 4th International Meshing Roundtable, Albuquerque, New Mexico, USA, 16-17 October 1995.

[36] J. Jenkins, M. DeAngelis. A Summary of Numerous Strain-Gage Load Calibrations on Aircraft Wings and Tails in a Technology Format. NASA Technical Memorandum 4804. Dryden Flight Research Center, Edwards, California, July 1997.